

University of Nottingham

UK | CHINA | MALAYSIA

MRes Research Project

# Prognostic significance of tissue-resident CD8+ T cells In Breast Cancer: An African Population


Lara Field

14308200

Supervisors

Dr. Judith Ramage

Dr. Ian Spendlove

School of Medicine

University of Nottingham

**CONTENTS:**

Abstract ..... 3
Acknowledgements ..... 4
COVID-19 Impact Statement ..... 5
Table of Contents ..... 6
List of Figures ..... 7
List of Tables ..... 8
Abbreviations ..... 8
References ..... 98

## Abstract

Compared to Caucasian breast cancer patients, African women present with notoriously more aggressive breast cancer tumours, at a younger age, with diagnosis at a later stage. These factors result in a higher mortality rate. Quantification of $CD8^+$ tumour infiltrating lymphocytes has been correlated with better prognosis in breast cancer. More recent evidence has found an effector memory T cell subtype termed tissue-resident memory CD8+ T ($T_{RM}$) cells to exist in the tumour microenvironment. CD8 $T_{RM}$ cells, identified by the expression of CD39, CD69 and CD103, reside in peripheral tissues including tumours, and the presence has been found to promote survival. However, the link between TILs/$T_{RM}$ infiltration has focused on Caucasian breast cancer patients, with the immune contexture of African women's breast cancers being poorly studied, despite the higher mortality rate. It is theorised that CD8 $T_{RM}$ density could serve as a prognostic predictor in African breast cancers too. By using a Breast cancer TMA assembled from Ghanaian women, an African population, the tumour microenvironment particularly the density of CD8+ $T_{RM}$ could be studied. Multiplex immunohistochemistry was successfully optimised to simultaneously detect CD4 and CD8 (T cell markers), CD103 ($T_{RM}$ marker) and CD39 (antigen-specific $T_{RM}$ marker) to identify 13 distinct immune phenotypes. The African breast cancer immune landscape was found to comprise of a diverse range of phenotypes with varying densities in the epithelia, stroma and total tumour. CD8+ $T_{RM}$s ($CD8^+CD103^+CD39^+$) density was found to be low, with the majority of CD8 cells being either single $CD8^+$ or $CD8^+CD39^+$. CD8 $T_{RM}$ density correlated with neoadjuvant chemotherapy, pre-menopausal age, and tumour location, but not patient survival. CD39 is immunosuppressive and $CD39^+$ single cells were the most prevalent phenotype in tumours. It was concluded that CD8 $T_{RM}$ not promoting survival was due to the high density of immune-suppressive cells present in the tumour or $T_{RM}$s being chronically exhausted. Thus, future analysis will investigate the importance of the immune subsets in the breast cancer environment, within the African population. Understanding the immune landscape of African breast cancer tumours will provide insight into future therapeutics.

## Acknowledgements

Firstly, I would like to that my supervisor Dr. Judith Ramage for giving me the opportunity to do such an exciting research project, and for her guidance and support throughout the year, despite the trials and tribulations of a pandemic and multiple lockdowns. I have gained invaluable skills from this experience. I would also like to thank Dr. Eric Gyan for constructing the TMA and patient clinical database, as well as collaborating with me to optimise the technique and obtain the data. This project would not have been possible without his moral support, allowing me to collaborate on analysing samples he collected, and for helpful conversations throughout. Additionally, I would like to thank Dr. Andrew Jackson for helpful discussions, particularly on the technical troubleshooting of the optimisation process, and for encouraging me to persevere. My second supervisor Dr. Ian Spendlove also provided guidance throughout the project, for which I am thankful for. I extend my thanks to all members of the Tumour Immunology group for their help navigating the lab and discussing my project in meetings, especially the PhD student Ilona Sica for patiently teaching me PBMC isolation and flow cytometry techniques.

I'd also like to thank the team at the University of Birmingham for allowing me to use their Quantitative pathology imaging systems, particularly Dr. Kelly Hunter and technician Ana Teodosio for attentively training me to use the technologies and understand the technique, as well as for scanning the slides on the Polaris.

Finally, I would not have been able to do this project without the unwavering support from my family and friends.

## COVID-19 Impact Statement

The entirety of the work for this Masters of Research degree was completed in the period of 1st October 2020 to September 2021, a period which fell during the COVID-19 pandemic. This presented a vast multitude of obstacles including but not limited to; delays to induction to the laboratory institute, COVID exposure-related isolations, government and institutional restrictions limiting face-to-face training, room occupancy and capacity to travel to University of Birmingham to scan slides.

These circumstances cumulated to reduce the capacity of laboratory and non-laboratory work that could be completed for this Masters of Research.

# Table of Contents


Chapter 1: Introduction ..... 10

Chapter 2: Materials and Methods ..... 27

2.1 Study cohort/population ..... 27

2.2 Standard and Multiplex Immunohistochemistry (IHC) Staining ..... 27

2.2.1 Overview of Methods ..... 27

2.2.2 Chromogenic IHC marker optimisation ..... 29

2.2.3 Monoplex Immunofluorescence (IF) Optimisation ..... 30

2.2.4 Spectral Library assembly ..... 31

2.2.5 Multiplex IF optimisation ..... 31

2.3 Immunofluorescence analysis ..... 32

2.4 Statistical Analysis ..... 33

Chapter 3: Results – Multiplex Immunohistochemistry ..... 34

3.1 Chromogenic Immunohistochemistry Optimisation ..... 35

3.1.1 Chromogenic Immunohistochemistry Optimisation of antibodies against CD8 and CD103 ..... 36

3.1.2 Chromogenic Immunohistochemistry Optimisation of antibodies against CD39 and Pan Cytokeratin ..... 38

3.1.3 Chromogenic Immunohistochemistry Optimisation of antibody against CD4 ..... 40

3.2 Monoplex Immunohistochemistry optimisation ..... 42

3.2.1 Allocation of Antibody-Opal Pairings ..... 44

3.2.2. Optimisation of Opal-Antibody conditions as Monoplex ..... 47

3.2.3. Monoplex Optimisation of CK-Opal780 ..... 49

3.2.4. Monoplex Optimisation of CD39-Opal570 ..... 51

3.2.5. Monoplex Optimisation of CD103-Opal690 ..... 53

3.2.6. Monoplex Optimisation of CD4 and CD8 Opal Pairings ..... 56

3.3 Multiplex IHC optimisation ..... 60

3.3.1. Allocation of Staining Order ..... 60

3.3.2. CD39 Opal570 was the main contributor to bleed through during multiplex IHC optimisation ..... 62

3.4 Training inform software for data acquisition ..... 70

3.5. Patient Characteristics ..... 74

3.6. Intra-tumoural phenotype population densities within African Breast Cancers ..... 79

3.7. Patients receiving neoadjuvant chemotherapy had higher $CD8^{+}CD103^{+}CD39^{+}$ epithelial, stromal and total tumour density. ..... 81

3.8. The presence of $CD8^+CD103^+CD39^+$ cells in the tumours of African breast cancer patients do not predict survival ..... 84
Chapter 4: Discussion ..... 87
4.1 The Optimisation Process ..... 87
4.2. Patient Demographics ..... 90
4.3. The immune landscape of African Breast cancer tumours ..... 91
4.4. The correlation of $CD8^+CD103^+CD39^+$ density with clinicopathological features and patient survival ..... 94
4.5. Future directions ..... 96
4.6. Conclusions ..... 97

## List of Figures

Figure 2.1: The Opal Multiplex Immunohistochemistry Principle. ..... 28
Figure 2.2: Flow diagram of the process of multiplex immunohistochemistry. ..... 28
Figure 3.1: Standard Chromogenic IHC staining of CD8 and CD103 ..... 36
Figure 3.2: Standard Chromogenic IHC staining of CD39 and Pan Cytokeratin. ..... 38
Figure 3.3: Standard chromogenic IHC staining of CD4. ..... 40
Figure 3.4: Monoplex Immunofluorescence Optimisation of CK-Opal780. ..... 49
Figure 3.5: Monoplex Immunofluorescence Optimisation of CD39-Opal570. ..... 51
Figure 3.6: Approaches to reduce background signal of CD103-Opal690. ..... 53
Figure 3.7: Monoplex Immunofluorescence Optimisation of CD103-Opal690. ..... 55
Figure 3.8: Monoplex Immunofluorescence Optimisation of antibody against CD4 ..... 56
Figure 3.9: Monoplex Immunofluorescence Optimisation of antibody against CD8 ..... 58
Figure 3.10: Opal570 bleed through to its adjacent channels ..... 65
Figure 3.11: Representative Image of the optimised multiplex IHC conditions established ..... 67
Figure 3.12: Representative Composite Images of the optimised multiplex IHC conditions ..... 68
Figure 3.13: Representative images of each phenotype present in Ghanaian breast cancer tissue after staining with a 5-plex IHC panel ..... 69
Figure 3.14: The Multiplex IHC staining and analysis process. ..... 72
Figure 3.15: Tissue segmentation of Ghanaian breast cancer TMA cores. ..... 73
Figure 3.16. Intra-epithelial phenotype population densities within African Breast Cancer tumours. 80
Figure 3.17: The presence of high numbers of CD8+CD103+CD39+ in the stroma of African breast cancer tumours is not a predictor of survival ..... 84
Figure 3.18: The presence of high numbers of CD8+CD103+CD39+ in the tumour epithelium of African breast cancer tumours is not a predictor of survival ..... 85

Figure 3.19: The presence of high numbers of CD8+CD103+CD39+ in the tumours of African breast cancer patients is not a predictor of survival.....86

## List of Tables

Table 2.1: Primary antibody details and conditions. .....30

Table 2.2: Multiplex IHC optimised conditions. .....32

Table 3.1: Opal Fluorophores Spectral Characteristics .....44

Table 3.2: Criteria for Opal Reporter staining on the Vectra Polaris .....48

Table 3.3: Signal intensities produced by different Opal780 concentrations. .....50

Table 3.4: Signal intensities produced by different Opal570 concentrations .....52

Table 3.5: Signal intensities produced by different Opal690 concentrations. .....55

Table 3.6: CD4 optimisation, paired with Opal620 and Opal520. .....57

Table 3.7: CD8 optimisation, paired with Opal520 and Opal620 .....59

Table 3.8: The Multiplex Optimisation Process of adjusting Opal concentrations to achieve suitable staining, with no bleed through.....63

Table 3.9: Multiplex IHC Panel Optimised for the Ghanaian Breast Cancer TMA .....66

Table 3.10: Summary table of the patient characteristics and their correlation with survival. .....78

Table 3.11: Correlations between the epithelial, stromal and total CD8+CD103+CD39+ T cell densities and different clinicopathological features in breast cancer cases .....83

## Abbreviations

APC – Antigen presenting cell

ATP – Adenosine triphosphate

BSA – Bovine serum albumin

CD - Cluster of differentiation

CTL - Cytotoxic T lymphocyte

CTLA-4 - Cytotoxic T lymphocyte-associated protein 4

CRC - Colorectal cancer

DAB – 3,3’-diaminobenzidine

DAPI - 4’,6-diamidino-2-phenylindole

DC – Dendritic cell

DFS – Disease free survival

DMSO - Dimethyl sulfoxide

ER – Estrogen receptor

HER2 – Human epidermal growth factor receptor 2

IHC – Immunohistochemistry

IL – Interleukin

LAG-3 – Lymphocyte activation gene-3

MHC – Major histocompatibility complex

MWT – Microwave treatment

PD-1 – Programmed death 1

PD-L1 – Programmed death ligand 1

PR – Progesterone receptor

TAM – Tumour associated macrophage

TCR – T-cell receptor

TIL – Tumour infiltrating lymphocyte

Treg – T regulatory cell

TGF-b – Transforming growth factor beta

TMA – Tissue microarray

TME – Tumour microenvironment

TNBC – Triple negative breast cancer

TRM – Tissue-resident memory T cell

TIM3 – T cell immunoglobulin and mucin domain-containing protein 3

# Chapter 1: Introduction

## 1.1. T cells

The T cells of our immune system serve a pivotal role in protection against infectious agents, as well as having a defined role of targeting cancer cells. In recent years, the value of host immune systems in cancer diagnosis and treatment has transformed the oncology field. Of note, tumour infiltrating lymphocyte (TIL) presence, comprising of T and B lymphocytes, has demonstrated prognostic significance in various cancers, such as melanoma (Clemente et al., 1996), colorectal cancer (CRC) (Naito et al., 1998) and breast cancer (Denkert et al., 2010). Furthermore, in both triple negative breast cancer (TNBC) and HER-2 breast cancer, TIL score was defined as a robust biomarker to predict patient response to immunotherapies such as anti-programmed cell death 1 (PD-1) antibodies (Loi et al., 2017, 2019). The growing role of TILs resulted in many immune infiltration classification systems, such as the Immunoscore being developed to classify tumours according to their immune infiltration (Galon & Bruni, 2012). However, immune infiltration scoring is not sufficient to predicting clinical outcome, as the specific immune cell phenotypes responsible need to be defined.

### CD8

T cells can be broadly categorised into T killer cells, expressing CD8, and T helper cells, expressing CD4, both of which are generated during an immune response. CD8 T cells become activated upon antigen stimulation, triggering the release of the cytotoxic

molecules perforin and granzymes, which rapidly kill the targeted cell (Linehan & Delamarre, 2019).

### CD4

$CD4^+$ T helper cells are classified as $T_H1$, $T_H2$, $T_H17$ and $T_{reg}$ (T regulatory cells), and $T_H1$ cells are particularly important in adaptive immunity by secreting IFN-γ and TNF to combat intracellular pathogens and tumour cells, while $T_{reg}$ cells are immunosuppressive (Park et al., 2019).

## T cell activation

T-cells undergo major structural changes when they interact with antigen-presenting cells (APCs), that results in cell cycle progression, activation, and expansion (Reicher & Barda-Saad, 2010). The mechanism through which T-cells are activated is thought to follow the three-signal hypothesis. The hypothesis is as follows; A T-cell that is antigen specific to an APC leads to the first signal. Then the second signal required is a co-stimulatory signal, notably CD28 on naïve T-cells are co-stimulatory receptors, CD28 binds to two co-stimulatory molecules: CD80 and CD86. The third signal has been found to be provided by inflammatory cytokines, IL-12 and type I interferons are thought to be required (Goral, 2011).Without the three signals T-cells do not produce a significant response.

## Memory T cells

Following the initial immune response, memory T cells are produced, where they persist in the tissue, facilitating an enhanced response upon re-exposure to the same antigen (Ahmed

& Gray, 1996). Over twenty years ago, two heterogenous memory T cell populations were identified, defined as the effector memory T ($T_{EM}$) cells, which reside in the peripheral tissues, and the central memory T ($T_{CM}$) cells, which circulate through the secondary lymphoid tissues (Sallusto et al., 1999). An additional population of terminally differentiated effector cells, termed $T_{EMRA}$, also exists, categorised by the re-expression of CD45RA (Sallusto et al, 2004).

## Effector memory

Effector memory cells are identified through their CD45RO+ and CD45RA- isoform expression, they differ from central memory cells because they lack the lymph node homing CCR7, so are CCR7-. Due to their lack of CCR7 they migrate to numerous peripheral sites in the tissue (Sallusto et al., 2004). Effector memory cells have been found to produce more effector cytokines than central memory T-cells though both have an effector functional capacity (Farber et al., 2014).

## Central memory

Central memory cells are less differentiated than effector memory cells, they are CD45RO+ CD45RA-and CCR7+, and have been found to produce more IL-2 than effector memory T-cells and have a higher proliferative capacity (Fearon et al., 2006).

## Terminally differentiated

T-cells differentiate through stages throughout their lifetime. Terminally differentiated effector memory cells (TEMRA) are more differentiated than central memory and effector memory cells. TEMRA memory cells include pre-effector 1 cells, pre-effector 2 cells and end

stage non-proliferative effector cells. TEMRA cells have been found to re-express CD45RA, which would usually be associated with naïve T-cells (Tian et al., 2017).

## $T_{RM}$ Cells

Speculation that some $T_{EM}$ cells may permanently reside in peripheral tissues to effectively perform immunosurveillance drove investigations within mouse models to pinpoint distribution of T cells within multiple tissue sites. As in most Immunology concepts, in vivo mouse model studies paved the path of discovery of a new tissue-resident T cell subtype (Szabo et al., 2019). More recently, a newly defined memory T cell population, the tissue-resident memory T ($T_{RM}$) cells have proven to be a superior cancer survival marker, compared to total TIL quantification. Initially, this memory T cell subset were found to remain resident in the skin, sensory ganglia and female reproductive tract upon clearance of a herpes simplex virus (HSV) infection, and that these cells could persist without local antigen presentation and were superiorly protective compared to their $T_{CM}$ cohort (Gebhardt et al., 2009; Mackay et al., 2012). These initial studies defined $T_{RM}$ cells to provide localised, tissue-intrinsic immunosurveillance, countering the initial theory that T cells continuously recirculate to survey tissues in transit. While the literature best outlines tissue residency for $CD8^+$ T cells, $CD4^+$ $T_{RM}$ have been identified. Though most $CD4^+$ memory T cells recirculate, $CD4^+$ $T_{RM}$ populations exist in various tissues, including the skin (Glennie et al., 2015), the lungs following infection (Teijaro et al., 2011) and in lung cancer tissue (Oja et al., 2018). CD4 and CD8 $T_{RM}$ cells were found to localise in different regions; $CD8^+$ $T_{RM}$ were found in the epithelium and $CD4^+$ $T_{RM}$ reside in the tissue parenchyma for both the skin and female reproductive tract (Iijima & Iwasaki, 2014).

## $T_{RM}$ Cell Features

The hallmark $T_{RM}$ cell feature is their lack of migration and recirculation. The existence of such populations has been proven in diverse tissue types via parabiosis, organ transplantation and antibody-mediated T cell depletion studies (Mueller & Mackay, 2016). Traditionally, the co-expression of two distinct cell surface markers have been defined to delineate $T_{RM}$ cells, CD69 and CD103. CD69 was originally established as an early activation marker, and serves as an indicator of tissue retention by its functional ability to antagonise the function of the S1PR1 tissue egress facilitator to promote early retention in peripheral tissues (Cyster & Schwab, 2012; Mackay et al., 2015). Based on its presence on a large proportion of CD4 and CD8 $T_{RM}$ cells in both mice and humans, CD69 is generally recognised as the canonical marker for $T_{RM}$ cells, identified by both functional and transcriptional studies. Indeed, CD69 is an early activation marker for most effector T cells to enable lymph node retention, but in $T_{RM}$ cells its expression is constitutive and not accompanied by other activation marker expression (Cepek et al., 1994).

The second cell surface marker is CD103, the $\alpha_E$ subunit of the $\alpha_E\beta_7$ integrin complex, which binds to E-cadherin on epithelial tissues to promote peripheral maintenance (MacKay et al., 2013). CD103 expression on $T_{RM}$ cells has been confirmed in various epithelial tissues, such as the skin epidermis (Masopust et al., 2010), but mice parabiosis and antibody depletion studies have identified $T_{RM}$ cells lacking CD103 expression in several tissues, including the female reproductive tract (Steinert et al., 2015). The inconsistent tissue type expression of CD103 is likely due to the $\alpha_E\beta_7$-E-cadherin interaction anchoring the CD103+ $T_{RM}$ cells within mucosal tissues where E-cadherin expression is enriched, inflating the expression of this cell surface phenotype compared to tissues with basal E-cadherin expression. CD103 expression

is also seen on the immunosuppressive Treg phenotype (CCR4+CTLA-4hi FOXP3+ CD103+CD25hi) in colon adenocarcinomas (Svensson et al., 2012). As such, one must heavily account for the phenotypic heterogeneity of the $T_{RM}$ cell subset when selecting a cell surface marker in experimentation. Still, *ITGAE* (CD103) transcriptional upregulation was categorised as a core signature marker for both CD4 and CD8 $T_{RM}$ cells, when comparing CD69+ and CD69– populations (Kumar et al., 2017). CD49a (integrin $\alpha_1$), which binds to the collagen-specific CD29 (integrin $\beta_1$), is also expressed by $T_{RM}$ cells, particularly in lung and skin populations (Cheuk et al., 2017; Purwar et al., 2011). This expression infers that CD49a may aid $T_{RM}$ adhesion near basement membranes of the epithelium.

## $T_{RM}$ Cell Development and Maintenance

The precise mechanism of how $T_{RM}$ cells differentiate remains to be elucidated, though it is likely that the generative process differs depending on the tissue type, and its disease state. Early on in T cell development, the fate of precursors to become memory T cells is determined by their CD127 expression and lack of killer cell lectin-like receptor subfamily G member 1 (KLRG1), distinguishing them from short-lived effector T cells ($KLRG1^+CD127^-$ phenotype) (Kaech et al., 2002). Despite initial studies conveying $T_{RM}$ cells originate from $KLRG1^-$ precursors (MacKay et al., 2013), it was recently found that the $CD8^+$ T cells which could downregulate KLRG1 can differentiate into memory cells including $T_{RM}$ cells, and these cells had a higher cytotoxic potential than those differentiating from $KLRG1^-$ precursors (Herndler-Brandstetter et al., 2018). Taken together, $T_{RM}$ precursor origin appears to be phenotypically diverse.

Upon triggering an immune response to infection, recently activated effector T cells, which have a heterogenous potential to become memory thus $T_{RM}$ cells, are primed to enter peripheral tissues and aid pathogen ablation (Kaech et al., 2002). Additional to KLRG1 expression, transcriptional signature studies in mouse and human $T_{RM}$ cells implicate an increasing library of transcription factors that promote their development. This includes the elevated expression of *Hobit* (the residency-defining transcription factor) with Blimp1 (Mackay et al., 2016) as well as Runx3 (which also promotes long term maintenance) (Milner et al., 2017), aryl hydrocarbon receptor (ARH) and Notch signalling (Kumar et al., 2017). Cytokines within the tissue microenvironment extrinsically probe effector T cells to become $T_{RM}$. Within the literature, TGFβ, IL-7, IL-15, and TNF, among others, have been identified to regulate $T_{RM}$ cells, though their relative importance and roles continue to be debated (Adachi et al., 2015; MacKay et al., 2013; Zhang & Bevan, 2013). Downregulation of Kruppel-like factor 2 (KLF2) which targets the S1PR1 gene, thus reduces tissue egress also appears important (Skon et al., 2013). It is important to note that most $T_{RM}$ development and maintenance knowledge derives from the viral $T_{RM}$ cell context. However, TGFβ is found in various tumours in high levels, including melanoma and breast cancer (E. Goldberg & L. Schwertfeger, 2010; Edwards et al., 2018), and was found to promote $T_{RM}$ development by stimulating CD103 expression (Edwards et al., 2018; El-Asady et al., 2005), as well as lung tumour TIL accumulation (Boutet et al., 2016). In the same melanoma study, IL-15 expression positively correlated with $T_{RM}$ cell accumulation (Edwards et al., 2018).

## Regulation and Maintenance of $T_{RM}$/Chemokines and $T_{RM}$

Establishment of $T_{RM}$ populations would need sufficient T cell expansion, as well as chemokine and cytokine priming. Cytokines play a key role in immune cell migration and cell function, including $T_{RM}$ cells (S. L. Park et al., 2019). $T_{RM}$ cells have been found to express CXCR3, CCR5 and CCR6 receptors, and also produce the chemokines CCL3, CCL4 and CCL5 (Hombrink et al., 2016). In fact, CXCR6 is a core signature $T_{RM}$ marker (Kumar et al., 2017) and a study found that its ligand CXCL16 promotes $T_{RM}$ establishment in the liver (Tse et al., 2014; Zaid et al., 2017). Mouse model studies confirmed the significance of CXCR3 expression, also linking CXCR3 and CXCR10 to $T_{RM}$ formation and maintenance (MacKay et al., 2013; Zaid et al., 2017). CXCL9 and 10 (whose receptor is CXCR3) mediate epithelial entry to mucosal surfaces infected with HSV-2, further conveying the importance of CXCR3 and its ligands in $T_{RM}$ migration (Shin & Iwasaki, 2012). On the other hand, lack of CCR7 expression, which normally promotes T cell egress from tissue, enhances $T_{RM}$ cell development (Debes et al., 2005). The precise mechanisms regulating $T_{RM}$ migration and maintenance remain to be categorised, but knowing which chemokines direct them to tissues may be of interest in harnessing the immune system to fight cancers.

## $T_{RM}$ cell function

The genetic transcript reveals $T_{RM}$ cells, including breast cancer-derived $T_{RM}$ cells, express elevated levels of the cytotoxicity-associated genes, GZMB and PRF-1, as well as pro-inflammatory cytokines, such as IFN-γ (Savas et al., 2018). From this, the potential functionality of $T_{RM}$ cells as critical immune sentinels either directly by lysis or indirectly by recruiting immune effector cells began. $T_{RM}$ cells were found to be generated by and protect against both viral and bacterial challenge, such as skin and sensory ganglia HSV, oral *Listeria*

*monocytogenes*, and even the immune-privileged brain vesicular stomatitis virus (VSV)(Gebhardt et al., 2009; Steinbach et al., 2016). Specifically for $CD4^+$ $T_{RM}$, evidence for a protective role in diverse anatomical sites continues to grow (Szabo et al., 2019). For example, in the female reproductive tract of mice models, $CD4^+$ $T_{RM}$ were found to crucially protect against HSV challenge (Iijima & Iwasaki, 2014), and in humans a HSV-specific $CD4^+$ $T_{RM}$ population was identified, conveying the role of these cells in viral infection (Posavad et al., 2017). Cytotoxic killing via GZMB and PRF-1 release may be facilitated by the CD103-E-cadherin interaction stably anchoring the $T_{RM}$ cell to its target cell (le Floc'h et al., 2011).

Aside from their direct cytotoxic function via the secretion of GZMB and PRF-1, $T_{RM}$ cells rapidly produce various cytokines, such as IFN-γ, IL-2 and TNF (Schenkel et al., 2014). During initial $T_{RM}$ cell explorations, Schenkel et al demonstrated CD8 $T_{RM}$ cells in a murine model elicited both innate and adaptive responses to *Vaccinia Virus* via these cytokine secretions (Schenkel et al., 2014). In one 2015 study, IFN-γ secretion by $T_{RM}$ cells ensued without cytotoxic activity in response to cognate antigen, and IFN-γ-secreting $T_{RM}$ provided superior viral protection compared to $T_{RM}$ derived from IFN-γ-deficient mice (McMaster et al., 2015). Combined, these studies show $T_{RM}$ cells to function in both a direct killing fashion and by propagating the body's immune response via cytokine signalling. But of course, the degree to which these mechanisms contribute to pathogenic immunity is heterogenous. More recently, the potential for the $T_{RM}$ to target cancer cells has been theorised.

## Breast Cancer

Breast cancer is the second most commonly diagnosed cancer worldwide, accounting for 11.6% of all cancer diagnoses, and in females alone, it is by far the cancer with the highest incidence and mortality, according to the GLOBOCAN 2018 study (Bray et al., 2018). It is a

highly heterogenous disease, categorised into subtypes based on their expression of HER2, estrogen receptor (ER), progesterone receptor (PR) and the level of the proliferation marker protein Ki-67. Luminal A tumours are ER and/or PR positive, HER2 negative, with low Ki-67. Luminal B tumours are ER and/or PR positive, HER2 positive/negative, with high Ki-67. TNBC or basal-like tumours are devoid of HER2, ER or PR expression (Schnitt, 2010).

## Breast Cancer in the African population

Breast cancer in African women is a highly understudied area. In sub-Saharan Africa, lat few population-based cancer registries, so the burden of breast cancer is assessed through hospital studies and the GLOBOCAN database. GLOBOCAN found in their 2020 report the incidence to be 38.3 per 100,000, the most common cancer among Ghanaian women, and a mortality rate of 18.1 per 100,000 (GLOBOCAN, 2020). This high mortality is largely due to socioeconomic factors leading to delayed diagnosis, with 49.5% of Ghanaian patients presenting at tumour grade 3 (Thomas et al, 2017).

African patients present most commonly with the highly aggressive TNBC, with this subtype accounting for 26% of African American breast cancer cases compared to just 16% of white Americans (Stark et al., 2010). This TNBC proportion is more pronounced in Ghanaian women, where 58.3% were of this subtype (Der et al., 2015).

## Immune landscape

Immunosurveillance is the process by which the body's immune system monitors, recognises and reacts to aberrant cells such as tumour cells. Though the concept of Cancer Immunosurveillance was originally conceived over 50 years ago, it was not until the last decade that the theory was validated experimentally. The tumour microenvironment includes a diverse range of different immune cells which interact with one another to create

a response favouring tumour killing, or alternatively create an environment which is immunosuppressive. Anti-tumour immune cells include cytotoxic T cells, helper T cells, natural killer (NK) cells and dendritic cells (DCs) (Bruni et al., 2020). In contrast, Treg cells, myeloid derived suppressor cells (MDSCs) and tumour-associated macrophages (TAMs) function to suppress the anti-tumour immune response to favour tumour progression and metastasis (Bruni et al., 2020). Tumours have evolved to evade and suppress the host immune system by promoting these suppressive immune cells.

## T Cells in Cancer

While both the innate and adaptive responses are involved in immunosurveillance, $CD8^+$ cytotoxic T killer cells are of particular importance via their ability to directly engage with and kill cancer cells.

Logically, the capability of $CD8^+$ T cells to perform this immunosurveillance function depends on their ability to access the tumour microenvironment, and only a small subset are able to do so (S. L. Park et al., 2019). For an individual to elicit an anti-cancer response, a sequence of events, collectively termed the Cancer-Immunity cycle needs to take place. In short, mutations created during carcinogenesis generate neoantigens which, in the right microenvironment, are captured and expressed on dendritic cell MHCs to activate and mobilise T cells (some of which further differentiate into $T_{RM}$ cells) to the tumour bed. Upon infiltrating the tumour, activated $CD8^+$ T cells kill cancer cells via their TCR interaction with the neoantigen (Chen & Mellman, 2013). As expected, many factors prevent the Cancer-Immunity cycle from functioning optimally in cancer patients, such as cancer antigens not

being detected, TME factors suppressing immunity and elimination of neoantigen-expressing cancer cells (termed immunoediting) (Motz & Coukos, 2013).

## TRM in Cancer

CD39 has been found to be expressed on $T_{RM}$ cells in the context of cancer (Duhen et al., 2018). CD39 is an integral membrane protein which, in tandem with CD73, catalyses the hydrolysis of ATP, consequently producing the immunosuppressive molecule adenosine (Maliszewski et al., 1994). Critically, CD4 and CD8 T cells express CD39 upon TCR activation (Raczkowski et al., 2018), for example by a cancer neoantigen, therefore CD39 expression can effectively distinguish tumour-specific T cells from bystander T cells (Duhen et al., 2018). The Duhen group identified a CD8 TIL group expressing both CD103 and CD39 to display a tissue-resident phenotype and ability to kill autologous cancer cells in six solid tumour types, including colorectal cancer (Duhen et al., 2018). Cell surface marker upregulation differing between tissues suggests $T_{RM}$ cells alter their expression depending on their specific microenvironment.

Aside from the CD marker expression distinguishing the $T_{RM}$ phenotype, upregulation of immune checkpoint (IC) inhibitors, including PD-1, CTLA-4, LAG-3, and TIM-3 have elevated expression in $T_{RM}$ cells derived from numerous solid tumours (Duhen et al., 2018). For example, upregulated IC inhibitor expression was identified in T cells in melanoma (Boddupalli et al., 2016), lung cancer (Clarke et al., 2019), and breast cancer (Savas et al., 2018). While this is traditionally a feature of T cell exhaustion ($T_{ex}$ cells) (Wherry, 2011), functional studies within both the viral (S. L. Park et al., 2018) and tumour context, such as lung cancer (Ganesan et al., 2017) show $T_{RM}$ cells displaying increased functionality. In fact,

exhaustion molecule expression mobilises $T_{RM}$ cells as prime IC inhibitor therapy targets, fuelling the research of these newly defined cells in the Cancer Immunology field.

Initial indications that $T_{RM}$ cells have anticancer effects stemmed from studies correlating $CD8^+$ tumour-infiltrating lymphocytes (TILs) with prognosis in cancers, such as melanoma (Haanen et al., 2006). In light of CD103 and CD69 cell markers delineating $T_{RM}$ cells, increasing evidence of their presence in tumours and correlation with improved patient outcomes has arisen. For example, in melanoma patients, CD103+CD8+ $T_{RM}$ better predicted improved survival than total CD8+ TIL presence (Edwards et al., 2018). Parallel evidence was also recorded in lung cancer patients, where CD103+ $T_{RM}$ cells predicted survival and displayed greater cytotoxic potential than $CD103^-$ T cells (Djenidi et al., 2015; Ganesan et al., 2017). In CRC, the prognostic potential of CD8 and CD103 markers, thus $T_{RM}$ phenotype has been reported. The $CD8^+$ T cell infiltration, $CD8^+CD103^+$ T cell quantity, and a higher $CD8^+CD103^+$ T cell:Total $CD8^+$ T cell ratio all correlated with improved OS. $CD8^+CD103^+$ T cell numbers also inversely correlated with both distant metastasis and age status (W. Hu et al., 2019). More recently, unpublished research from the Ramage group analysed the colorectal cancer immune landscape using multiplex immunohistochemistry (IHC), discovering that the density of triple positive cells ($CD8^+CD103^+CD39^+$), aligning with the phenotype of activated $T_{RM}$ cells, was independently prognostically significant.

For $CD4^+$ $T_{RM}$, a number of different phenotypes have been identified. Sarrabayrouse et al identified the presence of CD4+CD8αβ+CD103+ αβ T cells capable of killing autologous tumour cells in CRC samples (Sarrabayrouse et al., 2011), while another group isolated inducible Tregs ($CD4^+CD103^+LAP^+FoxP3^-$ IL-$10^+$) from CRC patients, and these cells were

significantly more immunosuppressive compared to the traditionally categorised FoxP3$^{+}$ Tregs (Scurr et al., 2014).

## T cells in Breast cancer

Despite breast cancer historically not being viewed as an immunogenic disease, evidence now shows immune infiltration to be an important aspect, particularly in TNBC and HER2+ tumours where 20% and 16%, respectively, are 50% infiltrated with TILs (Stanton & Disis, 2016). In all breast cancer types, TIL infiltration improves neoadjuvant chemotherapy response, a significant correlation with survival is only seen in the TNBC and HER2+ subtypes (Loi, 2013; Salgado et al., 2015).

## TRM in breast cancer

The superior predictive ability of CD103 and CD8 co-expression in TNBC than either marker alone was initially demonstrated using standard IHC on a TMA of 424 patients. CD103 expression was associated, not only with patient outcome, but also clinical-pathological features such as tumour grade, size and receptor expression (Wang et al., 2016). A 2020 study built upon Wang et al (2016) findings, using IHC to identify CD103, but not CD8, as a prognostic marker for OS and DFS (Park et al., 2020). The Savas group isolated and performed single-cell RNA sequencing (scRNA-seq) on breast cancer-derived T cells, where a $T_{RM}$ population was identified, namely high CD103 expression, immune checkpoint inhibitors, and low expression of tissue egress factors (Savas et al., 2018). Importantly, the expression of CD69 was not $T_{RM}$-specific, but was expressed on most TILs sequenced. The

'METABRIC' consortium data was also analysed, finding that in primary TNBC patients, the $T_{RM}$ gene signature predicted improved overall survival (OS) and relapse-free survival (RFS) better than CD8A expression alone. This $T_{RM}$-survival correlation is unique to TNBC, providing an explanation as to why TNBC patients have the highest response rates to anti-PD1 therapies, as $T_{RM}$ express PD1 so can mobilised by this immunotherapy to kill tumour cells (Savas et al., 2018).

In 2019, a group used quantitative immunofluorescence to show $CD103^{+}CD8^{+}$ $T_{RM}$ cells localised to, and were the major TIL type in breast cancer islands, and that most of this population also expressed CD69 (Egelston et al., 2019). Samples were divided according to relapse occurrence, with the relapse-free group showing a significantly greater $T_{RM}$ density in both the cancer islands and stroma. Consequently, a correlation between $T_{RM}$ cancer island density and RFS was seen. Furthermore, quantitative spatial analysis found that stromal $T_{RM}$ density in close proximity (0–25 μm) to cancer islands significantly correlated with RFS (Egelston et al., 2019). This study builds upon findings from the Savas group, strengthening the $T_{RM}$-prognosis relationship (Savas et al., 2018). Together, these data provide a strong argument for $CD8^{+}$ $T_{RM}$ cells as a prognostic marker, but there is a clear gap in the literature for investigating other $T_{RM}$ markers such as CD39 as a marker of antigen-specific $T_{RM}$, and the role of $CD4^{+}$ $T_{RM}$ cells in breast cancer immunosurveillance.

To this end, the immune landscape of breast cancer tumours, and the relation of $T_{RM}$ subtypes to patient prognosis have only begun to be defined, using both mouse and human models. Though, taken together, effector CD8 T cells have an important role in anti-tumour

immunity. $T_{RM}$ studies outlined in this review highlight the anti-cancer abilities of tumour-specific $T_{RM}$ cells, particularly CD8 $T_{RM}$.

## Aims and Methodology

Subsequent to current findings, this study intends to demonstrate the localisation of CD4 and CD8 $T_{RM}$ subsets to solid tumours and investigate their role in anti-cancer immunity thus how $T_{RM}$ density within tumours affects patient prognosis. In this thesis, it is hypothesised that together the markers CD8, CD103 and CD39 will identify activated, tumour-specific $T_{RM}$ cells, and that the density of this population in African Breast Cancer tumours will correlate with overall survival (OS) in these patients.

To investigate the role of these antigen-specific $T_{RM}$, multiplex IHC will be used to analyse the immune infiltration of cores from a cohort of Ghanaian breast cancer patients assembled onto TMAs. A critical aim of this project is to optimise a 5-colour multiplex IHC antibody panel, for the markers CD4, CD8, CD39, CD103 and CK.

The second main aim of the project is to phenotypically identify the types of immune cells infiltrating the tumours using the expression of 4 immune markers, thus inferring their effect on patient survival. CK will be used to distinguish the epithelia from the stroma within the tumours, to allow infiltration in each region to be individually assessed. The markers CD4 and CD8 delineate the T helper and T killer cell subtypes, respectively, while CD39, and CD103 have been highlighted to be canonical markers of $T_{RM}$ cells. The presence of $T_{RM}$ phenotypes will be correlated with clinical parameters to demonstrate their ability as a prognostic marker.

Through multiplex IHC, CD39+ (antigen-specific) $T_{RM}$ presence in tumours should exhibit more anti-cancer effects than CD39- $T_{RM}$ and therefore associate more strongly with survival. We aim to pinpoint the optimal marker combination for prognostic prediction to be CD8+CD103+CD39+, as previously shown in CRC, and hypothesise these marker combinations to be superior to CD8+ or CD8+CD103+.

# Chapter 2: Materials and Methods

## 2.1 Study cohort/population

Breast cancer tumour samples from patients who attended the Cape Coast Teaching Hospital, Ghana were collected for this study. 142 patients, including patients who received surgery followed by chemotherapy, or neoadjuvant chemotherapy, surgery and a further chemotherapy regime were included. Stage 4 patients were excluded. A formalin fixed paraffin embedded (FFPE) tissue microarray (TMA) was constructed with 2 peripheral cores and 1 central tumour core per patient, with cores being 1mm diameter and 4µm thickness. Patient clinicopathological data e.g. age, stage (TNM system, (Rosen & Sapra, 2021)), grade (UK grading system), histological type, hormonal status, survival time following surgery were obtained. TMA construction and clinical data gathering were carried out by Dr. Eric Gyan.

## 2.2 Standard and Multiplex Immunohistochemistry (IHC) Staining

### 2.2.1 Overview of Methods

Multiplex IHC is a novel technique which has revolutionised chromogenic IHC by enabling the simultaneous detection of up to 8 biomarkers in one protocol, even if such markers co-express (Stack et al., 2014). Opal multiplex IHC uses tyramide signal amplification (TSA), where opal fluorophores are conjugated to tyramide molecules. Similar to chromogenic IHC, antigen-bound primary antibodies are targeted by secondary antibodies liked to horse radish peroxidase (HRP). HRP enzymatically amplifies the Opal-TSA signal at the enzyme site as well as triggering it to bind to the secondary and primary antibodies, and the biomarker itself (as seen in **Figure 2.1**). Microwave treatment (MWT) can then be used to strip the antibodies, leaving Opal-TSA bound to the biomarker. Another primary and secondary

antibody can then be incubated with the tissue, with the reporter being another Opal-TSA, as shown in **Figure 2.2.**

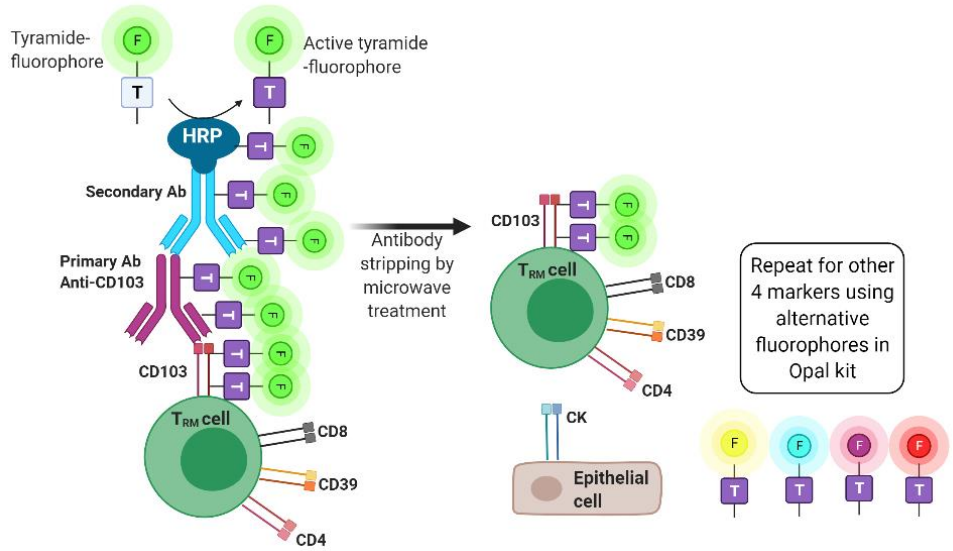



Figure 2.1: The Opal Multiplex Immunohistochemistry Principle. The biomarker is recognised by the primary antibody, bound to by HRP-conjugated secondary antibody, which activates tyramide within the Opal-TSA complex. Opal-TSA signal is amplified through the antibody complex down to the antigen itself. Microwave treatment strips the antibodies, leaving Opal-TSA bound. The process is repeated for each antigen, using a different primary antibody and Opal fluorophore. Figure assembled using Biorender.com.

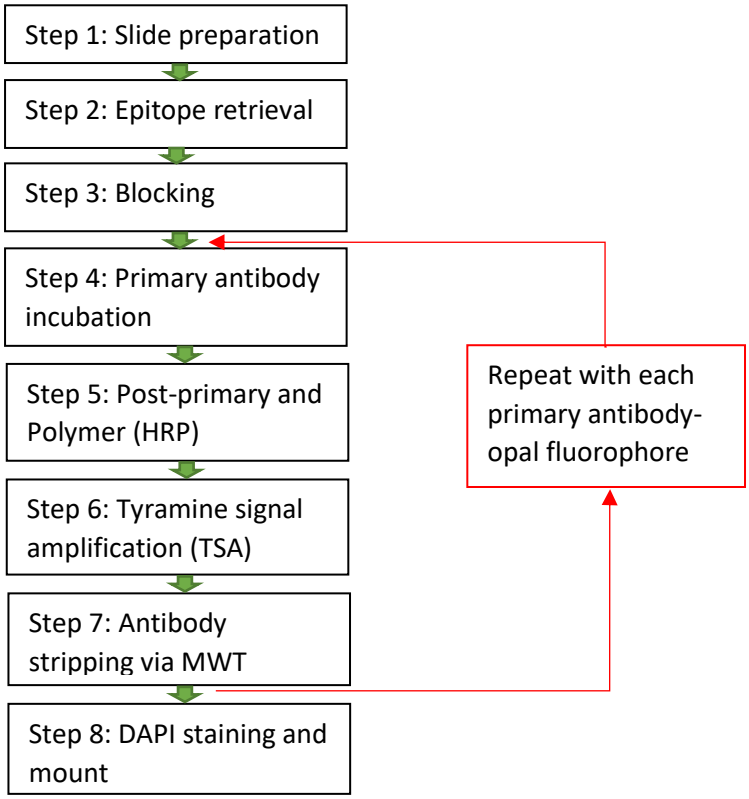



Figure 2.2: Flow diagram of the process of multiplex immunohistochemistry.

### 2.2.2 Chromogenic Immunohistochemistry marker optimisation

For the chromogenic IHC, staining was performed manually using the Novolink Polymer Detection kit (Leica Biosystems, catalog code: RE7150-K) following manufacturer's instructions, with antigen binding detected via horse-radish peroxidase (HRP) conversion of the diaminobenzidine (DAB), with haematoxylin counterstaining. Primary antibodies (**Table 2.1**) were diluted in Blocking Diluent (Akoya Biosciences).

Prior to IHC staining, all TMA slides were baked at 60°C for 10 minutes, then manually dewaxed and rehydrated by 2 times 5 minutes xylene, 3 times 2 minutes IMS and 5 minutes dH2O. Antigen retrieval was performed by microwave treatment (MWT), using the Whirlpool JT366 SL microwave oven in citrate buffer (pH 6) or AR6/AR9 buffer (Akoya Biosciences) for 90 seconds at 1000W and 20 minutes at 160W. Cooling methods included leaving at RT for 15 minutes or slow flooding with dH2O for 5 minutes.

Following first antigen retrieval, slide TMA core area were outlined with hydrophobic/PAP pen (ab2601, Abcam) and washed 2 x 5 minutes with TBST, prepared by either dissolving 1 TBST tablet (EMD Millipore, 524753-1EA) in 500mL dH2O or 1XTBS with 0.1% Tween-20, prepared with 10% Tween-20 aqueous solution (Thermofisher, 37520). Protein block and peroxidase block were applied for 5 minutes, washing in between (from this point washing refers to 3 times 5 minutes TBST, unless stated otherwise, and is performed between every reagent incubation. Primary antibody incubation (conditions), post-primary and polymer (both 30-minute incubations), followed by DAB (DAB chromogen diluted 1:20 in DAB substrate buffer) development for 5 minutes, and haemotoxylin counterstaining for 6 minutes. Slides were dehydrated and cleared by 3 times 2 minutes IMS, 2 times 5 minutes xylene, and mounted onto coverslips with DPX Mountant.

| Antibody | Clone | Species | Source | Concentration | Antigen Retrieval | Incubation period |
|---|---|---|---|---|---|---|
| CD8 | 4B11 | Mouse | Leica Biosystems | 1:200 | AR9 | 1 hour room temperature |
| CD4 | 368 | Mouse | Leica Biosystems | 1:50 | AR9 | 1 hour room temperature |
| CD103 | Ab129202 | Rabbit | Abcam | 1:250 | AR6 | 1 hour room temperature |
| CD39 | EPR20627 | Rabbit | Abcam | 1:100 | AR9 | Overnight at 4°C |
| Pan Cytokeratin | Ab27988 | Mouse | Abcam | 1:200 | AR9 | 1 hour room temperature |

*Table 2.1: Primary antibody details and conditions.* Primary antibody concentration, incubation conditions and antigen retrieval methods were determined by optimisation as detailed in Results 3.1.1.

### 2.2.3 Monoplex Immunofluorescence Optimisation

Using the primary antibody concentrations established in chromogenic IHC (visual interpretation of imaged slides), single immunofluorescence (IF) antibody optimisation was performed. Staining was performed manually using the blocks, post-primary and polymer reagents from the Novolink Polymer detection kit, and AR buffers, Blocking/Diluent, 1Xplus amplification diluent, and the fluorophores 4', 6-diamdino-2phenylindole (DAPI), Opal Polaris 520, Opal Polaris 570 and Opal Polaris 690 from the Opal 4 colour manual kit (catalog number: NEL810001KT). The additional fluorophore Opal Polaris 620 and the individual tyramide signal amplification fluorophore Opal Polaris 780 were incorporated into the multiplex. Antibody pairings to opal fluorophores were evaluated by considering opal brightness, marker abundance, marker co-expression and pairings previously used (within laboratory group or in literature). Chromogenic IHC optimised primary antibody conditions and a starting opal concentration of 1:100 in 1xplus amplification diluent were used. All opal reagents were applied and incubated for 10 minutes, covered from light, with the exception being Opal Polaris 780, requiring TSA-DIG 1:100 in 1xplus amplification diluent for 10

minutes, MWT 90 seconds at jet and 15 minutes at 160W in AR9 buffer, and a 1-hour incubation with Opal 780 (1:25-1:150 dilution in Blocking/Antibody diluent). Opal concentrations, antigen retrieval method and blocking conditions were adjusted accordingly based on staining analysis in inform software.

Once multiplex optimisation was achieved, monoplex slides were reproduced with the relevant number of antigen retrievals it would be exposed to, to assess staining consistency.

### 2.2.4 Spectral Library assembly

Alongside single IF antibody optimisation, a spectral library was created and assembled in the inform (Akoya biosciences) software for the unmixing and signal extraction of the multiplex images. Using CD8 (1:200, AR9), which reliably stains a high number of positive cells, was used in combination with all 5 opal fluorophores under the same conditions, excluding DAPI. A DAPI only library slide (no primary or opal staining) and an autofluorescence stain (no staining, but same conditions as library slides) were also created.

### 2.2.5 Multiplex Immunofluorescence optimisation

Once all antibody and opal pairs were optimised, they were combined into one multiplex protocol and their order and opal concentrations were further optimised to eliminate signal bleed through between adjacent channels. Specifically for multiplex, successive antigen stripping were by MWT 90 seconds at 1000W and 15 minutes at 160W in AR9 buffer. At this stage, slides could be left in post-cooled AR9 buffer at RT overnight if the experiment needed to be paused.

| Antibody | Position | Antigen retrieval | Fluorophore | Concentration |
|---|---|---|---|---|
| | | | Spectral DAPI | |
| CD4 | 3 | AR9 | Opal 520 | 1:175 |
| CD39 | 2 | AR9 | Opal 570 | 1:200 |
| CD8 | 4 | AR9 | Opal 620 | 1:100 |
| CD103 | 1 | AR6 | Opal 690 | 1:175 |
| Pan Cytokeratin | 5 | AR9 | Opal 780 | 1:150 |

*Table 2.2: Multiplex IHC optimised conditions.* Primary antibodies, Opal-TSA pairing and Opal concentration are displayed along with the antigen retrieval method and position placed in the multiplex panel.

## 2.3 Immunofluorescence analysis

Singleplex IHC images were taken using the Nikon E600 microscope.

Multiplex IHC optimisation slides were imaged using the Mantra (Akoya Biosciences) at 20X and whole slide set by the Vectra/Polaris (Akoya Biosciences), both situated at the University of Birmingham. The magnification of the further magnified images in the thesis were obtained digitally from the original 20X images. During monoplex and multiplex optimisation, opal-antibody pairings, signal intensity and bleed through of signal between channels were continuously assessed in inForm version 2.5.0 software by visual assessment and per-pixel staining intensity (taking the average and range of >80 positive cells across >8 representative cores for each condition). Target intensity ranges (listed in **Table 3.2**) and a signal to background ratio of 10:1 was aimed for.

Polaris whole slide scans were viewed in Phenochart to select representative cores to be imported into inform for creating the training project. Inform software training included tissue segmentation (specifically into epithelium or stroma), cell segmentation and cell phenotyping using the antibody markers labelled with opal fluorophores. Training algorithm

was then applied entire TMA and the statistical program R was used to translate data into excel sheets. Dr. Eric Gyan provided help throughout the optimisation, staining, imaging and analysis performed in this project.

## 2.4 Statistical Analysis

Cell densities generated by the immunofluorescence analysis were matched to patient cores, average densities were calculated for patients with multiple cores stained and matched to clinical data within SPSS. Epithelial, stromal and total tumour cell densities were classified as either high or low based on X-tile-generated threshold values giving a significant p value. Kaplan-Meier survival plots were generated to give statistical significance based on Log Rank Mantel-Cox to assess the survival effect of cell density within the tumour regions. Cell densities were also correlated with different clinico-pathological parameters including age, breast cancer subtype, grade and stage using a Chi-squared test.

# Chapter 3: Results – Multiplex Immunohistochemistry

Using the Opal TSA reagents to perform multiplex IHC, up to 6 immune biomarkers can be simultaneously detected on a single tissue of interest or TMA series. The technique builds upon single chromogenic IHC; Following antigen retrieval, mouse IgG primary antibodies are applied onto tissue to detect antigens such as CD8, followed by the post primary Rabbit anti-mouse IgG being applied to detect the primary antibody. The post primary is then recognised by the polymer (anti-rabbit Poly-HRP-IgG). While chromogenic IHC would then visualise these tissue-bound antibodies using DAB chromogen conversion, multiplex IHC uses Opal fluorophores to visualise antibody staining.

The end goal of this study was to fully optimise a 6-colour multiplex IHC protocol (including DAPI for cell nuclei visualisation) on a Ghanaian Breast Cancer TMA series. Unfortunately, offcuts of this TMA were limited, thus initial optimisation and imaging used offcut sections of a Nottingham Breast Cancer TMA FFPE block. Optimal staining conditions vary greatly between tissue types, hence why breast cancer offcuts were chosen for this development stage. Of course, validation of the Nottingham TMA staining conditions on the Ghanaian series was needed later on in the Optimisation process.

For this project, CD8, CD39, CD103, CD4 and Pan Cytokeratin (AE1/3) antibodies are being studied. Each primary antibody concentration was titrated according to manufacturer's guidelines and previous work within the lab that optimised primary antibody conditions for CD8, CD39 and CD103.

## 3.1 Chromogenic Immunohistochemistry Optimisation

Chromogenic IHC is the first step in the Multiplex IHC optimisation process, where the optimal primary antibody concentration can be determined. The primary antibody forms the surface on which the post primary antibody, polymer and Opal detection markers will bind. Therefore, it is important to identify the chromogenic IHC conditions which produce strong, specific staining for each primary antibody, as any non-specific binding at this stage would be amplified downstream creating inaccurate signal. Firstly, the suitable antigen retrieval (AR) buffer and heat-induced epitope retrieval (HIER) method are determined. Chromogenic IHC AR buffers include the pH 6.0 citrate buffer, and the pH 9.0 EDTA buffer, with the higher pH buffer being considered harsher and producing stronger staining. HIER methods include microwave treatment (heating at full power to boiling point then 20% power to gently heat over a 15-minute period), and the water bath method (heating below boiling point across a longer 20-minute period).

Secondly, the primary antibody concentration needs to be titrated to pinpoint the dilution that generates the highest quality staining, as well as the incubation time which can range from 30 minutes up to overnight. These conditions can then be translated into fluorescent monoplex IHC, and then all protocols compiled into one multiplex IHC panel.

### 3.1.1 Chromogenic Immunohistochemistry Optimisation of antibodies against CD8 and CD103

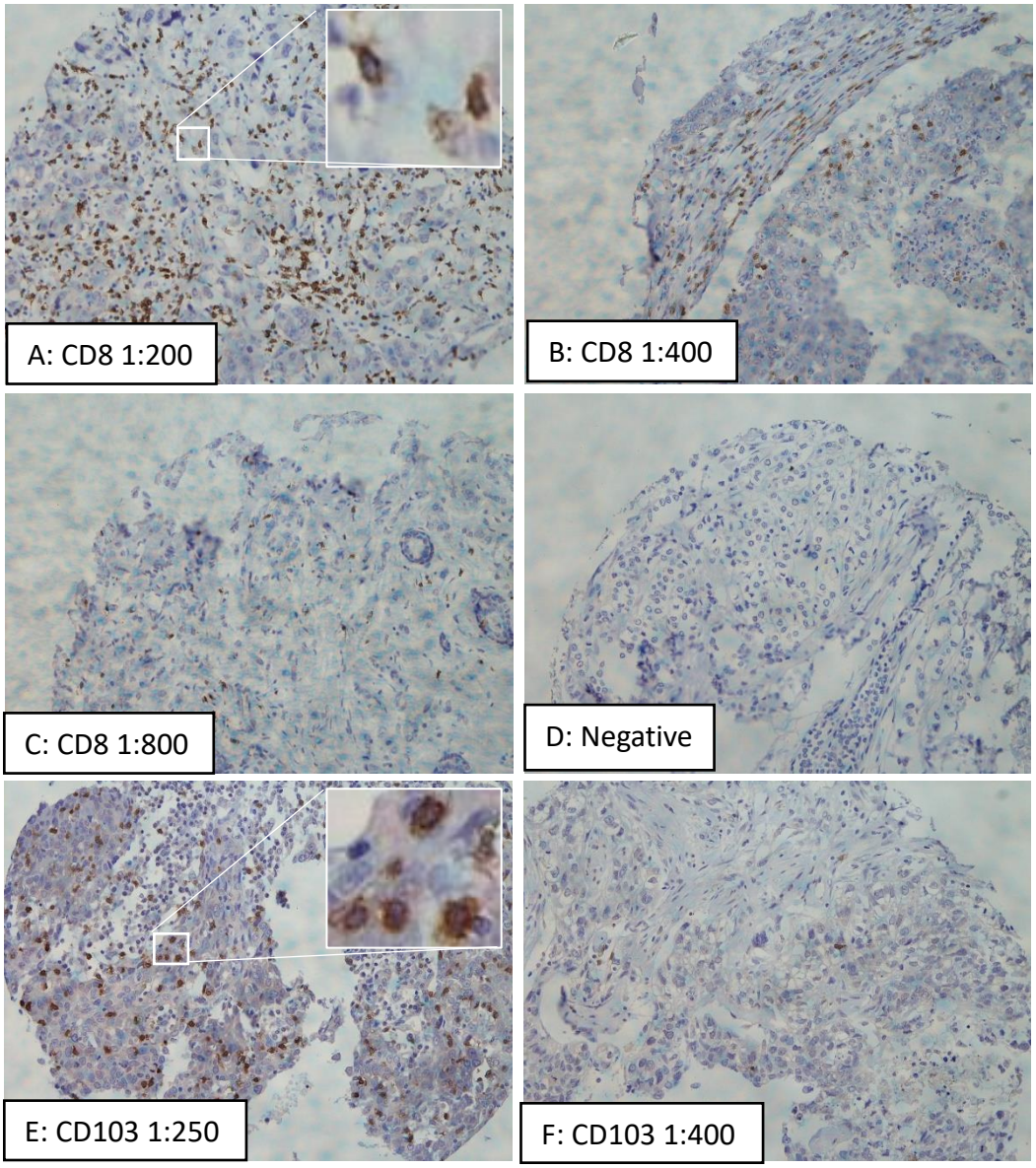



Figure 3.1: Standard Chromogenic IHC staining of CD8 and CD103

Representative cores of Breast Cancer TMA slides stained with anti-CD8 antibody at 1:200 (A), 1:400 (B) and 1:800 (C). (D) shows a representative core that received the same treatment excluding primary antibody as a control slide. Staining with anti-CD103 at 1:250 (E) and 1:400 (F) are shown. Images were imaged on the Nikon E600 and are displayed at 20X magnification. Inset images (large white boxes) represent 5.75 times (A) and 5.6 times (B) further magnified areas within the small white boxes.

Firstly, TMA slides were stained with anti-CD8 antibody at 1:200, 1:400 and 1:800 dilutions. As shown in **Figure 3.1 A** there was strong specific membrane staining with the anti-CD8 antibody, at 1:200. Staining was considered specific because there was low/no background

staining against positively stained cells and no non-specific staining seen on the negative slide (only DAPI visible as blue nuclei, no brown/red DAB staining, for example in, **Figure 3.1 D**). Slides were stained with the anti-CD103 antibody at 1:250 and 1:400 dilutions. The stronger membrane staining was observed at 1:250, as shown in **Figure 3.1 E**, with only faint background staining noted. Therefore, anti-CD8 1:200 and anti-CD103 1:250 antibody concentrations were chosen.

### 3.1.2 Chromogenic Immunohistochemistry Optimisation of antibodies against CD39 and Pan Cytokeratin

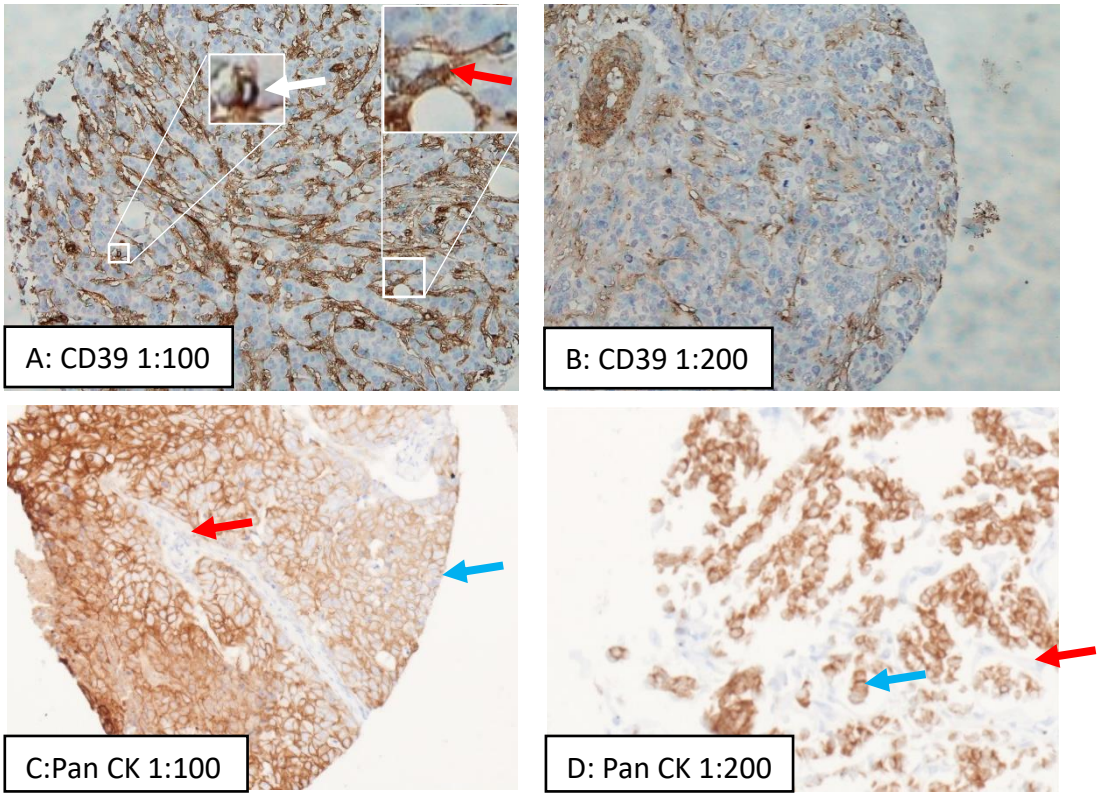



Figure 3.2: Standard Chromogenic IHC staining of CD39 and Pan Cytokeratin. Representative cores of Breast Cancer TMA slides stained with anti-CD39 antibody at 1:100 (A) and 1:200 (B). In (A), the white arrow indicates a lymphocyte stained with anti-CD39, while the red arrow shows CD39 staining of the stroma. Staining with anti-CK at 1:100 (C) and 1:200 (D) are shown. The red arrows in (C) and (D) point to the unstained stroma, while the blue arrows indicate epithelial regions which have been stained with anti-CK antibody. CD39 stained slides were imaged at 20X on the Nikon E600 while CK slides were imaged at 20X by the Mantra on the brightfield setting. Inset images (large white boxes) represent 5 times (A - left) and 3.75 times (A - right) further magnified areas within the small white boxes.

Based on the manufacturer datasheet and previous data within the group, anti-CD39 antibody was applied to TMA slides at 1:100 and 1:200 dilutions. As indicated by the white arrow in **Figure 3.2 A**, anti-CD39 staining was shown to present as bold ring-shaped staining of the membrane, as well as more elongated cell membrane staining, shown by the red arrow in **Figure 3.2 A**. The bold ring-shaped cell membrane staining seen in the figure is indicative of CD39 expression on lymphocytes, similar to that of CD8 and CD103. This is the

staining of interest in this research project. However, as CD39 is involved in the adenosine pathway it is also highly expressed in the stroma, as indicated by the red arrow in **Figure 3.2 A** as more elongated cell membrane staining (indicative of fibroblast CD39 staining). As the lymphocyte CD39 staining was much more defined at 1:100, this concentration was chosen.

Pan cytokeratin (CK) specifically stains epithelial regions, and was added into the panel to distinguish epithelium from stroma to easily assess lymphocyte density within these regions. As indicated by the blue arrows in **Figure 3.2 C** and **D**, both 1:100 and 1:200 anti-CK antibody titrations strongly stained the epithelial cells. CK specificity was observed as there was no background staining in the stroma, indicated by the red arrow in **Figure 3.2 C** and **D**. Accurate epithelial staining was confirmed by visually assessing pathological structures using DAPI alone and crosschecking this with CK staining. Accordingly, as both antibody titrations distinguished tumour and stromal regions, the lower concentration of 1:200 sufficed.

### 3.1.3 Chromogenic Immunohistochemistry Optimisation of antibody against CD4

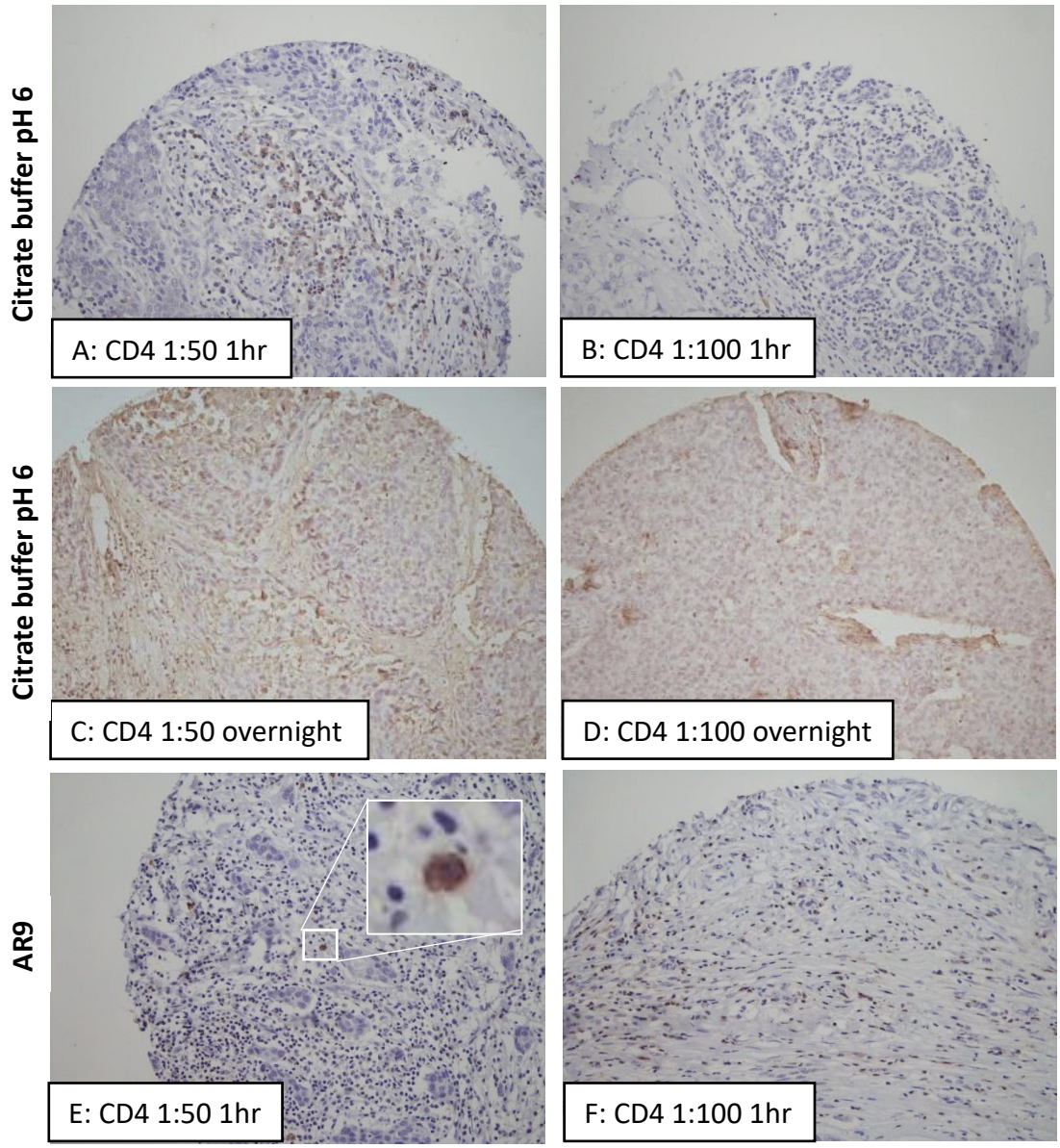



Figure 3.3: Standard chromogenic IHC staining of CD4. Representative cores of Breast Cancer TMA slides stained with anti-CD4 antibody. Using pH 6 citrate buffer, anti-CD4 was applied for 1 hr at 1:50 (A) and 1:100 (B) and overnight at 1:50 (C) and 1:100 (D). Using AR9 buffer (AkoyaBio), anti-CD4 was applied for 1 hr at 1:50 (E) and 1:100 (F). All slides were imaged on the Nikon E600 and displayed at 20X magnification. Images were imaged on the Nikon E600 and are displayed at 20X magnification. Inset image in E (large white box) represents 6.2 times further magnified area within the small white box.

Initially for the CD4 staining conditions, the pH 6.0 citrate buffer was used for antigen retrieval prior to applying 1:50 and 1:100 anti-CD4 titrations. As can be seen in **Figure 3.3 A** and **B**, 1hr incubation following citrate buffer antigen retrieval produced very faint staining.

Therefore, overnight incubation at the same dilutions was trialled, as displayed in **Figure 3.3 C** and **D**, producing stronger staining but also stronger background signal, making it difficult to pinpoint the positive cells. As neither incubation nor concentration could improve staining quality, the antigen retrieval method was adjusted, switching to the AR9 buffer, which is a pH 9.0 antigen retrieval buffer. AR9 buffer was used as it is a stronger antigen retrieval option. As shown in **Figure 3.3 E** and **F**, these conditions yielded strong, specific membrane staining.

## 3.2 Monoplex Immunohistochemistry optimisation

Multiplex IHC involves the Tyramide system amplification (TSA) system, where TSA is converted and polymerised by HRP, causing it to bind to the primary and secondary antibodies, as well as the antigen itself. This clever amplification means that microwave treatment (MWT) can strip the antibodies, but leave the TSA and fluorescing reporter bound to the antigen, as depicted in **Figure 2.1**. Additionally, cell nuclei are visualised using DAPI rather than haematoxylin and eosin.

TSA can be conjugated to one of 8 Opal fluorophores. Each Opal has unique excitation and emission peaks, outlined in **Table 3.1,** enabling individual detection by the quantitative pathology imaging system; the Mantra and the Vectra Polaris. Both imaging systems can detect all 8 opal fluorophores, as shown in the table below. The Mantra can quickly capture images of individual regions or cores at 10X, 20X and 40X magnification, but the downfall is that these regions are user-selected allowing for selection bias and the time-consuming process of selecting and scanning each region. Also, there is a difference in opal signal detection between the two imaging systems, with the ratios for each opal detailed in **Table 3.1**. In recent developments, the Vectra Polaris functionality was enhanced to scan whole slides at 40X magnification in a rapid, automated fashion without the need to select regions for scanning. Importantly, this function is only compatible with the certain Opals, termed the MOTIF$^{TM}$ Opals, indicated in the table below. Opals compatible with the MOTiF technology (integrated into the Vectra Polaris) were solely considered to utilise its ability to rapidly generate unmixed whole slide scans up to 40X magnification view.

For the initial optimisation process, the Mantra was used to quickly capture representative cores across the TMA to guide the steps of assay development. The Vectra Polaris was used to rapidly scan the fully optimised whole slides, therefore the staining conditions achieved when imaging on the Mantra needed to be validated on the Vectra Polaris later in assay development.

### 3.2.1 Allocation of Antibody-Opal Pairings

Following the identification of the optimal chromogenic IHC staining parameters, the next stage in assay development was to pair each primary antibody to one of the opal fluorophores in a monoplex condition (only one antibody and opal per slide). It is vital to do this to identify which opal and antibody best pair together, such that the staining is strong and specific, before all the antibody-opals are applied to one slide, referred to as a multiplex slide.

Antibody-opal pairings are allocated based on a number of factors, with the first factor of condition in this project being the abundance of the marker in the tissue of interest, pairing the highly abundant markers with the weaker opals. The opal brightness/intensities relative to one another are listed in **Table 3.1**.

| Fluorophore | Excitation | Emission | Brightness | Intensity Ratio Mantra:Polaris | MOTIF (Vectra Polaris Whole slide scanning) |
|---|---|---|---|---|---|
| **Spectral DAPI** | **358nm** | **461nm** | **-** | **1:1.5** | ✓ |
| Opal Polaris 480 | 450nm | 500nm | Highest | 1:2.6 | ✓ |
| **Opal 520** | **450nm** | **500nm** | **Highest** | **1:0.9** | ✓ |
| Opal 540 | 523nm | 536nm | Medium | N/A | ✗ |
| **Opal 570** | **550nm** | **570nm** | **Medium** | **1:0.7** | ✓ |
| **Opal 620** | **588nm** | **616nm** | **Medium** | **1:1** | ✓ |
| Opal 650 | 627nm | 650nm | Highest | N/A | ✗ |
| **Opal 690** | **676nm** | **694nm** | **Low** | **1:1** | ✓ |
| **Opal Polaris 780** | **750nm** | **770nm** | **Lowest** | **1:2.4** | ✓ |

*Table 3.1: Opal Fluorophores Spectral Characteristics*. Columns 1-4 display the opals and their spectral excitation and emission wavelengths, and their relative fluorophore brightness. Column 5 shows the opal intensity detection ratio on the Polaris, compared to the Mantra imaging systems, with green indicating higher detection by the Polaris, and red indicating higher detection on the Mantra, and yellow indicating the same detection by both systems. The remaining column indicates which Opals are MOTIF, compatible with the 40X whole slide scanning function of the Vectra Polaris. In bold are the opals selected to use in this project.

Importantly, all markers in the panel had the potential to co-express, therefore it was vital to allocate opal-pairings wisely in a monoplex setting, and then verify this in a multiplex condition by combining all antibody-opal pairings into one protocol and checking there was no signal interference between the opals.

A major factor influencing the initial staining parameters was the conditions used in a previously optimised 3-colour multiplex colorectal cancer protocol within Dr. Ramage's research group staining for CD8, CD39 and CD103. This previous project used the Opal 4-colour kit, which contains Opal520, Opal570 and Opal690 plus DAPI for nucleus visualisation. In the early stages of their work, CD39 was paired with Opal690, as CD39 was the most abundant marker in their 3-antibody panel so it was logical to allocate it to Opal690, the weakest opal out of the 3 (see **Table 3.1** for opal brightness). Out of the two remaining markers, CD103 was the highest expressing marker in the epithelial region, so was initially paired with Opal570, leaving the least abundant marker, CD8, with the brightest fluorophore Opal520. During the optimisation process, it was discovered that swapping CD39 and CD103 opals produced better staining, resulting in their final panel CD8-Opal520, CD39-Opal570 and CD103-Opal690.

With these previous opal pairings in mind, CD4 and CK needed to be paired with the individual fluorophores Opal620 and Opal780. As revealed by the chromogenic staining in **Figure 3.2 C** and **D** above, CK is highly abundant in breast cancer tissue, being expressed on all epithelial regions, thus it was allocated the weakest opal fluorophore, Opal780. CK was also a marker of low priority, as its involvement in the panel was to distinguish epithelia

from stroma, unlike all other markers being used to specifically phenotype single cells, further validating the decision to allocate it to the weakest fluorophore. CD4 expression was far less than CK, so could be reasonably paired with Opal620, a medium intensity opal. Notably, these antibody-opal pairings were assessed for their suitability when optimising the conditions of staining and titrating opal dilutions in the next stage of optimisation. Most commonly, the pairings may be revised if the staining intensity of one antibody-opal remains too high even with very low opal concentrations, or too low even at high opal concentrations, with the latter being more concerning due to the reagent consumption.

### 3.2.2. Optimisation of Opal-Antibody conditions as Monoplex

Alongside identifying antibody-opal pairings, the staining conditions for each of these as monoplex slides also needed to be found. Similar to the primary antibody optimisation using chromogenic IHC, the conditions to optimise included the antigen retrieval method, opal concentration, and adjusting the blocking step if any significant background signal emerged at the monoplex stage. As part of the opal staining kits, two antigen retrieval buffers are included: AR6 (a pH 6.0 buffer) and AR9 (a pH 9.0 buffer) with AR9 yielding the strongest opal staining due to its harsher pH. Therefore, it was decided that all antibody staining began with AR9 buffer to retrieve antigens with MWT as the starting point. The recommended starting opal concentration of 1:100 was used for all opals, with the exception of the Opal780 procedure which began with a 1:100 TSA-DIG solution followed by 1:25 Opal780.

During monoplex optimisation, the signal intensity was assessed for each antibody-opal pairing as detailed in **Methods Section 2.3** to achieve opal-specific target intensity ranges (listed in **Table 3.2**) and a signal to background ratio of 10:1. If intensities were too high or low, opal dilutions were increased or decreased, respectively. Where background signal was more than 10% of the positive cell intensities, the blocking step was adjusted as well as primary antibody and opal concentrations.

It is important to note that monoplex optimisation can only go so far; conditions can be refined to achieve the target signal intensity and background signal but these perfect values may not directly translate to a multiplex slide setting. Cross-channel bleed through may emerge when all antibody-opal protocols are combined as multiplex. Bleed through refers to the leakage of one channel's fluorescent signal into a (usually spectrally adjacent) channel, for example if the signal is high. Akoya Biosciences recommend keeping the intensities below 20 counts to minimise this occurring. Consequently, further opal concentration tweaking would be required, so the monoplex and multiplex optimisations were performed in parallel, after the initial monoplex conditions were refined.

| **Reporter** | **Target Exposure Time (m/s)** | **Target Intensity** |
|---|---|---|
| DAPI | 5 | 50-100 |
| Opal520 | 5-10 | 10-50 |
| Opal570 | 10-20 | 10-30 |
| Opal620 | 25-100 | 10-30 |
| Opal690 | 25-100 | 5-20 |
| Opal780 | 25-100 | 1-10 |

*Table 3.2: Criteria for Opal Reporter staining on the Vectra Polaris*. The reporters used in this project are displayed in the first column, with the exposure time (auto adjusted by the Vectra Polaris imaging system to achieve the best imaging quality) and target intensity ranges for each opal.

### 3.2.3. Monoplex Optimisation of CK-Opal780

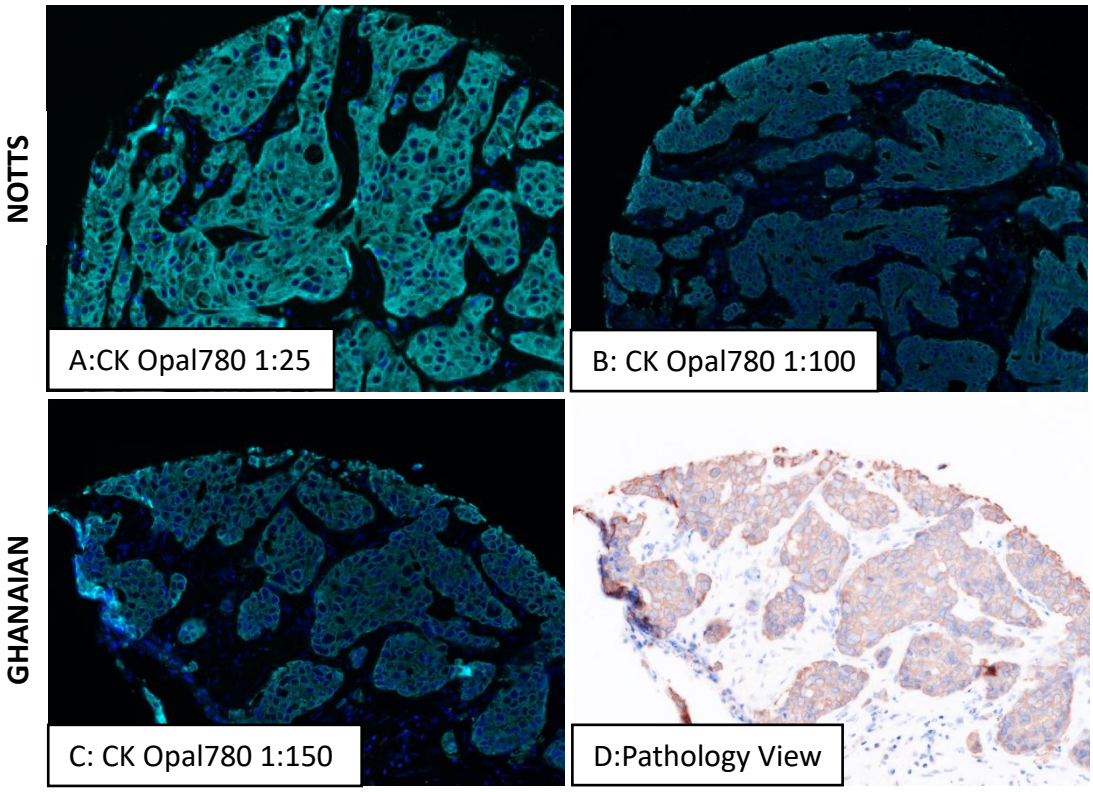



Figure 3.4: Monoplex Immunofluorescence Optimisation of CK-Opal780. Representative cores of Breast Cancer TMA slides of the Nottingham cohort and the Ghanaian cohort were stained with anti-CK, and paired with the fluorescent reporter Opal780. Opal780 signal has been visualised with the colour cyan. Opal780 was applied at 1:25 (A) and 1:100 (B) for 10 minutes on the Nottingham cohort TMA. The Ghanaian cohort TMA was stained with Opal780 at 1:150 (C). (D) shows the identical core and staining as in (C) but visualised with pseudo-DAB. All slides were imaged on the Mantra and displayed at 20X magnification.

As shown in **Figure 3.4 A** as the bold cyan staining, CK-Opal780 yielded strong epithelial staining at the recommended starting concentration of 1:25, and produced negligible background staining of the stroma. This result confirmed CK-Opal780 to be a suitable pairing. For this Opal fluorophore, it was important to note that the signal intensity is detected at 2.4 times the level when scanned on the Polaris than on the Mantra, as shown in **Table 3.1**. However, as seen in **Table 3.3**, the signal intensity counts were significantly above the target range of 0.42-4.2 counts on the Mantra. Therefore, Opal780 at 1:50 (not shown in Figure) was stained, still producing highly intense staining. At a 1:100 titration, shown in **Figure 3.4 B**, staining remained strong, so the conditions were then repeated on

the Ghanaian breast cancer TMA, which again produced strong staining (figure not shown).

A further dilution of 1:150 was performed to decrease the signal further, as shown in **Figure 3.4 C**.

| TMA | Opal780 Dilution | Signal Intensity (Mantra) |
|---|---|---|
| Nottingham | 1:25 | 8.3 (4-9) |
| | 1:50 | 7 (2.5-11) |
| | 1:100 | 3.5 (1.5-6) |
| | 1:150 | 1.3 (1-4) |
| Ghanaian | 1:150 | 2 (1-6) |
| ***Target range*** | | **0.42-4.2 (conversion)** |

*Table 3.3: Signal intensities produced by different Opal780 concentrations.* Nottingham and Ghanaian breast cancer TMA slides were stained with anti-CK and different concentrations of Opal780 and imaged on the Mantra. Using the inform software, the staining intensity was routinely measured by taking the average and range of >80 cells across 8 cores. Target range on the Polaris is 1-10, with the Mantra conversion (1:2.4 detection ratio Mantra:Polaris) shown in the table.

A 1:150 concentration was selected, as it produced staining within the range, as shown in **Table 3.3. Figure 3.4 D** displays the same core but with pseudo-DAB staining to aid the visualisation of tissue pathology to confirm specific epithelial staining. Critically, comparing **Figure 3.4 C** with **A** and **B** shows that like the Nottingham TMA, clear epithelial cell staining was observed on the Ghanaian TMA, conveying that the staining parameters successfully translate to the TMA of interest.

### 3.2.4. Monoplex Optimisation of CD39-Opal570

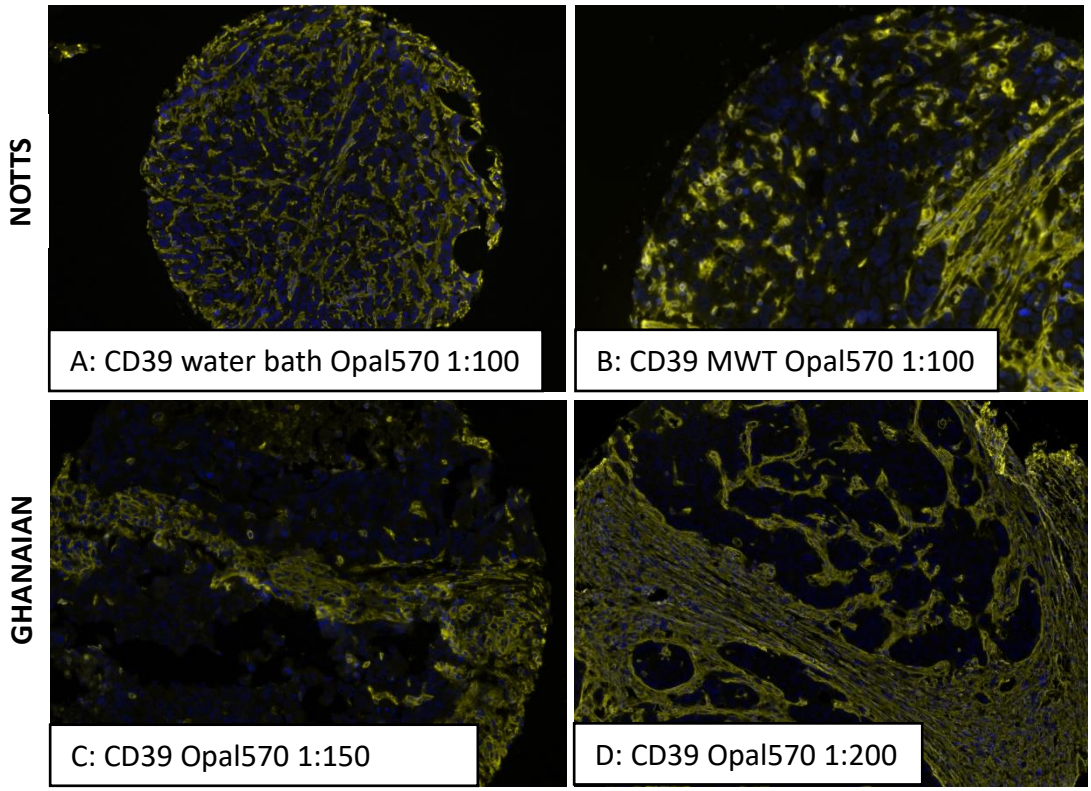



Figure 3.5: Monoplex Immunofluorescence Optimisation of CD39-Opal570. Representative cores of Breast Cancer TMA slides of the Nottingham cohort and the Ghanaian cohort were stained with anti-CK, and paired with the fluorescent reporter Opal570. Opal570 signal has been visualised with the colour yellow. Opal570 was applied at 1:100 to (A) and (B) for 10 minutes on the Nottingham cohort TMA. In (A), antigen retrieval was performed using the water bath HIER method, giving an average intensity of 5 at 10X and in (B), microwave treatment (MWT) was used, giving an average intensity of 13 at 10X. The Ghanaian cohort TMA was stained with Opal570 at 1:150 (C) and 1:200 (D). All slides were imaged on the Mantra and displayed at 20X magnification, except for (A) which was imaged at 10X.

From previous work with CRC tissue, CD39-Opal570 was found to produce strong, specific staining on CRC tissue when antigen retrieval was performed using AR9 buffer, with the HIER method being the water bath, as opposed to MWT. Thus, these conditions were used as a starting point for breast cancer tissue optimisation (**Figure 3.5 A**). The fluorophore Opal570, is detected at a lower intensity on the Polaris (0.7:1 Polaris:Mantra, as shown in **Table 3.1**).

| TMA | Opal570 Dilution | Signal Intensity (Mantra) |
|---|---|---|
| Nottingham | 1:100 | 29 (14-41) |
| | 1:125 | 24 (15-33) |
| | 1:150 | 9 (7-14) |
| Ghanaian | 1:125 | 15 (5-26) |
| | 1:150 | 8 (5-24) |
| ***Target range*** | | **14.3-42.9 (conversion)** |

*Table 3.4: Signal intensities produced by different Opal570 concentrations*. Nottingham and Ghanaian breast cancer TMA slides were stained with anti-CD39 and different concentrations of Opal570 and imaged on the Mantra. Using the inform software, the staining intensity was routinely measured by taking the average and range of >80 cells across 8 cores. Target range on the Polaris is 10-30, with the Mantra conversion (1:0.7 detection ratio Mantra:Polaris) shown in the table.

As shown in **Figure 3.5 A** and **B**, the water bath HIER method produced less intense staining (average of 5) than MWT (average of 13) in the same AR9 buffer, confirming the necessity for tissue-specific optimisation. At the same opal concentration, intensity was visually lower, so the conditions generating strong specific staining within the target range were MWT with AR9 buffer. As previous multiplex experiences found Opal570 to be prone to spectral bleed through, the opal concentration was diluted to minimise this risk. Opal570 dilutions of 1:125, 1:150 and 1:200 were applied to the Nottingham TMA and Ghanaian TMA, with intensity measurements shown in **Table 3.4** and representative Ghanaian cores for 1:150 and 1:200 shown in **Figure 3.5**. At this stage, 1:125 produced staining within the target range.

### 3.2.5. Monoplex Optimisation of CD103-Opal690

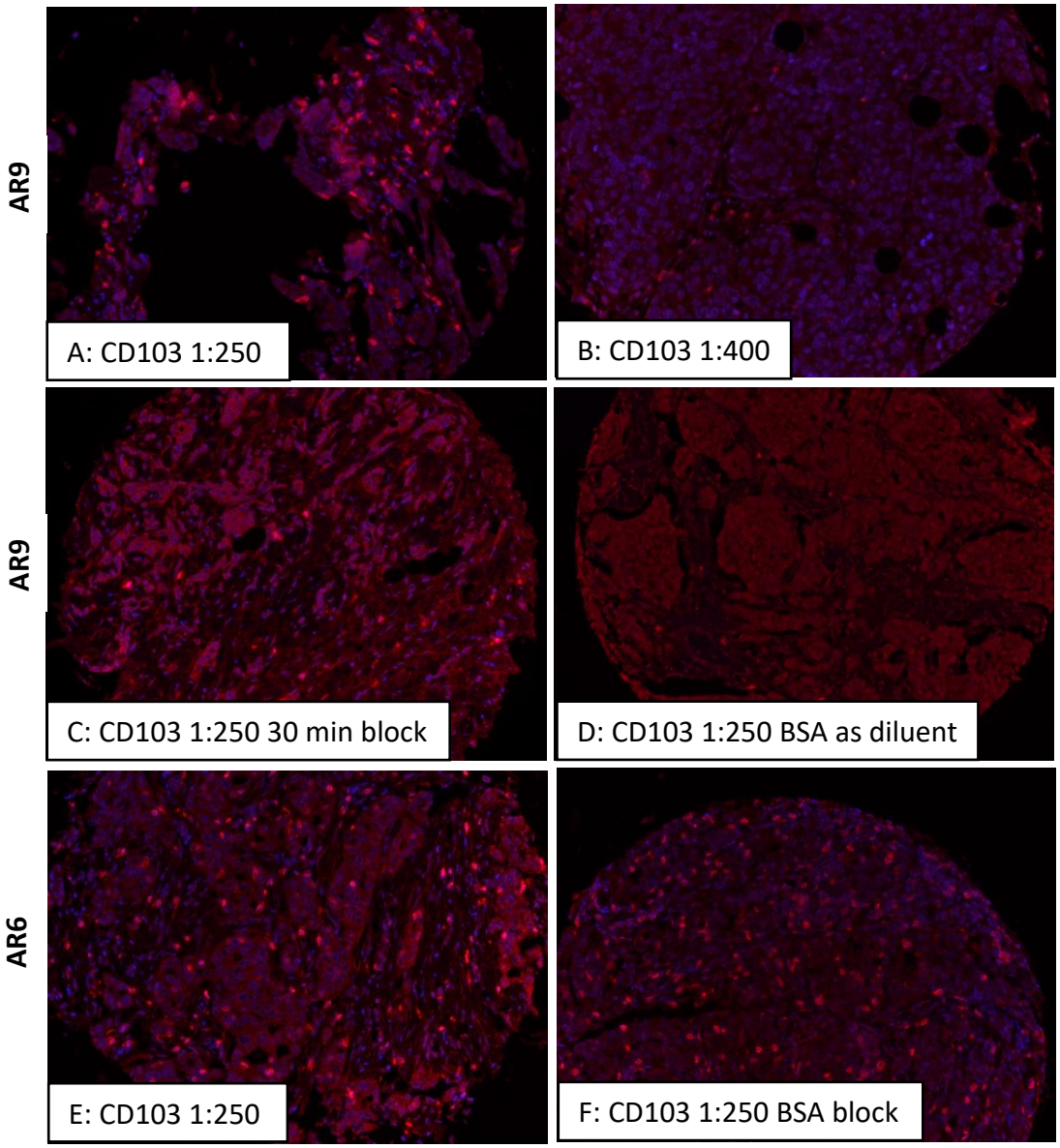



Figure 3.6: Approaches to reduce background signal of CD103-Opal690. Representative cores of Breast Cancer TMA slides of the Nottingham cohort were stained with anti-CD103, and paired with the fluorescent reporter Opal690. Opal690 signal has been visualised with the colour red. Opal690 was applied at 1:100 for 10 minutes to all 4 conditions, with AR6/AR9 indicating the antigen retrieval buffer pH used. In (A) and (B), standard multiplex IHC protocol was used (2x5 minutes blocking steps) and anti-CD103 dilutions 1:250 in (A) and 1:400 (B) applied. (C) received 2x30 minutes blocking, while (D) used 1XBSA solution as the primary antibody diluent. (E) and (F) samples received AR6 (antigen retrieval at pH 6), and (F) received an additional 1XBSA blocking step. All slides were imaged on the Mantra and displayed at 20X magnification.

CD103-Opal690, with an opal concentration of 1:100, strongly stained the positive cells, but also had significant non-specific background staining, as seen in **Figure 3.6 A** by the bright fluorescing cells against a background of signal throughout the tissue. Numerical assessment

saw the background intensity being up to 50% that of the positive cells. A range of approaches to stop background staining were trialled. Firstly, primary antibody dilution was increased to 1:400, but as shown in **Figure 3.6 B**, the effect of this simply dampened the positive signal but did not reduce background staining. Therefore, it was deduced that the blocking stage of the protocol needed to be adjusted. Increasing the blocking incubation times up to 30 minutes made no improvement to the background staining, as the background signal is much higher across the core when comparing **Figure 3.6 C** to **A**, making it more difficult to identify positive cells.

Next, BSA solution was substituted as the primary antibody diluent to compete with antibody binding, in the hopes to block non-specific binding. However, as seen in **Figure 3.6 D**, this approach simply dampened positive signal and background remained similar to **Figure 3.6 A**. As such, the antigen retrieval method was addressed, hypothesising that a less harsh AR6 buffer would hopefully resolve the issue. Cell staining became clearer and sharper against the background as shown in **Figure 3.6 E**. An additional blocking step with BSA solution was incorporated into the protocol, and this, combined with the gentler pH6 to retrieve epitopes, produced less nonspecific background staining, presented in **Figure 3.6 F**. Following successful CD103-Opal690 background signal reduction at the starting concentration of 1:100, it was then important to titrate the antibody to a suitable range to minimise bleed through risk when incorporating it into a multiplex panel. **Figure 3.6 F,** and **3.7 A** and **B** show that 1:100, 1:150 and 1:200 titrations produced strong staining, and validation of 1:200 in the Ghanaian TMA confirmed the intensity to remain within the target intensity range, as shown in **Table 3.5**. However, when validating the conditions in the

multiplex (see Section 3.3.2), the signal appeared weaker, thus the concentration was lowered marginally to 1:175 as shown in **Figure 3.7 C** and **Table 3.5**.

| **TMA** | | **Opal690 Dilution** | **Signal Intensity (Mantra)** | **Signal Intensity (Polaris)** |
|---|---|---|---|---|
| Nottingham | | 1:100 | 12 (5-21) | |
| | | 1:150 | 8 (6-12) | |
| | | 1:200 | 7 (3-11) | |
| Ghanaian | 1:175 | 15 (4-28) | | |
| | 1:200 | 9 (5-18) | | |
| ***Target range*** | | **5-20** | **5-20** | |

*Table 3.5: Signal intensities produced by different Opal690 concentrations.* Nottingham and Ghanaian breast cancer TMA slides were stained with anti-CD103 and different concentrations of Opal690 and imaged on the Mantra. All slides received AR6 antigen retrieval with an additional 1X BSA blocking step. Using the inform software, the staining intensity was routinely measured by taking the average and range of >80 cells across 8 cores. Target range on the Polaris and Mantra is 5-20, shown in the table.

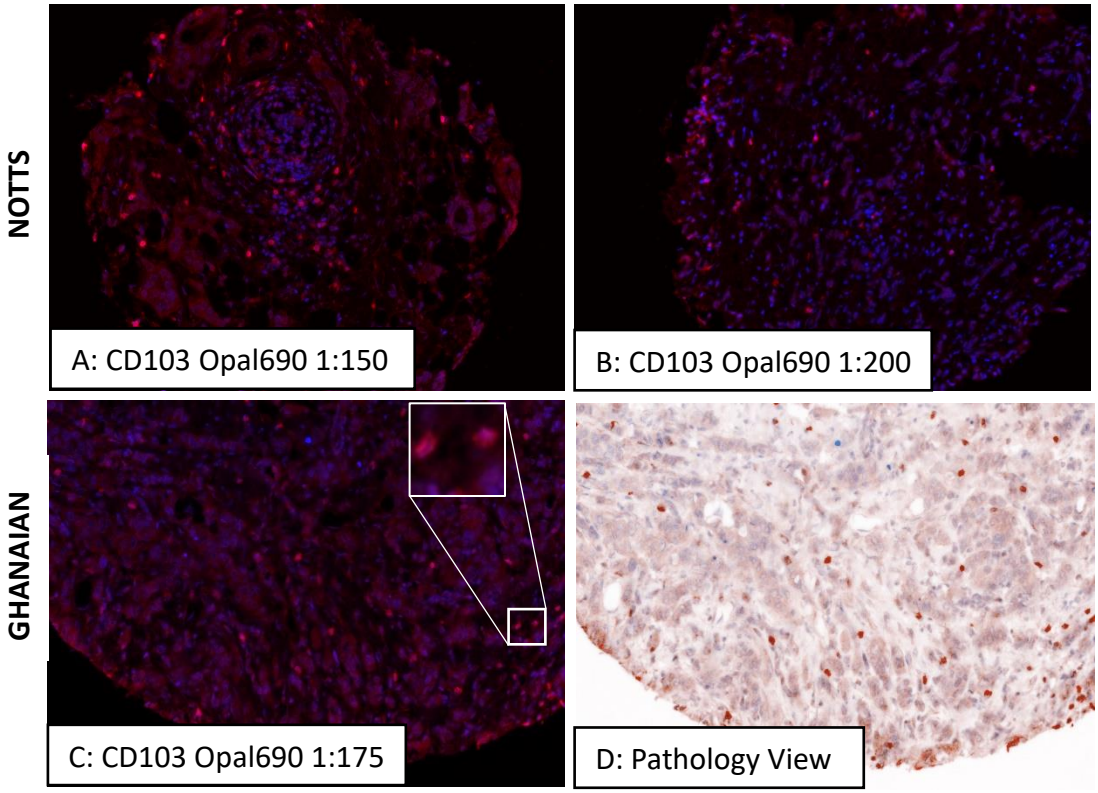



Figure 3.7: Monoplex Immunofluorescence Optimisation of CD103-Opal690. Representative cores of Breast Cancer TMA slides of the Nottingham and Ghanaian cohort were stained with anti-CD103, and paired with the fluorescent reporter Opal690. Opal690 signal has been visualised with the colour red and was applied at 1:150 (A) and 1:200 (B). The Ghanaian cohort TMA was stained with Opal690 at 1:175 (C). (D) shows the identical core and staining as in (C) but visualised with pseudo-DAB. All slides were imaged on the Mantra and displayed at 20X magnification. Inset image in C (large white box) represents 3.45 times further magnified area within the small white box.

### 3.2.6. Monoplex Optimisation of CD4 and CD8 Opal Pairings

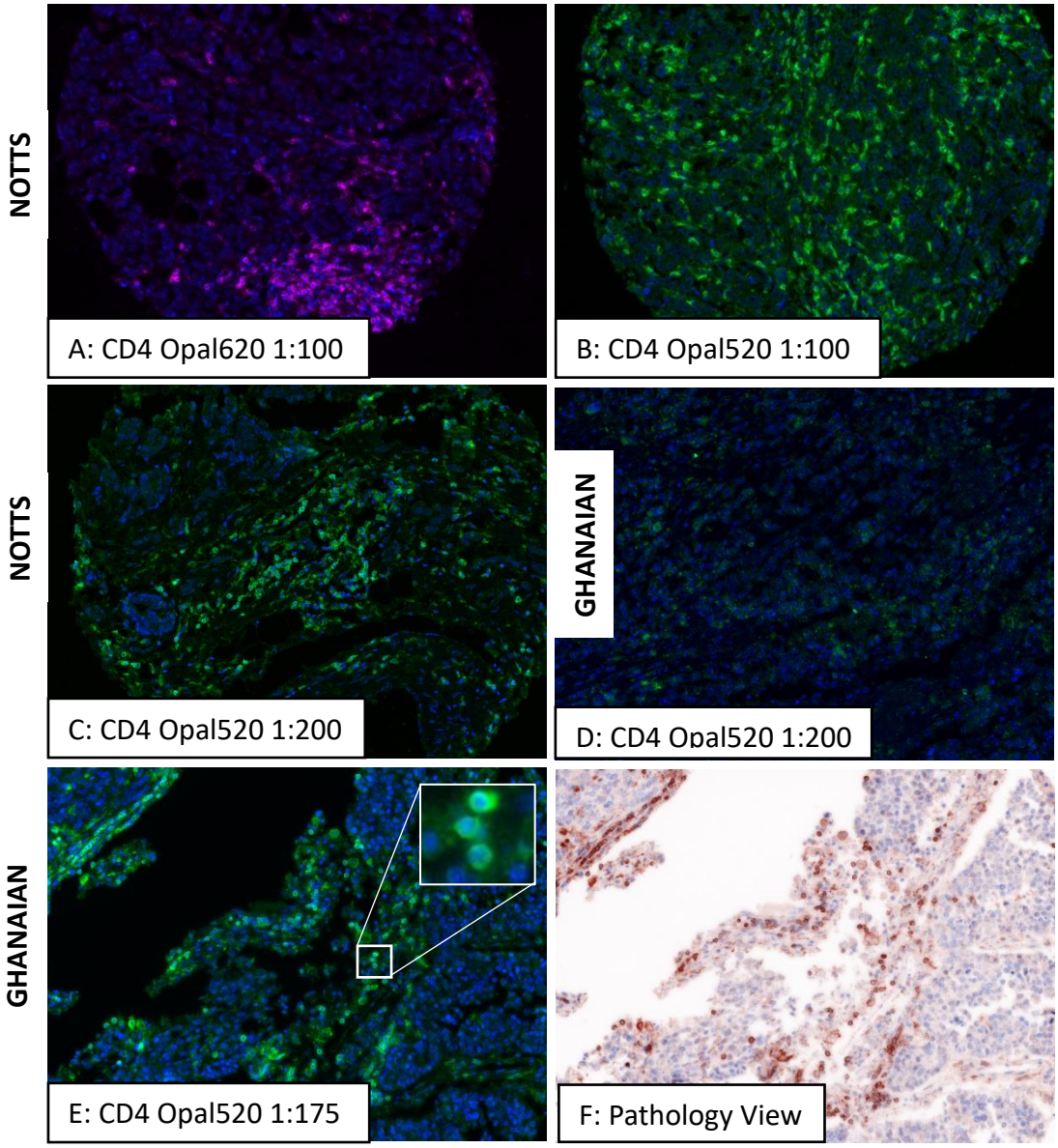



Figure 3.8: Monoplex Immunofluorescence Optimisation of antibody against CD4**.**
Representative cores of Breast Cancer TMA slides of the Nottingham cohort and the Ghanaian cohort were stained with anti-CD4, and paired with the fluorescent reporter Opal520 and Opal620, both applied for 10 minutes. Opal520 signal has been visualised with the colour green, while Opal620 has been visualised with magenta. Opal620 was applied at 1:100 (A). Opal520 was applied at 1:100 (B) and 1:200 (C). The Ghanaian cohort TMA was stained with Opal520 at 1:200 (D) and 1:175 (E). (F) shows the identical core and staining as in (E) but visualised with pseudo-DAB. All slides were imaged on the Mantra and displayed at 20X magnification. Inset image in E (large white box) represents 4.8 times further magnified area within the small white box.

During monoplex optimisation, CD4 was paired with the mediumly intense Opal620. CD4 staining produced very weak signal even at the recommended starting concentration 1:100, with intensity counts averaging at 4 as shown in **Table 3.6**, with staining represented in

**Figure 3.8 A**. As both the primary antibody and opal at high concentrations produced weak staining, the logical next step was to swap the opal pairings. Staining of the spectral library showed that CD8 reliably stained at the same Opal620 concentration (1:100) with an average of 20 intensity counts.

| **TMA** | **Opal620 Dilution** | **Signal Intensity (Mantra)** |
|---|---|---|
| Nottingham | 1:100 | 4 (3-12) |
| ***Target range*** | | **10-30** |
| | **Opal520 Dilution** | |
| Nottingham | 1:100 | 60 (40-78) |
| | 1:200 | 30 (25-50) |
| Ghanaian | 1:175 | 42 (25-50) |
| | 1:200 | 12 (9-20) |
| ***Target range*** | | **11.1-55.5** |

*Table 3.6: CD4 optimisation, paired with Opal620 and Opal520.* Nottingham and Ghanaian breast cancer TMA slides were stained with anti-CD4 and different concentrations of Opal520 and Opal620, followed by imaging on the Mantra. Using the inform software, the staining intensity was routinely measured by taking the average and range of >80 cells across 8 cores. Opal520 target range on the Polaris is 10-50, with the Mantra conversion (1:0.9 detection ratio Mantra:Polaris) shown in the table. Opal620 detection is the same on the Mantra and Polaris.

Accordingly, CD4 and CD8 opal pairings were swapped, pairing CD4 with the brightest fluorophore Opal520, which produced a significantly higher average signal of 60 at 1:100. As shown in **Figure 3.8 B**, this very high signal was accompanied with some residual background staining. This was easily resolved by titrating the opal to 1:200, as shown in **Figure 3.8 C**. However, when the same conditions were applied to the Ghanaian TMA, staining became very faint and positive cell staining became difficult to pinpoint (see **Figure 3.8 D**). As the intensity was still measured within the target range at an average of 12, Opal520 dilution was only slightly raised to 1:175, causing robust CD4 staining to return.

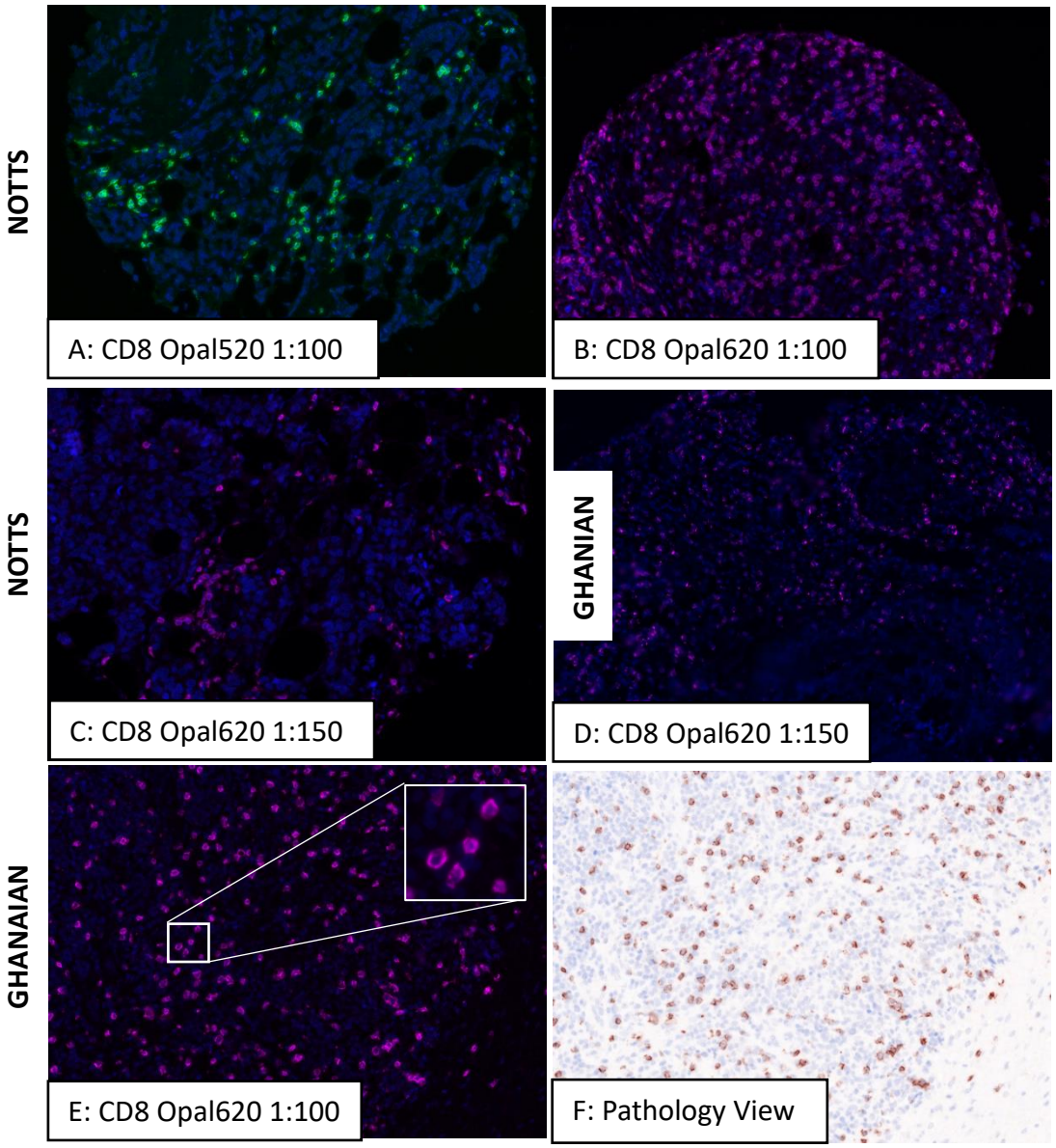



Figure 3.9: Monoplex Immunofluorescence Optimisation of antibody against CD8

Representative cores of Breast Cancer TMA slides of the Nottingham cohort and the Ghanaian cohort were stained with anti-CD8, and paired with the fluorescent reporter Opal520 and Opal620, both applied for 10 minutes. Opal520 signal has been visualised with the colour green, while Opal620 has been visualised with magenta. Opal520 was applied at 1:100 (A). Opal620 was applied at 1:100 (B) and 1:150 (C). The Ghanaian cohort TMA was stained with Opal620 at 1:150 (D) and 1:100 (E). (F) shows the identical core and staining as in (E) but visualised with pseudo-DAB. All slides were imaged on the Mantra and displayed at 20X magnification. Inset image in E (large white box) represents 2.8 times further magnified area within the small white box.

**Figure 3.9 A** and **B** confirms the strong, reliable staining of CD8 with both Opal520 and Opal620 at 1:100, thus validating the decision to swap opal pairing with CD4. With Opal620 being of medium intensity, a dilution of 1:150 produced positive staining within the target

range as shown in **Table 3.7**, represented in **Figure 3.9 C.** The same conditions produced significantly weaker staining on the Ghanaian breast cancer tissue, thus the opal concentration was returned to the starting dilution of 1:100, as shown in **Figure 3.9 E**. The notable signal intensity decrease was notable for all antibody-opal pairings in the Ghanaian breast cancer TMA, indicated in the Monoplex Optimisation figures as the need to bring most opal concentrations up after optimising in the Nottingham TMA slides. These significant disparities are reflective of the variation between the conditions the tumour biopsies received following removal, fixation and right up to microtome slicing.

| **TMA** | **Opal520 Dilution** | **Signal Intensity (Mantra)** | **Signal Intensity (Polaris)** |
|---|---|---|---|
| Nottingham | 1:100 | 64 (50-70) | |
| ***Target range*** | | **11.1-55.5** | **10-50** |
| | **Opal620 Dilution** | | |
| Nottingham | 1:100 | 20 (15-30) | |
| | 1:150 | 18 (12-25) | |
| Ghanaian | 1:100 | 12 (7-16) | |
| | 1:150 | 11 (4-16) | |
| ***Target range*** | | **10-30** | **10-30** |

*Table 3.7: CD8 optimisation, paired with Opal520 and Opal620***.** Nottingham and Ghanaian breast cancer TMA slides were stained with anti-CD8 and different concentrations of Opal520 and Opal620, followed by imaging on the Mantra. Using the inform software, the staining intensity was routinely measured by taking the average and range of >80 cells across 8 cores. Opal520 target range on the Polaris is 10-50, with the Mantra conversion (1:0.9 detection ratio Mantra:Polaris) shown in the table. Opal620 detection is the same on the Mantra and Polaris.

## 3.3 Multiplex IHC optimisation

### 3.3.1. Allocation of Staining Order

Having established the optimal staining parameters singly, all the protocols were combined into one multiplex panel. The order of antibodies applied to the TMA was designed based on the stability of each antibody-opal staining pair and previous optimisation findings. As an antibody is placed later in the staining order, it will be exposed to more antigen retrieval rounds, which can either uncover more antigens thus positive cells, or degrade the already uncovered antigens. Therefore, it was important to find a balance between these two effects when allocating antibody-opal pairings to each position.

In the Monoplex Optimisation section, it was found that CD103-Opal690 was prone to non-specific background staining which was visibly stronger when an AR9 buffer was used, which was predicted to worsen with increased MWT. It was the only antibody-opal pairing to require the less harsh AR6 antigen retrieval method, while all other antibodies required AR9, meaning that if CD103-Opal690 was placed after any of the other antibodies it would be exposed to AR9 thus increasing its background staining. Therefore, it was logical to allocate this pairing to position 1.

The co-expression of all markers in this study could potentially result in the umbrella effect occurring; this term refers to opal-TSA binding to an antigen and its surrounding membrane region inhibiting the binding of subsequent primary antibodies on the same cell membrane. Therefore, if a highly expressing marker such as CK in the epithelium is placed earlier in the panel, significant Opal-TSA could be deposited onto the membrane such that

CD8/CD4/CD39/CD103 antigens could be blocked. The umbrella effect is exaggerated by highly expressed markers are paired with the brightest fluorophores (Taube et al., 2020).

To reduce the risk of blocking other marker binding, CK was allocated the weakest opal (already established in Monoplex Optimisation section) and placed last in the sequence. Furthermore, CK being lowest in priority of staining quality, it could be placed anywhere in the sequence. This was due to the potential antigen exposure or degradation that occurs with increased MWT at latter positions would be least impactful on the project if given to CK. As Opal780 cannot be exposed to MWT, unlike the other opals, this antibody-opal pairing needed to be placed in the last position. Visual analysis of the intensity range of CK staining in position 1 and 5 was done to validate this. At a concentration of 1:25 Opal780 and a TSA-DIG concentration of 1:100, the staining range of CK-Opal780 was 1-5 counts at both position 1 and 5 at 10X magnification.

Allocation of CD103 in Position 1, and CK in position 5 left CD4, CD8 and CD39 to positions 2-4. Previous researchers optimally placed CD39 in Position 1 but the Monoplex optimisation showed CD39 to be more stable than CD103, so it was provisionally placed in position 2, followed by CD4 and CD8 in positions 3 and 4.

To validate antibody-opal positioning, monoplex slides were stained with the appropriate number of antigen retrievals (for example, at position 3 the tissue would receive 1 AR6 and 2 AR9 rounds) and visually assessed, finding similar staining patterns compared to position 1.

### 3.3.2. CD39 Opal570 was the main contributor to bleed through during multiplex IHC optimisation

Following the establishment of the antibody order, the monoplex protocols were combined into one multiplex staining protocol, and opal concentrations needed to be amended according to staining intensities and spectral bleed through. Primarily, unmixing signal with a spectral library assembled from the tissue of interest eliminates bleed-through. However, if one opal has a very high intensity it may be more prone to this, and/or if its adjacent channel has lower intensities and consequently needs a higher exposure time to view signal it may detect and unmix the bright neighbouring channel's intensity.

**Table 3.8** shows the different opal concentration combinations trialled to find the optimum staining parameters, and the resulting signal intensities generated from the conditions as detected on the Polaris imaging system. As previously mentioned, the monoplex and multiplex optimisations were performed in parallel, with initial multiplex conditions being applied to the Nottingham cohort TMA before moving onto the Ghanaian cohort. CK-Opal780 reliably stained at an Opal780 concentration of 1:150 throughout the multiplex optimisation. Though, multiple troubleshoot attempts were required for all other antibodies, in particular CD39-Opal570 and its spectrally adjacent antibody-opal pairings CD4-Opal520 and CD8-Opal620. Firstly, in panel 1, Opal520 1:200, Opal570 1:125, Opal620 1:150, Opal690 1:200 and Opal780 1:150 concentrations were used. On the optimisation tissue, Opal520, Opal570 and Opal780 concentrations stained suitably, giving signal intensity that was within the target range of 10-30. As for Opal690, staining was strong and specific but did produce some slight bleed through to the Opal780 channel, as lymphocyte membrane staining in the same position as in Opal690 channel could be seen. In the

Opal620 channel, no positive CD8 staining was seen, only bleed through from Opal570, as seen in **Figure 3.10 D** below as the faint stromal staining pattern similar to that seen in the CD39-Opal570 channel (**Figure 3.10 C**), indicated that staining at this concentration was too high. Therefore, Opal570 and Opal690 concentrations were decreased in the revised panel.

| Panel | TMA | Antibody-opal pair | Opal concentration | Intensity (range) |
|---|---|---|---|---|
| 1 | Nottingham | CD4-Opal520 | 1:200 | 11 (7-20) |
| | | CD39-Opal570 | 1:125 | 13 (5-15) |
| | | CD8-Opal620 | 1:150 | 0.6 (0.1-0.8) |
| | | CD103-Opal690 | 1:200 | 12 (4-14) |
| | | CK-Opal780 | 1:150 | 0.9 (0.4-3.6) |
| 2 | Nottingham | CD4-Opal520 | 1:200 | 4.9 (2-7) |
| | | CD39-Opal570 | 1:150 | 13.1 (6-33) |
| | | CD8-Opal620 | 1:150 | 23 (6-29) |
| | | CD103-Opal690 | 1:250 | 1.6 (0.8-2) |
| | | CK-Opal780 | 1:150 | 1.3 (1-3) |
| 3 | Ghanaian | CD4-Opal520 | 1:175 | 45 (22-65) |
| | | CD39-Opal570 | 1:150 | 5 (3-10) |
| | | CD8-Opal620 | 1:100 | 6 (2-10.9) |
| | | CD103-Opal690 | 1:175 | 1.4 (1-1.6) |
| | | CK-Opal780 | 1:150 | 3.5 (0.8-8) |
| 4 | Ghanaian | CD4-Opal520 | 1:175 | 28 (16-37.5) |
| | | CD39-Opal570 | 1:200 | 8.6 (4-18) |
| | | CD8-Opal620 | 1:100 | 5.1 (2-6.8) |
| | | CD103-Opal690 | 1:175 | 5 (2-7.2) |
| | | CK-Opal780 | 1:150 | 1.5 (1-3) |

*Table 3.8: The Multiplex Optimisation Process of adjusting Opal concentrations to achieve suitable staining, with no bleed through*. The antibody-opal pairing is shown with the opal concentration used. All opals were applied for 10 minutes. All intensities were measured using ~80 cells across 8 cores, imaged on the Polaris. In green, the opal concentrations used in the fully optimised panel are highlighted.

As expected, when Opal570 was further diluted, Opal620 stained well with no bleed through, shown by strong staining in **Figure 3.10 H** though the adjustment instead caused bleed through to the Opal520 channel but positive CD4 staining was still easy to distinguish, as seen in **Figure 3.10 F**. At 1:250, Opal690 staining was quite weak and from the monoplex optimisation results, it was observed that all opals, except for Opal780, had noticeably

weaker staining when applied to the Ghanaian TMA, compared to the Nottingham/optimisation TMA. This led us to use higher opal concentrations for Opals 520, 620 and 690 when a multiplex panel was applied to the Ghanaian TMA in panel 11. Opal780 stained well at 1:150 as a monoplex slide so this concentration was used again, and the nature of Opal570 bleed through on the Ghanaian TMA could not be predicted, so the same concentration was used. Opals 620, 690 and 780 stained suitably in this panel, therefore these concentrations were selected. As seen previously in Panel 8, Opal570 signal bled through to the 520 channel but in the Ghanaian TMA, the effect was more pronounced (shown in **Figure 3.10 J**), giving and Opal520 intensity of an average of 45. Finally, when decreasing Opal570 concentration to 1:200, the optimised multiplex IHC panel conditions (seen in **Table 3.9**) were reached. Despite some of the opal intensity averages being below the target range, these conditions produced strong staining for each antibody in the panel, with minimal background signal and no cross-channel bleed through.

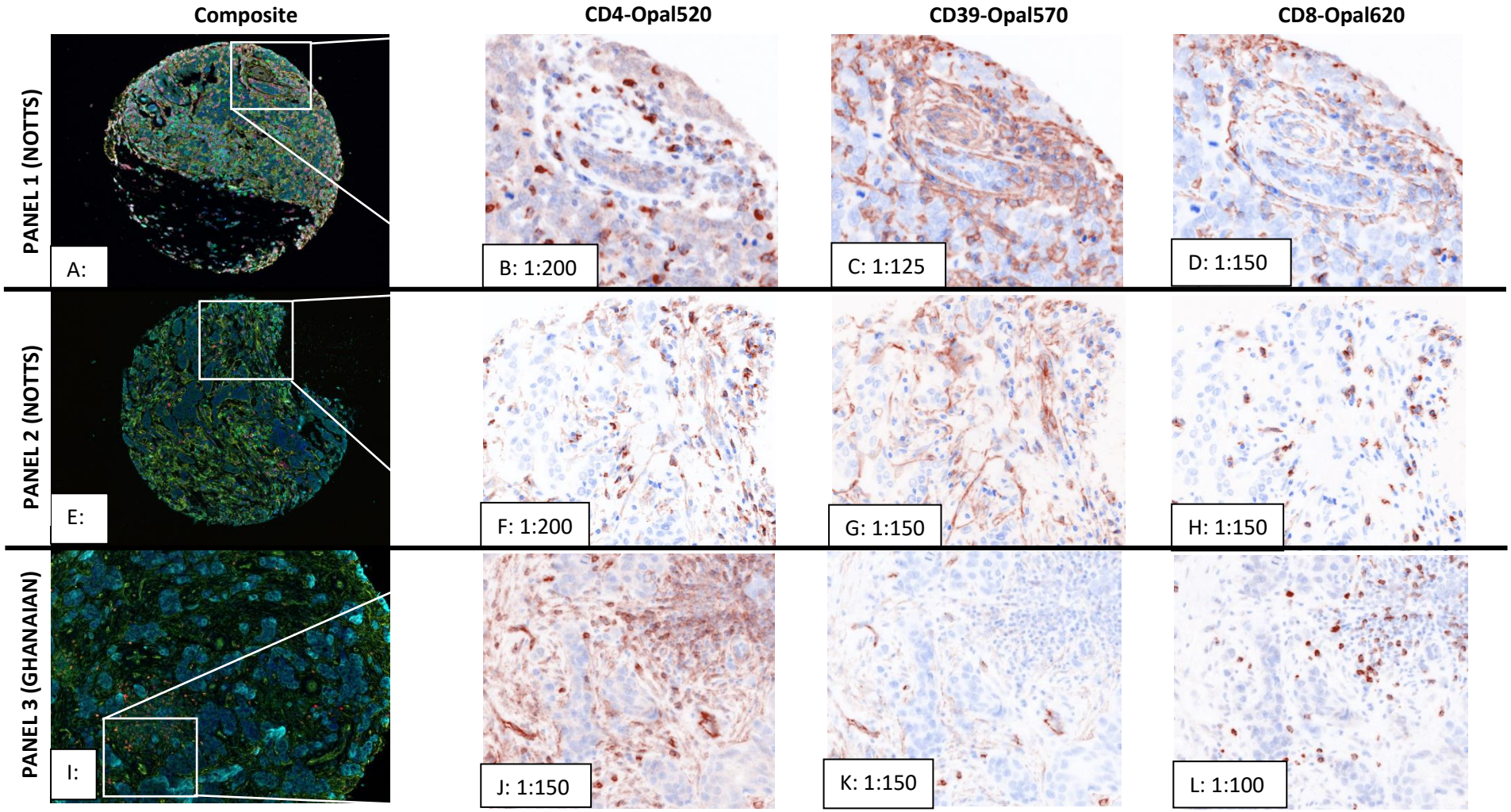



Figure 3.10: Opal570 bleed through to its adjacent channels**.** Representative cores from the Nottingham and Ghanaian TMA series were stained with the antibody-opal panel; CD4-Opal520, CD39-Opal570, CD8-Opal620, CD103-Opal690 and CK-Opal780. Each row shows different views of a representative core from Optimisation Panel 1, 2 and 3. From left to right, column 1 shows the composite images, and higher magnification of the same cores as the pseudo-DAB view of individual channels. Column 2 shows the Opal520 channel, Column 3 shows Opal570 and the last column shows Opal620. Panel composites were imaged at 10X and further magnified images represents 3.2 times further magnified area within the small white boxes.

| Antibody | Position | Fluorophore | Concentration |
|---|---|---|---|
| CD4 | 3 | Opal 520 | 1:175 |
| CD39 | 2 | Opal 570 | 1:200 |
| CD8 | 4 | Opal 620 | 1:100 |
| CD103 | 1 | Opal 690 | 1:175 |
| Pan Cytokeratin | 5 | Opal 780 | 1:150 |

*Table 3.9: Multiplex IHC Panel Optimised for the Ghanaian Breast Cancer TMA*. The primary antibodies, the opals they were paired with, and the opal concentration used are shown, as well as the position that the antibody-opals were applied to the TMA slide.

**Table 3.9** shows the conditions which were used to stain the full set of Ghanaian breast cancer TMA slides, and a representative core stained with these conditions is shown in **Figure 3.11**, which shows each antibody-opal pairing results. Composite images of two representative cores are shown in **Figure 3.12.** From visually assessing cores such as the one displayed in **Figure 3.11**, it was evident that the staining was strong and specific for the markers of interest. However, to validate this observation, examples of each of the potential phenotypes (defined by one or multiple combined markers) that would be present in the samples were visualised, as shown in **Figure 3.13**. Importantly, the figure shows strong positive staining of each antibody-opal with no bleed through to neighbouring channels being shown across all the cellular phenotypes. This validation was important because if bleed through was present, then the inform software may incorrectly identify that signal as positive staining. Prior to staining the full TMA set, a trial project was run using the Panel 4 optimisation slides to ensure that the inform software could be trained to recognise each marker.

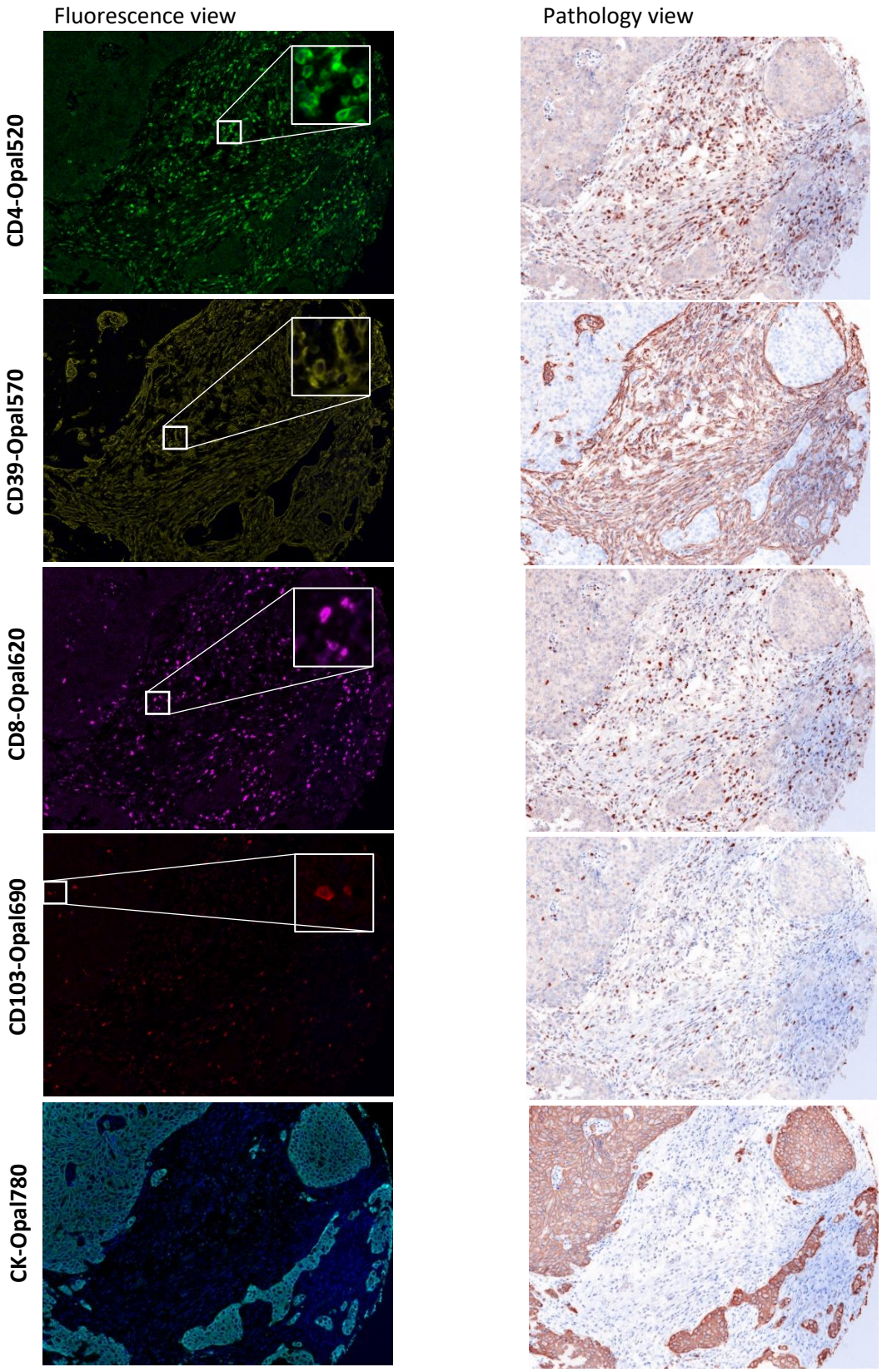



Figure 3.11: Representative Image of the optimised multiplex IHC conditions established**.** Ghanaian breast cancer cores were stained with 5 antibody-opals, with each row presenting a different antibody. The two columns show the same core but as fluorescent and pseudo-DAB staining views (nuclear/DAPI staining excluded). Images displayed at 20X magnification. Inset images (large white box) represents 4.2 times further magnified area within the small white boxes.

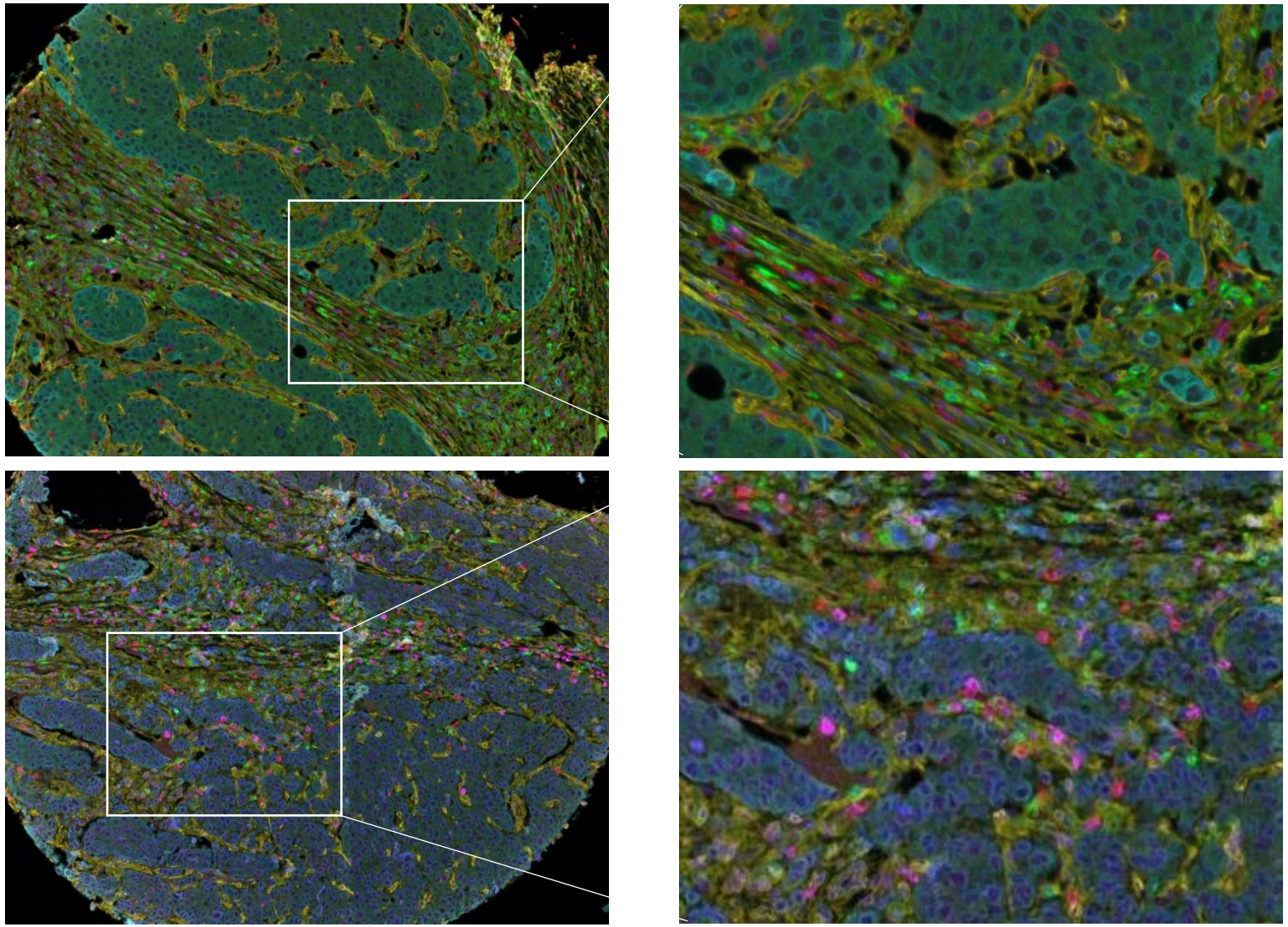


Figure 3.12: Representative Composite Images of the optimised multiplex IHC conditions**.** Ghanaian breast cancer cores stained with 5 antibody-opals. Images were taken at, and displayed at 20X magnification (left), and 2.6 times further magnified area within the small white boxes (right).

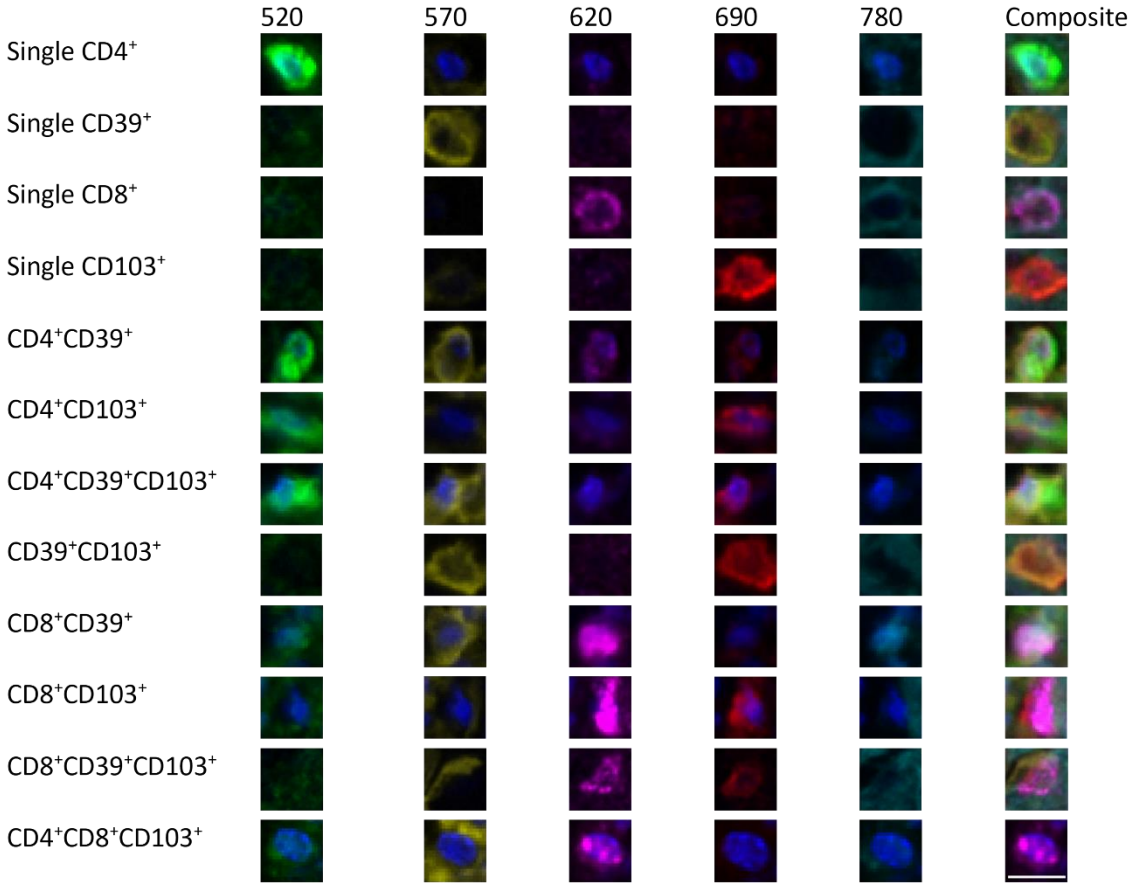



Figure 3.13: Representative images of each phenotype present in Ghanaian breast cancer tissue after staining with a 5-plex IHC panel**.** Ghanaian breast cancer cores were stained with 5 antibody-opals. Each phenotype of interest is shown in the rows (if a marker is not shown, assume negative expression). Each column shows the individual channels, with the last column showing the composite view. Images were taken on the Polaris at 20X, with images further magnified (representative bottom right scale bar = 10µm).

## 3.4 Training inform software for data acquisition

Adequate optimisation of the multiplex panel was confirmed by visual analysis and numerical analysis of signal intensities. However, it was vital to ensure that the staining produced by the protocol could be used on the inform software to segment tumour into epithelia and stroma, segment cells, and phenotype these cells. A flowchart of the process is shown in **Figure 3.14.** Following the whole slide scanning on the Polaris, the slides were viewed in the program Phenochart, where a number of cores were selected as training images and imported into inform. Inform was programmed to use the CK-Opal780 staining to categorise epithelium from stroma, and example tissue regions for both categories were selected on a range of different cores to ensure the software correctly segmented the tissue across the whole TMA set. The background i.e. slide areas with no tissue was also categorised to eliminate any non-specific staining being included in the analysis. Representative cores and their tissue segmentation by inform are shown in **Figure 3.15** below.

The DAPI staining was then used to aid the identification and segmentation of individual cells within the cores. Parameters including the minimum DAPI signal intensity, minimum cell size and splitting sensitivity were adjusted to achieve the most accurate cell segmentation. Cell membranes were also outlined, using the CK and CD8 staining as a guide. After tissues and cells were segmented as accurately as possibly, 5 examples of each phenotype were identified and shown to the software before training the phenotype classifier to assign phenotypes to each cell in the training project cores. Cells with no staining of interest were also trained as ‘others’ and were emitted from the numerical output. Importantly, the phenotypes assigned by the software were critically assessed and

corrected if a cell was incorrectly classified, and the software was re-trained repeatedly until the cells were correctly phenotyped. The algorithm created by this training project was then applied to all cores in the Ghanaian TMA series to quantify the different immune cell phenotypes infiltrating the tumours.

RStudio was then used to run the package PhenoptrReports to consolidate all the inform output and translate it into an excel sheet, to give cell counts, cell densities, among other analyses for each core.

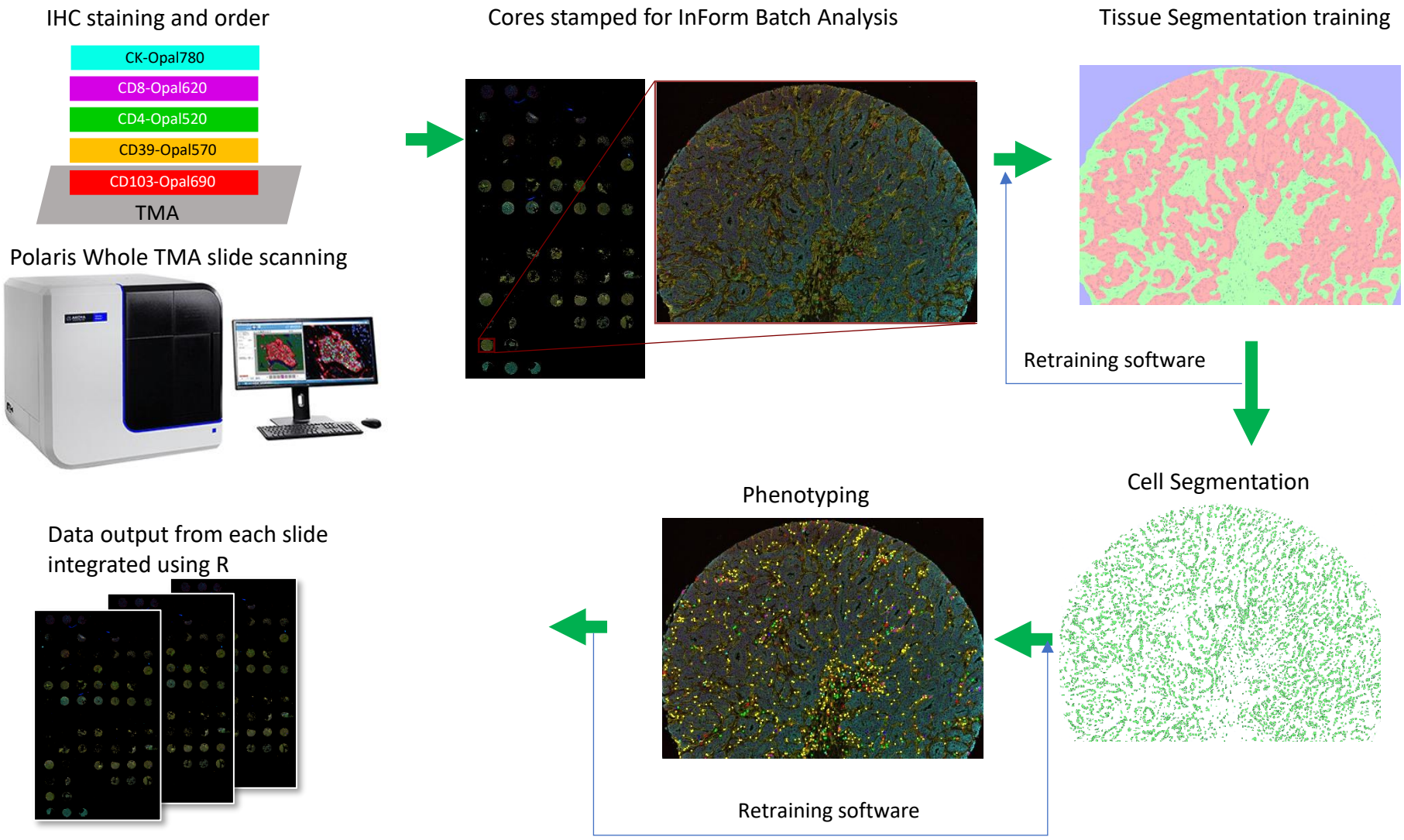



Figure 3.14: The Multiplex IHC staining and analysis process. Examples cores were imaged on the Polaris, and displayed at 20X.

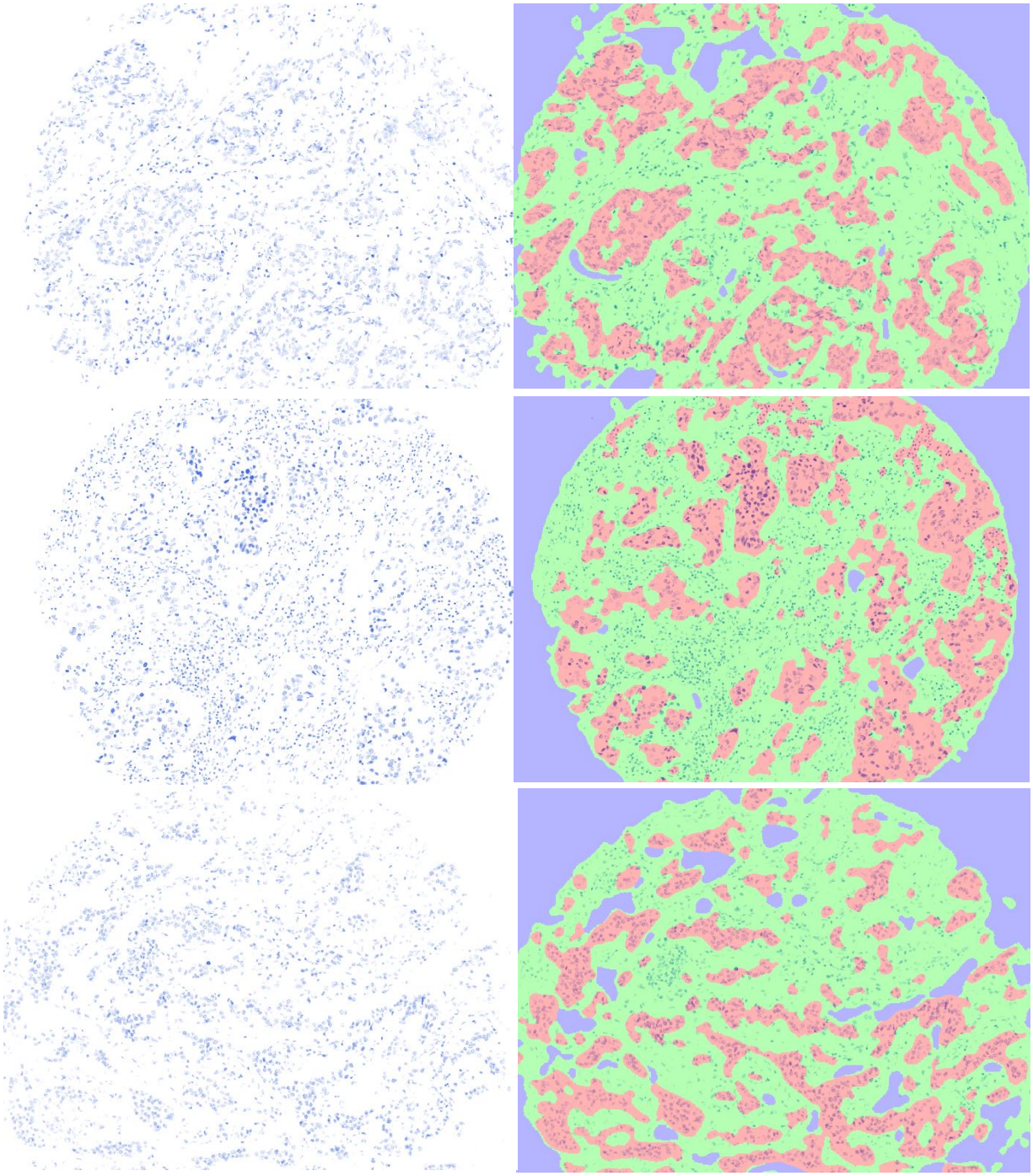


Figure 3.15: Tissue segmentation of Ghanaian breast cancer TMA cores. Representative cores from the Ghanaian breast cancer TMA are shown with just the DAPI view to visualise tissue pathology, and on the right, the tissue segmentation performed by the inform tissue analysis software. In red are the epithelial regions, green represents the stromal regions and blue represents the areas of the slide with no tissue. Images were taken on the Polaris. Images were obtained and are displayed at 20X magnification.

## 3.5. Patient Characteristics

The study cohort consisted of 142 cases of invasive breast cancer diagnosed at Department of Pathology, Cape Coast Teaching Hospital, Ghana. Patient Clinical data and clinicopathological data were obtained from the Histopathology registry. A follow-up of patients was between 2015-2019. Ethical clearance was obtained from the Cape Coast Teaching Hospital's Ethical Review Board. The Tissue Microarray were constructed using archival FFPE blocks from patients' samples submitted to the pathology department for histopathology diagnosis. Three replicate cores were taken from each patient sample; 2 cores from the periphery of the tumour and 1 core from the centre. Of this cohort, those with minimal patient follow-up information were excluded from the analysis. Additionally, cores were lost from the TMA during staining, usually due to MWT or washing off, and some cores were excluded from analysis due to the core being incomplete (<20% of core) or having no identifiable cells.

Of the 97 patients remaining in the TMA array that were analysed after these exclusions, 69.3% had died from breast cancer, and 30.7% (or 62.9 dead, 27.8 alive, 9.3 missing data) were alive. All patients were female and their demographics are shown in **Table 3.10.** In particular, higher frequencies of patients presented with Grade 2 (35%) and Grade 3 (52%), than the least severe Grade 1 (13%), with similar frequencies being seen for tumour stage and the Nottingham Prognostic Index (NPI) (Galea et al., 1992). Though, only tumour grade and NPI significantly correlated with patient survival.

In terms of their hormonal status/molecular subtype, 30.9% were Luminal A, 9.6% Luminal B, 12.8% HER2+, and the most common type was TNBC, accounting for 46.8% of patients. Molecular subtype correlated with survival significantly, as shown in (**Table 3.10**) with TNBC patients having the shortest mean survival time post-surgery out of the groups. Only the PR and ER expression correlated with prolonged survival significantly, with HER2 expression not being advantageous.

Furthermore, lymph node involvement, histological type, tumour laterality and beast quadrant location did not correlate with survival.

All patients received surgery to remove the tumour/s, but those with more advanced or larger tumours received adjuvant chemotherapy prior to surgery. Consequently, patients who received adjuvant chemotherapy had a significantly shorter mean survival, shown by the highly significant P value.

| Parameter | | N (%) | Mean survival (months) | SE | 95% confidence interval | | Survival distribution (Log rank Mantel-Cox) of cohort | |
|---|---|---|---|---|---|---|---|---|
| | | | | | Lower | Upper | Chi-square | P value |
| Age | Premenopausal (<50 years) | 50 (52.1) | 16.69 | 2.221 | 12.34 | 21.04 | 2.693 | 0.101 |
| | Postmenopausal (≥50 years) | 46 (47.9) | 23.91 | 2.875 | 18.27 | 29.54 | | |
| | Overall | 96 (100) | 20.73 | 1.939 | 16.93 | 24.53 | | |
| Tumour Grade | 1 | 12 (13.5) | 32.43 | 4.27 | 24.06 | 40.8 | 14.033 | **<0.001** |
| | 2 | 31 (34.8) | 22.96 | 3.43 | 16.24 | 29.69 | | |
| | 3 | 46 (51.7) | 12.2 | 1.466 | 9.32 | 15.07 | | |
| | Overall | 89 (100) | 20.4 | 1.963 | 16.55 | 24.24 | | |
| Tumour stage | 1 | 6 (8.5) | Samples too small to perform Kaplan-Meier | | | | | |
| | 2 | 23 (32.4) | | | | | | |
| | 3 | 42 (59.2) | | | | | | |
| Nottingham Prognostic Index | Good | 2 (4.2) | Samples too small to perform Kaplan-Meier | | | | | |
| | Moderate | 19 (39.6) | | | | | | |
| | Poor | 27 (56.3) | | | | | | |
| Hormonal status/molecular subtype | Luminal A | 29 (30.9) | 29.83 | 3.723 | 22.53 | 37.13 | 12.252 | **0.007** |
| | Luminal B | 9 (9.6) | 18 | 4.056 | 10.05 | 25.95 | | |
| | HER2+ | 12 (12.8) | 20.3 | 4.269 | 11.93 | 28.67 | | |
| | TNBC | 44 (46.8) | 13.31 | 1.708 | 9.96 | 16.66 | | |

| | | | | | | | | |
|---|---|---|---|---|---|---|---|---|
| | Overall | 94 (100) | 21.55 | 1.987 | 17.65 | 25.44 | | |
| ER | Positive | 24 (24.7) | 31.45 | 4.025 | 23.56 | 39.34 | 8.447 | **0.004** |
| | Negative | 73 (75.3) | 15.62 | 1.609 | 12.47 | 18.78 | | |
| | Overall | 97 (100) | 21.05 | 1.941 | 17.24 | 24.85 | | |
| PR | Positive | 29 (29.9) | 28.57 | 3.845 | 21.03 | 36.1 | 5.354 | **0.021** |
| | Negative | 68 (70.1) | 16.83 | 1.853 | 13.19 | 20.46 | | |
| | Overall | 97 (100) | 21.05 | 1.941 | 17.24 | 24.85 | | |
| HER2 | Positive | 20 (21.7) | 19.44 | 3.345 | 12.88 | 25.99 | 0.479 | 0.489 |
| | Negative | 72 (78.3) | 20.31 | 2.165 | 16.07 | 24.56 | | |
| | Overall | 92 (100) | 21.03 | 1.98 | 17.15 | 24.91 | | |
| Lymph node involvement | Involved | 40 (81.6) | 18.8 | 2.334 | 14.23 | 23.38 | 0.36 | 0.548 |
| | Not involved | 9 (18.4) | 21 | 4.462 | 12.26 | 29.75 | | |
| | Overall | 49 (100) | 19.31 | 2.128 | 15.14 | 23.48 | | |
| Neoadjuvant chemotherapy | Yes | 57 (69.5) | 13.83 | 1.538 | 10.81 | 16.84 | 15.735 | **<0.001** |
| | No | 25 (30.5) | 30.59 | 3.095 | 24.52 | 36.66 | | |
| | Overall | 82 (100) | 19.55 | 1.754 | 16.11 | 22.99 | | |
| Histological type | Invasive ductal carcinoma | 89 (91.8) | Samples too small to perform Kaplan-Meier | | | | | |
| | Invasive lobular carcinoma | 4 (4.1) | | | | | | |
| | Invasive colloid carcinoma | 1 (1) | | | | | | |
| | DCIS | 1 (1) | | | | | | |

| | | | | | | | | |
|---|---|---|---|---|---|---|---|---|
| | Tubular carcinoma | 1 (1) | | | | | | |
| | Lymphocytic lymphoma | 1 (1) | | | | | | |
| | Overall | 97 (100) | | | | | | |
| Laterality | Right | 51 (53.7) | 19.74 | 2.422 | 14.99 | 24.48 | 0.006 | 0.936 |
| | Left | 44 (46.3) | 19.93 | 2.702 | 14.63 | 25.22 | | |
| | Overall | 95 (100) | 20.73 | 1.939 | 16.93 | 24.53 | | |
| Quadrants | Outer quadrants | 16 (29.6) | 20.56 | 3.445 | 13.81 | 27.31 | 1.827 | 0.401 |
| | Inner quadrants | 6 (11.1) | 12 | 2.236 | 7.62 | 26.38 | | |
| | Central | 32 (59.3) | 18.57 | 2.611 | 13.45 | 23.69 | | |
| | Overall | 54 (100) | 19.95 | 1.994 | 15.05 | 22.86 | | |

*Table 3.10: Summary table of the patient characteristics and their correlation with survival.* For each clinicopathological parameter, the frequency of patients in each group are shown as well as the valid percentage, as some patients had variables missing. Survival distribution was performed by Kaplan-Meier in SPSS for each parameter. For parameters where group sample sizes are too small, these have been left blank.

## 3.6. Intra-tumoural phenotype population densities within African Breast Cancers

For each core, the cells were categorised into one of 13 phenotypes based on the positive expression of CD4, CD8, CD103 and CD39. Phenotype counts and cell densities were calculated by the inform software for each tumour region. Unstained cells were allocated as other and counted within each tissue type. Epithelial, stromal and total areas were used to calculate cell densities for each core and region. For patients who had more than one core stained, average cell densities were calculated. **Figure 3.16** presents the phenotype densities for each patient plotted as a dot, with the black line marking the median density. Phenotypes are delineated only by the positive markers, for example $CD4^+$ represents $CD4^+CD8^-CD103^-CD39^-$.

As can be seen in the plot, cell densities of the different phenotypes infiltrating the epithelium of breast cancer patients were highly variable. By far, the population with the highest median density marker was $CD39^+$ (648.4), followed by $CD8^+$ (222.9) and $CD8^+CD39^+$ (180.2) phenotypes. Interestingly, the median densities for single $CD8^+$ and double positive $CD8^+CD39^+$ were markedly higher than single $CD4^+$ (98.12) and double positive $CD4^+CD39^+$ (66.49) populations, but the opposite was seen when comparing the triple positive populations $CD4^+CD103^+CD39^+$ (12.41) and $CD8^+CD103^+CD39^+$(0). Median densities for $CD103^+$ and $CD39^+CD103^+$ were relatively low, while $CD4^+CD103^+$ and $CD8^+CD103^+$ double positive populations were zero. A small population of $CD4^+CD8^+CD39^+$ cells (0) was also observed.

From the dot plot it is apparent that most patients had low densities for all phenotypes (except $CD39^+$, $CD8^+$ and $CD8^+CD39^+$), shown by a high number of dots at the lower end of the density scale. Due to the vast amount of data generated by the multiplex IHC staining, the CD8 TP (triple positive, $CD8^+CD103^+CD39^+$) population was focused on for more in-depth survival analysis and correlation with clinicopathological parameters. Specifically, CD8 TP density was correlated with overall survival (OS), with OS being the percentage of patients alive during the time of diagnosis to the most recent follow-up.

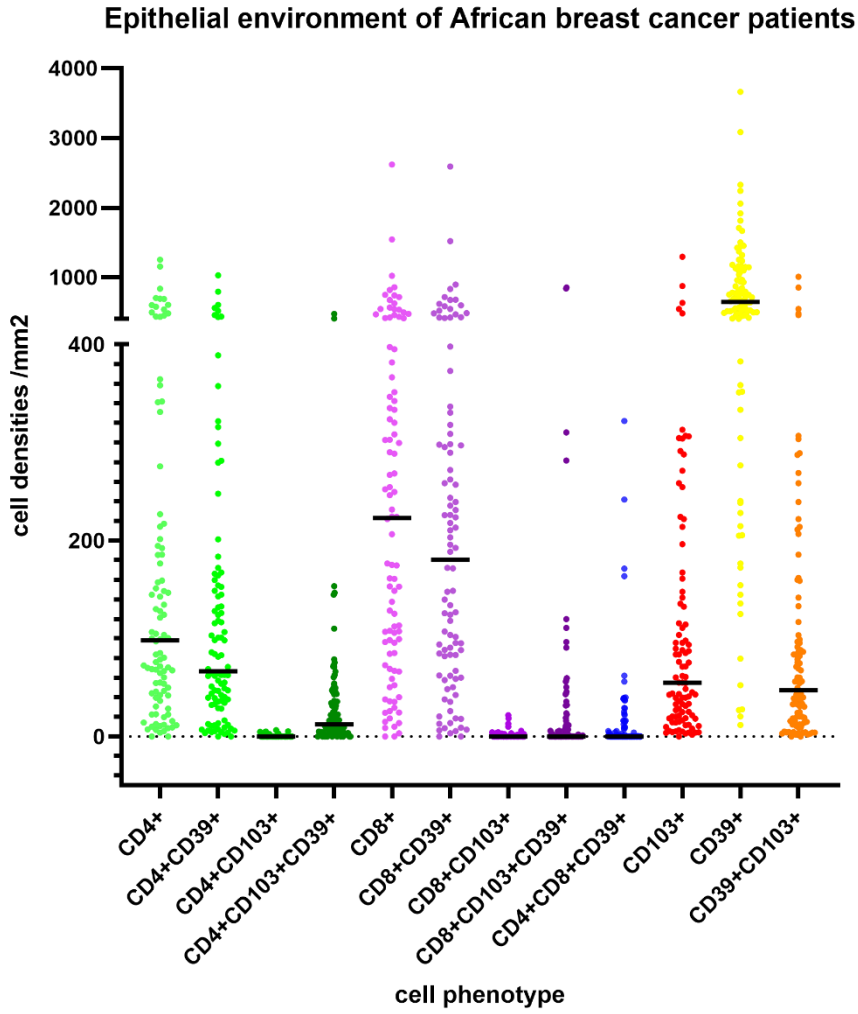



Figure 3.16. Intra-epithelial phenotype population densities within African Breast Cancer tumours. Cell densities of different T cell phenotypes have been plotted, with each dot representing a patient, and the lines marking the median density. The different shades of green indicate the single, double and triple $CD4^+$ phenotypes, while the purple shades indicate the single, double and triple $CD8^+$ phenotypes. Descending medians: $CD39^+$ (648.4), $CD8^+$ (222.9), $CD8^+CD39^+$ (180.2), $CD4^+$ (98.12), $CD4^+CD39^+$ (66.49), $CD103^+$ (54.74), $CD39^+CD103^+$ (46.97), $CD4^+CD103^+CD39^+$ (12.41). $CD4^+CD103^+$, $CD8^+CD103^+$, $CD8^+CD103^+CD39^+$ and $CD4^+CD8^+CD39^+$ had medians of 0.

## 3.7. Patients receiving neoadjuvant chemotherapy had higher $CD8^+CD103^+CD39^+$ epithelial, stromal and total tumour density.

$CD8^+CD103^+CD39^+$ (referred to as CD8 TP) were the phenotype of interest in this study, thus the correlation between CD8 TP density and clinicopathological factors was explored, as shown in **Table 3.11** below. As observed by the p values generated by the cross-tabulation Chi-squared tests, there was no significant correlation seen between CD8 TP density and patient tumour grade, stage, hormonal status, histopathological type, receptor expression, NPI, and lymph node involvement for stromal, epithelial and total tumour regions. Notably, whether a patient received neoadjuvant chemotherapy or not significantly correlated with CD8 TP density for all 3 tumour region categories. It was found that of patients with high total tumour CD8 TP density, 91% had received neoadjuvant chemotherapy, while only 9% had not.

Stromal CD8 TP density was found to be linked to patient age, with pre-menopausal patients (<= 50 years) accounting for 75% of high density CD8 TP counts, and post-menopausal patients accounting for just 25%. The tumour location was also linked to total tumour CD8 TP density. Specifically, 73% of high CD8 TP density patients had tumours located in the right breast compared to 27% with left-located tumours. Furthermore, whether the tumour was located in the inner quadrants, outer quadrants or the centre of the breast significantly correlated with total tumour CD8 TP density.

| | Epithelial TP CD8+CD103+CD39+ T cells | | | Stromal TP CD8+CD103+CD39+ T cells | | | Total Tumour TP CD8+CD103+CD39+ T cells | | |
|---|---|---|---|---|---|---|---|---|---|
| | **Low (%)** | **High (%)** | **P-value** | **Low (%)** | **High (%)** | **P-value** | **Low (%)** | **High (%)** | **P-value** |
| **Age** | | | | | | | | | |
| Premenopausal (<50) | 37 (48) | 13 (68) | 0.111 | 38 (47.5) | 12 (75) | **0.044** | 36 (49) | 14 (64) | 0.217 |
| Postmenopausal (≥ 50) | 40 (52) | 6 (32) | | 42 (52.5) | 4 (25) | | 38 (51) | 8 (36) | |
| **Tumour grade** | | | | | | | | | |
| 1 | 9 (12.5) | 3 (18) | 0.797 | 10 (13) | 2 (14) | 0.503 | 9 (13) | 3 (15) | 0.576 |
| 2 | 26 (36) | 5 (29) | | 28 (37) | 3 (21) | | 26 (37.7) | 5 (25) | |
| 3 | 37 (51.5) | 9 (53) | | 37 (50) | 9 (65) | | 34 (49.3) | 12 (60) | |
| **Tumour stage** | | | | | | | | | |
| 1 | 5 (9.1) | 1 (6.3) | 0.674 | 6 (10.3) | 0 (0) | 0.270 | 5 (9.6) | 1 (5.3) | 0.611 |
| 2 | 19 (34.5) | 4 (25) | | 20 (34.5) | 3 (23.1) | | 18 (34.6) | 5 (26.3) | |
| 3 | 31 (56.4) | 11 (68.8) | | 32 (55.2) | 10 (76.9) | | 29 (55.8) | 13 (68.4) | |
| **Nottingham Prognostic Index (NPI)** | | | | | | | | | |
| Good | 2 (5.3) | 0 (0) | 0.756 | 2 (5.1) | 0 (0) | 0.484 | 2 (5.7) | 0 (0) | 0.620 |
| Moderate | 15 (39.5) | 4 (40) | | 14 (35.9) | 5 (55.6) | | 13 (37.1) | 6 (46.2) | |
| Poor | 21 (55.3) | 6 (60) | | 23 (59) | 4 (44.4) | | 20 (57.1) | 7 (53.8) | |
| **Hormonal status** | | | | | | | | | |
| Luminal A | 24 (31.2) | 5 (29.4) | 0.987 | 25 (31.3) | 4 (28.6) | 0.978 | 27 (34.6) | 6 (30) | 0.975 |
| Luminal B | 7 (9.1) | 2 (11.8) | | 8 (10) | 1 (7.1) | | 7 (9) | 2 (10) | |
| HER2+ | 10 (13) | 2 (11.8) | | 10 (12.5) | 2 (14.3) | | 10 (12.8) | 2 (10) | |
| TNBC | 36 (46.8) | 8 (47.1) | | 37 (46.3) | 7 (50) | | 34 (43.6) | 10 (50) | |
| **ER** | | | | | | | | | |
| Positive | 19 (24.4) | 5 (26.3) | 0.859 | 20 (24.7) | 4 (25) | 0.979 | 19 (25.3) | 5 (22.7) | 0.803 |
| Negative | 59 (75.6) | 14 (73.7) | | 61 (75.3) | 12 (75) | | 56 (74.7) | 17 (77.3) | |
| **PR** | | | | | | | | | |
| Positive | 23 (29.5) | 6 (31.6) | 0.858 | 25 (30.9) | 4 (25) | 0.640 | 22 (29.3) | 7 (22.7) | 0.823 |
| Negative | 55 (70.5) | 13 (68.4) | | 56 (69.1) | 12 (75) | | 53 (70.7) | 15 (77.3) | |
| **HER2** | | | | | | | | | |
| Positive | 16 (21.1) | 4 (25) | 0.728 | 17 (21.5) | 3 (23.1) | 0.900 | 16 (21.9) | 4 (21.1) | 0.935 |

| | | | | | | | | | |
|---|---|---|---|---|---|---|---|---|---|
| Negative | 60 (78.9) | 12 (75) | | 62 (78.5) | 10 (76.9) | | 57 (78.1) | 15 (79) | |
| **Lymph node involvement** | | | | | | | | | |
| Involved | 30 (81.1) | 10 (83.3) | 0.861 | 32 (84.2) | 8 (72.7) | 0.386 | 30 (85.7) | 10 (71.4) | 0.243 |
| Not involved | 7 (18.9) | 2 (16.7) | | 6 (15.8) | 3 (27.3) | | 5 (14.3) | 4 (28.6) | |
| **Neoadjuvant chemotherapy** | | | | | | | | | |
| Yes | 40 (63.5) | 17 (89.5) | **0.031** | 42 (63.6) | 15 (93.8) | **0.019** | 37 (61.7) | 20 (90.9) | **0.011** |
| No | 23 (36.5) | 2 (10.5) | | 24 (36.4) | 1 (6.2) | | 23 (38.3) | 2 (9.1) | |
| **Histological type** | | | | | | | | | |
| Invasive Ductal Carcinoma | 71 (91) | 18 (94.7) | 0.957 | 74 (91.4) | 15 (93.8) | 0.962 | 68 (90.7) | 21 (95.5) | 0.942 |
| Invasive Lobular Carcinoma | 3 (3.8) | 1 (5.3) | | 3 (3.7) | 1 (6.2) | | 3 (4) | 1 (4.5) | |
| DCIS | 1 (1.3) | 0 (0) | | 1 (1.2) | 0 (0) | | 1 (1.3) | 0 (0) | |
| Invasive Colloid Carcinoma | 1 (1.3) | 0 (0) | | 1 (1.2) | 0 (0) | | 1 (1.3) | 0 (0) | |
| Lymphocytic Lymphoma | 1 (1.3) | 0 (0) | | 1 (1.2) | 0 (0) | | 1 (1.3) | 0 (0) | |
| Tubular Carcinoma | 1 (1.3) | 0 (0) | | 1 (1.2) | 0 (0) | | 1 (1.3) | 0 (0) | |
| **Laterality** | | | | | | | | | |
| Right | 37 (48.7) | 14 (73.7) | 0.051 | 42 (53.2) | 9 (56.3) | 0.821 | 35 (47.9) | 16 (72.7) | **0.041** |
| Left | 39 (51.3) | 5 (26.3) | | 37 (46.8) | 7 (43.8) | | 38 (52.1) | 6 (27.3) | |
| **Quadrants involved** | | | | | | | | | |
| Outer | 10 (23.8) | 6 (50) | 0.129 | 11 (26.2) | 5 (41.7) | 0.291 | 8 (20.5) | 8 (53.3) | **0.033** |
| Inner | 6 (14.3) | 0 (0) | | 6 (14.3) | 0 (0) | | 6 (15.4) | 0 (0) | |
| Central | 26 (61.9) | 6 (50) | | 25 (59.5) | 7 (58.3) | | 25 (64.1) | 7 (46.7) | |

*Table 3.11: Correlations between the epithelial, stromal and total CD8+CD103+CD39+ T cell densities and different clinicopathological features in breast cancer cases*. Cross tabulation of clinicopathological features is displayed with the number and percentage of patients within each subgroup for high and low CD8 TP density. High or low density of $CD8^+CD103^+CD39^+$ T cells was defined using X-tile. Correlations were performed using a chi-squared test. Significant P values are in bold.

## 3.8. The presence of $CD8^+CD103^+CD39^+$ cells in the tumours of African breast cancer patients do not predict survival

Kaplan-Meier survival plots were generated for CD8 TP densities within the stromal, epithelial regions as well as the total tumour area. As shown in **Figure 3.17, 3.18 and 3.19 A**, CD8 TP high or low density did not correlate with improved or worsened survival for any tissue category. Additionally, the total tumour CD8 TP density Kaplan-Meier plot was stratified to assess the correlation of density with survival for TNBC patients specifically. CD8 TP density did not correlate with survival for this subset of patients, as shown in **Figure 3.19**.

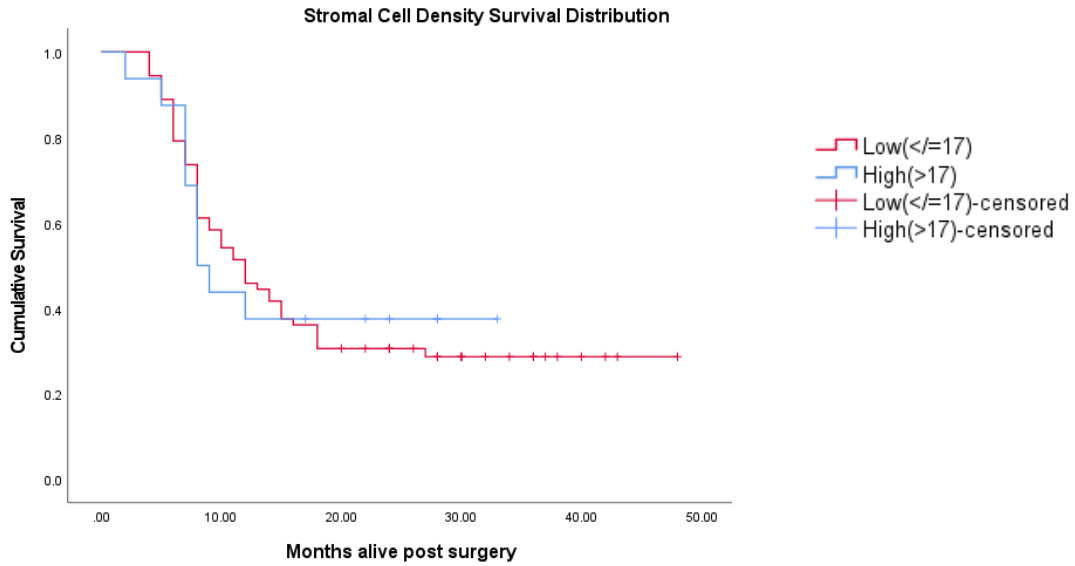



Figure 3.17: The presence of high numbers of CD8+CD103+CD39+ in the stroma of African breast cancer tumours is not a predictor of survival**.** Tumours from Ghanaian breast cancer patients were stained in multiplex immunohistochemistry for CD4, CD8, CD103, CD39 and CK, and CD8+CD103+CD39+ density was quantified using inform software. Using X-tile a low cell density was defined as </=17 cells/$mm^2$ and a high cell density was >17 cells/$mm^2$. 72 patients had a low density, while 16 patients had a high density. A Kaplan-meier plot was generated using survival status and months alive post-surgery. P = 0.882 (not significant).

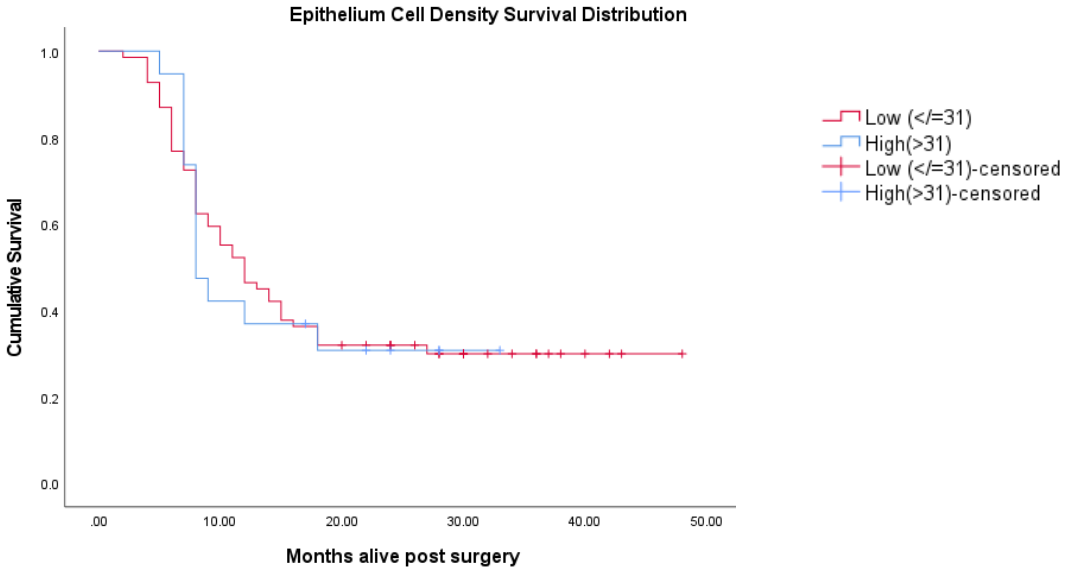



Figure 3.18: The presence of high numbers of CD8+CD103+CD39+ in the tumour epithelium of African breast cancer tumours is not a predictor of survival**.** Tumours from Ghanaian breast cancer patients were stained in multiplex immunohistochemistry for CD4, CD8, CD103, CD39 and CK, and CD8+CD103+CD39+ density was quantified using inform software. Using X-tile a low cell density was defined as </=31 cells/mm$^2$ and a high cell density was >31 cells/mm$^2$. 69 patients had a low density, while 19 patients had a high density. A Kaplan-meier plot was generated using survival status and months alive post-surgery. P = 0.945 (not significant).

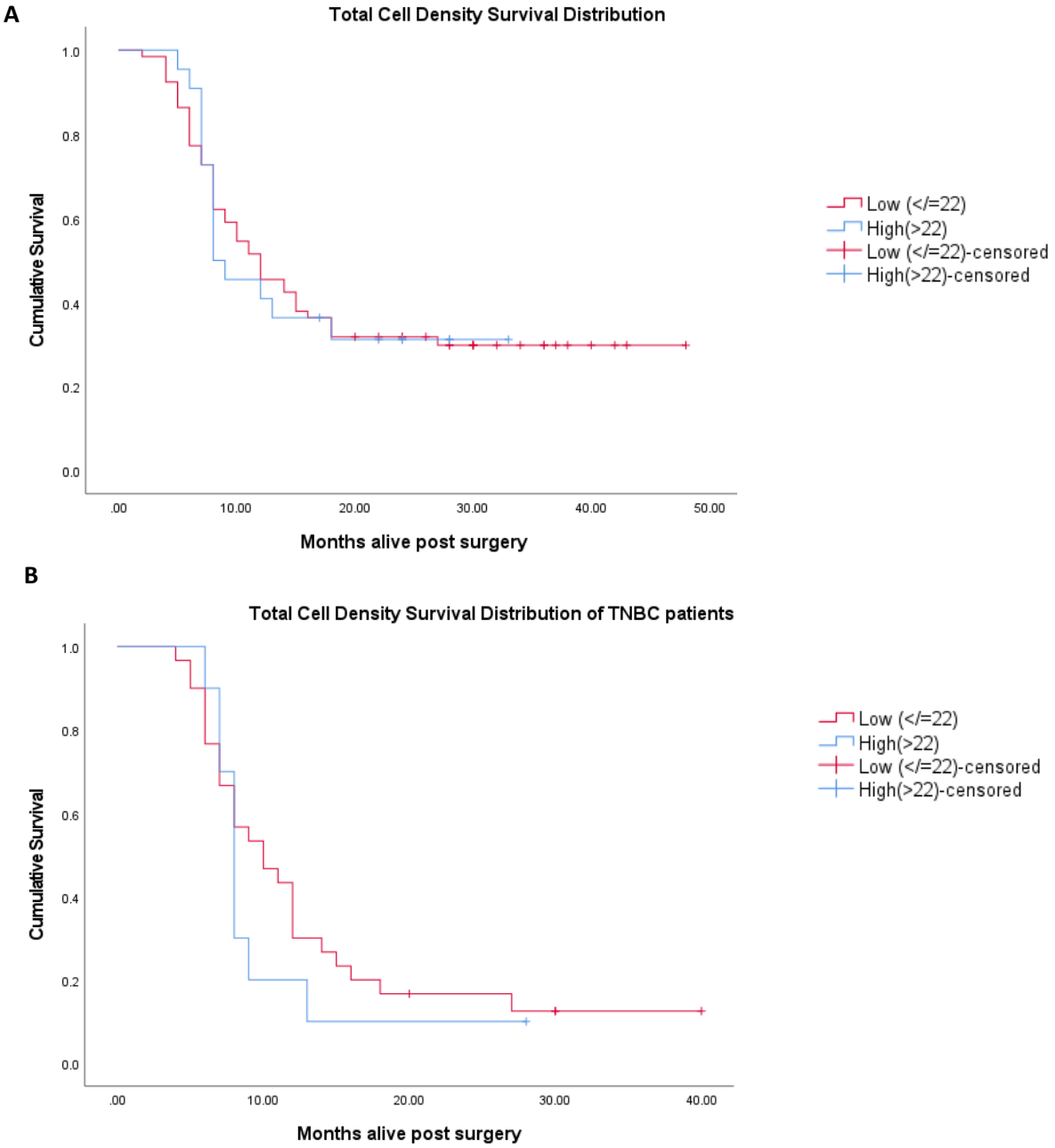



Figure 3.19: The presence of high numbers of CD8+CD103+CD39+ in the tumours of African breast cancer patients is not a predictor of survival**.** Ghanaian breast cancer patients were stained in multiplex immunohistochemistry for CD4, CD8, CD103, CD39 and CK, and CD8+CD103+CD39+ density was quantified using inform software. Using X-tile a low cell density was defined as </=22 cells/mm$^2$ and a high cell density was >22 cells/mm$^2$. A Kaplan-Meier plot was generated using survival status and months alive post-surgery for all patients (P = 0.882, not significant), and TNBC patients alone (P = 0.970, not significant). Analysing all patients together found 66 patients had a low density, while 22 patients had a high density. Specific analysis of TNBC patients found 30 individuals had a low density, and 10 patients had a high density.

# Chapter 4: Discussion

This study clearly showcases the successful optimisation of a 5-panel multiplex IHC, including 4 immune cell biomarkers to categorise more than 12 distinct phenotypes in the epithelial and stromal regions of breast cancer tumours. Robust trouble-shooting overcame not only tissue-type specific optimisation hurdles, but also TMA-specific issues, which was especially crucial due to the tumour tissue conditions post-surgery varying greatly across countries. For the first time in the literature, this study applied the multiplex IHC technique to breast cancer tissues from an African population, an understudied population with notoriously more aggressive tumours, and a critically high mortality rate ((Der et al., 2015; Ohene-Yeboah & Adjei, 2012; Stark et al., 2010; Thomas et al., 2017)). Focussing specifically on $CD8^+CD103^+CD39^+$ T cells (CD8 $T_{RM}$ phenotype), several clinicopathological parameters correlated with an increased CD8 $T_{RM}$ density, including age, whether neoadjuvant chemotherapy was received, tumour laterality and location. Kaplan-Meier survival analysis found no correlation between stromal, epithelial, and total tumour cell density and improved prognosis, even when TNBC patients were studied in isolation.

## 4.1. The Optimisation Process

As detailed in Chapter 3, initial optimisation involved conventional IHC to identify the specificity of the antibodies and their optimal concentrations. Optimal conditions including the appropriate antigen retrieval method for each antigen, antibody positions and opal concentration were obtained using monoplex IHC and the full multiplex IHC protocol. Despite the same tissue type being used throughout, differences in staining were seen when translating the Nottingham-optimised conditions to the Ghanaian cohort, emphasising the

need for TMA-specific optimisation. A tissue-specific spectral library was also assembled, which accounted for staining and autofluorescence variations unique to breast cancer tissue. This contrasts what is performed in studies published in the literature (Pulsawatdi et al., 2020; Sun et al., 2021), where the majority of the optimisation uses, and the spectral library is assembled from tonsil tissue. Using the tissue and TMA of interest throughout optimisation prevented set-backs which inevitably arising when moving from a control tissue such as tonsil, to the target tissue.

Antigen retrieval pH value was found to be critical to achieving optimal staining quality, as established previously in the literature (Pulsawatdi et al., 2020; Sun et al., 2021). In some cases, reagents supplied by the Opal vendor, Akoya Biosciences, did not give the best staining results. For example, the opal kit blocking buffer did not achieve optimal non-specific staining. Instead, a 1X BSA additional blocking step was found to control background staining.

This project also saw the importance of finding an antigen retrieval method that suits the majority of/all of the biomarkers in the panel. Following previous work done within the group on CRC tissue, AR9 buffer was initially used for all monoplex antibody-opals to allow easy integration of all protocols into one. Though, this was not possible due to the harshness of AR9 creating too much background signal for CD103-Opal690.

An overarching theme that was seen during this labour-intensive process was that the parameters determined as optimal by one step often need to be adjusted further when translated to the next step in the protocol, usually due to the emergence of bleed-through.

With the ordering of antibody-opal pairs, the optimal positioning of each pair was not always possible. For example, CD4-Opal520 which had some background signal could have benefited from being positioned first to limit the antigen retrieval exposures, but this was not possible due to the specific parameters required for clear CD103-Opal690 staining. Another step in the optimisation process was to verify that the staining conditions were the same on the Polaris, as on the Mantra which was used in the initial stages. Translating the conditions onto the Polaris required minimal effort, as long as the Mantra:Polaris signal difference was factored in when optimising the opal concentrations. This study continually assessed the Mantra-captured intensities by converting the target intensity (given for Polaris intensity) to the Mantra values.

Upon fully optimising the multiplex panel and staining the TMA slide set, the images were analysed in inform. Tissue and cell segmentation training were accomplished relatively efficiently, enabled due to the accurate epithelial CK staining distinguishing epithelium from stroma, and DAPI evenly staining the cell nuclei. Training the software to recognise phenotypes could be done using two approaches: Assigning multi-marker phenotypes to the cells in one project, or training different projects to recognise each of the markers and then merging the data together to give all the multi-marker combinations. This project used the approach of assigning all multi-marker phenotypes in one project, which allowed the accurate selection of at least 5 examples of each phenotypes. Though this was often time-consuming for the rarer triple positive populations, it did enable the software to show what phenotypes it was assigning to each cell so errors could be easily rectified. This approach allowed the identification of a $CD4^{+}CD8^{+}CD39^{+}$ population of cells which otherwise would not have been focused on if doing individual marker projects and merging them. It would be

interesting to use the other training approach and analyse the difference in cell phenotyping.

Multiple factors led to the sample size of 97 analysable patients compared to the total cohort of 142 cases. Firstly, the numerous rounds of MWT and repetitive washes caused a number of cores to be lost from the slide. This highlights one of the limitations of multiplex IHC, though this sample size is still a great achievement considering this cohort's immune infiltration has never been studied in multiplex IHC. Among the patients, full clinicopathological profiling was often not achieved due to limited ability to follow up patients after treatment.

## 4.2. Patient Demographics

In alignment with existing literature on Ghanaian breast cancer, higher frequencies of patients presented at the later stages 2 and 3 than seen in Caucasians (Thomas et al., 2017), and the most common hormonal type diagnosed was TNBC (Der et al., 2015). A high mortality rate and pre-menopausal diagnosis age were seen, in agreement with literature on Ghanaian women (GLOBOCAN 2020., Ohene-Yeboah & Adjei, 2012).

Patients within this study are diverse in terms of molecular pathology, histological type, and tumour location, reflective of the established concept of breast cancer being a highly heterogenous disease and consequently each subtype of cancer responding optimally to different treatment regimes (Sorlie et al, 2003). However, in contrast to the complex array of treatment avenues used in developed countries (treatment reviewed by Loibl et al, 2021), socioeconomical constraints prevent such treatment plans being accessed in Ghana, patients only received surgery and in some cases, neoadjuvant chemotherapy.

## 4.3. The immune landscape of African Breast cancer tumours

Within the breast cancer tumour microenvironment, many types of immune cells have been identified, and the immune system has the dual capability to inhibit or promote tumour establishment, expansion and metastasis (Nagarajan & Mcardle, 2018). Broadly, the anti-tumour immune cells are activated cytotoxic T cells ($CD8^+$), type 1 T helper cells ($CD4^+$ $T_H1$ cells) and NK cells. A number of pro-tumour immune cells collaborate to suppress the anti-tumour immune response, including Tregs (expressing CD4, CD39, and FoxP3), $T_H2$ cells, MDSCs and TAMs (Nagarajan & Mcardle, 2018).

This study used a 5-plex IHC to profile and quantify the diverse range of the different phenotype densities, but the specific phenotypes of interest were $CD8^+$ cells expressing CD39 and CD103, referred to hereon as CD8 TPs. Certainly, such complex and informative immune contexture data on African breast cancer patients has not been published. This study found low median densities of $CD4^+CD103^+$, $CD4^+CD103^+CD39^+$, $CD8^+CD103^+$ and $CD8^+CD103^+CD39^+$. It is established in the literature that CD103 marks CD4 and CD8 T cells as tissue-resident memory cells, or $T_{RM}$ (Savas et al, 2018), with CD103 as an independent marker, or co-expression with CD8 correlating with a better prognosis in breast cancers (Park et al, 2020; Wang et al, 2016; Egelston et al, 2019). Among this African cohort, low median densities of both double positive $T_{RM}$ and TP $T_{RMs}$ cells were seen, indicating tumours were poorly infiltrated with $T_{RM}$ cells.

This study found high $CD8^+$ and $CD8^+CD39^+$ median densities, which could be identifying two populations of effector T cell: bystander and tumour-specific effector T cells (Simoni et al, 2018). The expression of CD39 on CD8 T cell populations was previously found to distinguish tumour-specific effector T cells ($CD8^+CD39^+$) from bystander effector T cells ($CD8^+$) not

functionally involved in targeting the tumour (Simoni et al, 2018). From this literature it could be theorised that a high $CD8^+CD39^+$ density would correlate with survival, while a high $CD8^+$ density would not.

Building upon this theory, CD39 expression on CD8 $T_{RM}$ cells ($CD8^+CD103^+$) may distinguish them as tumour-specific, as shown by the Duhen group finding CD8 TP cells from a number of solid tumours (not including breast) were tumour antigen-specific and -reactive (Duhen et al, 2018). It could be postulated that the density of CD8 TPs identified in this breast cancer study would correlate with improved survival if this marker combination were truly identifying tumour-specific CD8 $T_{RM}$ cells. Evidence for high $CD39^+$ expression on $CD8^+$ $T_{RM}$ cells predicting luminal breast cancer survival has recently emerged (Losurdo et al, 2021). Though, the group performed flow cytometry of minced tumour samples, eliminating the immune cell spatial context and density that this multiplex IHC study provides.

Within this study, the highest median density was the single positive $CD39^+$ cells. CD39, an ectonucleotidase producing the immunosuppressive molecule adenosine, is expressed on B cells, fibroblasts, NK cells, Tregs, MDSCs, activated or memory CD4 T cells as well as the already discussed CD8 T cells (Allard et al, 2017)**.** Upon staining the African TMA, the inform software was trained to quantify only lymphocyte sized $CD39^+$ cells, therefore the CD39 single cells in this African cohort could include B cells such as Bregs and NK cells. It could be hypothesised that the high number of cells expressing CD39 without any T cell markers could be producing adenosine, which could accumulate in the tumour and suppress other immune cells. Sun *et al*, 2010 found that CD39 inhibition by POM-1 alleviated the tumour-induced suppression of $CD4^+$ and $CD8^+$ proliferation and increased CTL- and NK-cell cytotoxicity.

$CD4^+$ single T cells populations stained in this project would comprise of T helper cells including $T_H1$, $T_H2$, $T_H17$ as well as T regulatory cells. Further research could perform cytokine profiling to isolate which T helper cell types are dominating the breast cancer landscape, and a Th2-skewed response would be expected (Campbell et al, 2005). Treg cells would also be stained as $CD4^+CD39^+$ population in this study, it was found that >90% of Tregs expressed CD39 (Tøndell et al, 2020). Extensive data has suggested that $CD39^+$ Tregs are highly immune-suppressive, for example, $CD4^+CD39^+FoxP3^-$ Tregs were ~50-fold more suppressive compared to $FoxP3^+$ Tregs (Scurr et al, 2014). More recently, $CD39^+$ Tregs have been found to inhibit NK cell anti-tumour immunity in vivo and in vitro (Hu et al., 2017).

$CD103^+$ single density was high, aside from $T_{RM}$ cells, CD103 is expressed by Tregs, dendritic cells, as well as subset of NK cells (Marquardt et al, 2019). As $CD103^+$ Tregs would also be expressing CD4, and dendritic cells are seldom in tumours, the high CD103 in this cohort is likely NK cells. In breast cancer, higher tumour-infiltrating NK cells frequencies were seen in patients whose tumours had not spread to the lymph nodes (Rezaeifard et al, 2021). Future analysis of this African breast cancer cohort could incorporate the NK marker CD56 into the multiplex panel to study the effect on patient survival.

A rare subtype $CD4^+CD8^+CD39^+$ were discovered in this study. CD4/CD8 dual positivity was initially only thought to occur in the early T cell development stages, but a breast cancer study found $CD4^+CD8^+$ T cells with a similar cytotoxic potential to effector memory T cells (Desfrançois et al, 2009). Translating the theory that CD39 delineates tumour-specific T cells to the dual $CD4^+CD8^+$ phenotype could mean that in the context of this African breast cancer study, $CD4^+CD8^+CD39^+$ expression could be identifying another tumour-specific T cell subtype.

## 4.4. The correlation of $CD8^+CD103^+CD39^+$ density with clinicopathological features and patient survival

Specific focus on the correlation between the clinicopathological features and CD8 TP cell densities within the epithelia, stroma and total tumour found a high density for all correlated with neoadjuvant chemotherapy. Neoadjuvant chemotherapy was given to patients with larger, more aggressive tumours before surgically resecting the tumour (from which the TMAs were constructed). From this link it could be inferred that the treatment increases the number of CD8 TP cells infiltrating the tumour, or promotes the expression of CD39 and/or CD103 on already resident CD8 T cells. Neoadjuvant chemotherapy also correlates with a worse prognosis in this cohort. Whether these cells existed in the tumour prior to chemotherapy is not known but one study on African-American patients observed lower pathological complete response (pCR) to neoadjuvant chemotherapy than in Caucasians. Difference in immune infiltration/types of cells present may account for this difference (Killelea et al., 2015).

Analysis of CD8 TP density in this cohort found that younger patients had a higher density than patients in the post-menopausal category. For African breast cancer patients, this finding is novel, though studies using standard IHC showed CD8 TIL was significantly higher in younger patients (Abdou et al, 2020).

Kaplan Meier survival analysis found no significant correlation between epithelial, stromal or total tumour CD8 TP density and survival, in contrast to what was theorised. Though, the analysis of the different phenotypic densities clearly conveys the complex composition of immune cells within the breast cancer TME, and the cellular interactions that could be at

play. The correlation of one phenotype with survival is insufficient in assessing its function in the tumour as the whole immune contexture needs consideration.

It is highly plausible that the CD8 TPs identified in this study are highly potent and specific to the tumour, as proposed by the current research (Egelston et al, 2019; Duhen et al, 2018). The prognostic benefit may not be reflected due to these cells being functionally exhausted or being antagonised by pro-tumour immune-suppressive mechanisms that are likely present in the patients in the current study. Importantly, a gene expression profiling study found a higher proportion of exhausted CD8 TILs in black breast cancer patients than Caucasian patients (Yao et al, 2021). Exhaustion was defined by EOMES expression in combination with exhaustion markers such as PD-1 and LAG-3. In this study, CD8 TP cells may be of this exhausted phenotype, incapable of targeting the tumour, and therefore not improving survival. Cellular exhaustion could also explain that despite seeing higher CD8 TP immune infiltration in younger patients, this did not correlate with survival. However, T cell exhaustion is reversible, with immune checkpoint blockades such as anti-PD-1 successfully re-igniting anti-tumour T cell function, including in breast cancer (Nagarajan & Mcardle, 2018; Zarour, 2016)**.**

Critically, CD8 TP and CD8 $T_{RM}$ ($CD8^+CD103^+$) were among the lowest mean density phenotypes, compared to other phenotypes such as $CD39^+$, $CD4^+$ and $CD4^+CD39^+$. In the context of this study, these phenotypes may represent immune-suppressive Tregs, and the high CD39 expression may be accumulating adenosine in these microenvironments. In breast cancer, CD4+ was found to correlate with a poorer survival, (Huang et al, 2015). CD4 in this literature and the current project would also be identifying Th2 cells: Treatment-naïve breast cancers were found to sway towards Th2 response, which has been associated

with poorer survival (Campbell et al, 2005). The immune-suppressive Tregs could be co-existing with the CD8 TPs that may have the potential to be potent against tumour cells if these immunosuppressive cells weren't present. Immunosuppressive Tregs have already been found to abrogate the ability of $CD39^{high}$ CD8 $T_{RM}$s to predict survival so this is a highly plausible mechanism for this project's findings.

## 4.5. Future directions

Undoubtedly, the impressive optimisation of a 5 marker multiplex IHC panel on such an understudied African population has provided notable insight into the tumour microenvironment of these highly aggressive tumours. Further analysis of the data generated by this project needs to be achieved. For example, assessing whether there is a correlation between CD8 TP and $CD4^{+}$/$CD4^{+}CD39^{+}$ densities could indicate whether immune-suppressive Treg cells are potentially antagonising the anti-cancer effect of CD8 TPs. A positive correlation between the populations could confirm this mechanism. This project also calculated the nearest neighbour for each phenotype, thus the proximity of CD8 TPs with Tregs could be assessed in the future. It is hoped that in cases where Tregs and CD8 TPs are further in proximity to one another, CD8 TP anti-tumour function may be evident when performing analysis.

It is important to note all patients received similar treatment plans, that were not specifically tailored to their hormonal receptor expression, and other clinical features as done in developed countries (where most Cancer Immunology research is carried out). Reproducing the research done in this project on a Caucasian TMA (such as the Nottingham Breast Cancer TMA) would generate comparative data of the breast cancer immune landscape, as the African patients have already demonstrated a difference in TIL density.

Additionally, to address the finding that neoadjuvant chemotherapy is linked to a high CD8 TP density, it would be useful to analyse cell densities before and after chemotherapy. For example, if a high density existed in the tumour prior to chemotherapy, could this predict pathological complete response. Alternatively, the treatment itself may promote CD8 TP generation, and that immunotherapy could be beneficial in this context.

## 4.6. Conclusions

In summary, this project portrays the successful optimisation of the innovative technique, multiplex IHC, on a TMA assembled from Ghanaian breast cancer patients. It defined the densities of immune phenotypes present in the tumour microenvironment of these notably aggressive tumours, including a population of CD8 TPs, which have been portrayed in the literature as antigen-specific functional $T_{RM}$ cells. However, a good prognosis was observed when high CD8 TPs infiltrated tumours, suggesting that extensive immunosuppression could be antagonising their function. The novel insight that this study has given into the immune contexture of African breast cancer patients could suggest new therapies targeting the immune-suppressive populations may be beneficial in the future.

## References


Abdou, Y., Attwood, K., Cheng, T.-Y. D., Yao, S., Bandera, E. v., Zirpoli, G. R., Ondracek, R. P., Stein, L., Bshara, W., Khoury, T., Ambrosone, C. B., & Omilian, A. R. (2020). Racial differences in CD8+ T cell infiltration in breast tumors from Black and White women. *Breast Cancer Research 2020 22:1*, *22*(1), 1–10. https://doi.org/10.1186/S13058-020-01297-4

Adachi, T., Kobayashi, T., Sugihara, E., Yamada, T., Ikuta, K., Pittaluga, S., Saya, H., Amagai, M., & Nagao, K. (2015). Hair follicle-derived IL-7 and IL-15 mediate skin-resident memory T cell homeostasis and lymphoma. *Nature Medicine*, *21*(11), 1272–1279. https://doi.org/10.1038/nm.3962

Ahmed, R., & Gray, D. (1996). Immunological memory and protective immunity: Understanding their relation. *Science*, *272*(5258), 54–60. https://doi.org/10.1126/science.272.5258.54

Allard, B., Longhi, M. S., Robson, S. C., & Stagg, J. (2017). The ectonucleotidases CD39 and CD73: Novel checkpoint inhibitor targets. *Immunological Reviews*, *276*(1), 121–144. https://doi.org/10.1111/IMR.12528

Boddupalli, C. S., Bar, N., Kadaveru, K., Krauthammer, M., Pornputtapong, N., Mai, Z., Ariyan, S., Narayan, D., Kluger, H., Deng, Y., Verma, R., Das, R., Bacchiocchi, A., Halaban, R., Sznol, M., Dhodapkar, M. v., & Dhodapkar, K. M. (2016). Interlesional diversity of T cell receptors in melanoma with immune checkpoints enriched in tissue-resident memory T cells. *JCI Insight*, *1*(21). https://doi.org/10.1172/jci.insight.88955

Boutet, M., Gauthier, L., Leclerc, M., Gros, G., de Montpreville, V., Theret, N., Donnadieu, E., & Mami-Chouaib, F. (2016). TGFβ signaling intersects with CD103 integrin signaling to promote T-Lymphocyte accumulation and antitumor activity in the lung tumor microenvironment. *Cancer Research*, *76*(7), 1757–1769. https://doi.org/10.1158/0008-5472.CAN-15-1545

Bray, F., Ferlay, J., Soerjomataram, I., Siegel, R. L., Torre, L. A., & Jemal, A. (2018). Global cancer statistics 2018: GLOBOCAN estimates of incidence and mortality worldwide for 36 cancers in 185 countries. *CA: A Cancer Journal for Clinicians*, *68*(6), 394–424. https://doi.org/10.3322/caac.21492

Bruni, D., Angell, H. K., & Galon, J. (2020). The immune contexture and Immunoscore in cancer prognosis and therapeutic efficacy. In *Nature Reviews Cancer* (Vol. 20, Issue 11, pp. 662–680). Nature Research. https://doi.org/10.1038/s41568-020-0285-7

Cepek, K. L., Shaw, S. K., Parker, C. M., Russell, G. J., Morrow, J. S., Rimm, D. L., & Brenner, M. B. (1994). Adhesion between epithelial cells and T lymphocytes mediated by E-cadherin and the αeβ7 integrin. *Nature*, *372*(6502), 190–193. https://doi.org/10.1038/372190a0

Chen, D. S., & Mellman, I. (2013). *Review Oncology MeetsImmunology: The Cancer-Immunity Cycle*. https://doi.org/10.1016/j.immuni.2013.07.012

Cheuk, S., Schlums, H., Gallais Sérézal, I., Martini, E., Chiang, S. C., Marquardt, N., Gibbs, A., Detlofsson, E., Introini, A., Forkel, M., Höög, C., Tjernlund, A., Michaëlsson, J., Folkersen, L., Mjösberg, J., Blomqvist, L., Ehrström, M., Ståhle, M., Bryceson, Y. T., & Eidsmo, L. (2017). CD49a Expression Defines Tissue-Resident CD8+ T Cells Poised for Cytotoxic Function in Human Skin. *Immunity*, *46*(2), 287–300. https://doi.org/10.1016/j.immuni.2017.01.009

Clarke, J., Panwar, B., Madrigal, A., Singh, D., Gujar, R., Wood, O., Chee, S. J., Eschweiler, S., King, E. v., Awad, A. S., Hanley, C. J., McCann, K. J., Bhattacharyya, S., Woo, E., Alzetani, A., Seumois, G., Thomas, G. J., Ganesan, A. P., Friedmann, P. S., … Vijayanand, P. (2019). Single-cell transcriptomic analysis of tissue-resident memory T cells in human lung cancer. *Journal of Experimental Medicine*, *216*(9), 2128–2149. https://doi.org/10.1084/jem.20190249

Clemente, C. G., Mihm, M. C., Bufalino, R., Zurrida, S., Collini, P., & Cascinelli, N. (1996). Prognostic value of tumor infiltrating lymphocytes in the vertical growth phase of primary cutaneous melanoma. *Cancer*, *77*(7), 1303–1310. https://doi.org/10.1002/(SICI)1097-0142(19960401)77:7<1303::AID-CNCR12>3.0.CO;2-5

Cyster, J. G., & Schwab, S. R. (2012). Sphingosine-1-phosphate and lymphocyte egress from lymphoid organs. In *Annual Review of Immunology* (Vol. 30, pp. 69–94). Annu Rev Immunol. https://doi.org/10.1146/annurev-immunol-020711-075011

Debes, G. F., Arnold, C. N., Young, A. J., Krautwald, S., Lipp, M., Hay, J. B., & Butcher, E. C. (2005). Chemokine receptor CCR7 required for T lymphocyte exit from peripheral tissues. *Nature Immunology*, *6*(9), 889–894. https://doi.org/10.1038/ni1238

Denkert, C., Loibl, S., Noske, A., Roller, M., Müller, B. M., Komor, M., Budczies, J., Darb-Esfahani, S., Kronenwett, R., Hanusch, C., von Törne, C., Weichert, W., Engels, K., Solbach, C., Schrader, I., Dietel, M., & von Minckwitz, G. (2010). Tumor-associated lymphocytes as an independent predictor of response to neoadjuvant chemotherapy in breast cancer. *Journal of Clinical Oncology : Official Journal of the American Society of Clinical Oncology*, *28*(1), 105–113. https://doi.org/10.1200/JCO.2009.23.7370

Der, E. M., ChB, M., Gyasi, R. K., Tettey, Y., Edusei, L., Bayor, M. T., Jiagge, E., Gyakobo, M., Merajver, S. D., & Newman, L. A. (2015). *Triple-Negative Breast Cancer in Ghanaian Women: The Korle Bu Teaching Hospital Experience*. https://doi.org/10.1111/tbj.12527

Desfrançois, J., Derré, L., Corvaisier, M., Mével, B. le, Catros, V., Jotereau, F., & Gervois, N. (2009). Increased frequency of nonconventional double positive CD4CD8 αβ T cells in human breast pleural effusions. *International Journal of Cancer*, *125*(2), 374–380. https://doi.org/10.1002/IJC.24366

Djenidi, F., Adam, J., Goubar, A., Durgeau, A., Meurice, G., de Montpréville, V., Validire, P., Besse, B., & Mami-Chouaib, F. (2015). CD8 + CD103 + Tumor–Infiltrating Lymphocytes Are Tumor-Specific Tissue-Resident Memory T Cells and a Prognostic Factor for Survival in Lung Cancer Patients . *The Journal of Immunology*, *194*(7), 3475–3486. https://doi.org/10.4049/jimmunol.1402711

Duhen, T., Duhen, R., Montler, R., Moses, J., Moudgil, T., de Miranda, N. F., Goodall, C. P., Blair, T. C., Fox, B. A., McDermott, J. E., Chang, S. C., Grunkemeier, G., Leidner, R., Bell, R. B., & Weinberg, A. D. (2018). Co-expression of CD39 and CD103 identifies tumor-reactive CD8 T cells in human solid tumors. *Nature Communications*, *9*(1), 1–13. https://doi.org/10.1038/s41467-018-05072-0

E. Goldberg, J., & L. Schwertfeger, K. (2010). Proinflammatory Cytokines in Breast Cancer: Mechanisms of Action and Potential Targets for Therapeutics. *Current Drug Targets*, *11*(9), 1133–1146. https://doi.org/10.2174/138945010792006799

Edwards, J., Wilmott, J. S., Madore, J., Gide, T. N., Quek, C., Tasker, A., Ferguson, A., Chen, J., Hewavisenti, R., Hersey, P., Gebhardt, T., Weninger, W., Britton, W. J., Saw, R. P. M.,

Thompson, J. F., Menzies, A. M., Long, G. V., Scolyer, R. A., & Palendira, U. (2018). CD103+ tumor-resident CD8+ T cells are associated with improved survival in immunotherapy-naïve melanoma patients and expand significantly during anti-PD-1 treatment. *Clinical Cancer Research*, *24*(13), 3036–3045. https://doi.org/10.1158/1078-0432.CCR-17-2257

Egelston, C. A., Avalos, C., Tu, T. Y., Rosario, A., Wang, R., Solomon, S., Srinivasan, G., Nelson, M. S., Huang, Y., Lim, M. H., Simons, D. L., He, T. F., Yim, J. H., Kruper, L., Mortimer, J., Yost, S., Guo, W., Ruel, C., Frankel, P. H., … Lee, P. P. (2019). Resident memory CD8+ T cells within cancer islands mediate survival in breast cancer patients. *JCI Insight*, *4*(19). https://doi.org/10.1172/jci.insight.130000

El-Asady, R., Yuan, R., Liu, K., Wang, D., Gress, R. E., Lucas, P. J., Drachenberg, C. B., & Hadley, G. A. (2005). TGF-β-dependent CD103 expression by CD8+ T cells promotes selective destruction of the host intestinal epithelium during graft-versus-host disease. *Journal of Experimental Medicine*, *201*(10), 1647–1657. https://doi.org/10.1084/jem.20041044

Farber, D. L., Yudanin, N. A., & Restifo, N. P. (2014). Human memory T cells: generation, compartmentalization and homeostasis. *Nature Reviews. Immunology*, *14*(1), 24. https://doi.org/10.1038/NRI3567

Fearon, D. T., Carr, J. M., Telaranta, A., Carrasco, M. J., & Thaventhiran, J. E. D. (2006). The rationale for the IL-2-independent generation of the self-renewing central memory CD8+ T cells. *Immunological Reviews*, *211*, 104–118. https://doi.org/10.1111/J.0105-2896.2006.00390.X

Galea, M. H., Blamey, R. W., Elston, C. E., & Ellis, I. O. (1992). The Nottingham prognostic index in primary breast cancer. *Breast Cancer Research and Treatment 1992 22:3*, *22*(3), 207–219. https://doi.org/10.1007/BF01840834

Galon, J., & Bruni, D. (n.d.). Approaches to treat immune hot, altered and cold tumours with combination immunotherapies. *Nature Reviews Drug Discovery*. https://doi.org/10.1038/s41573-018-0007-y

Ganesan, A. P., Clarke, J., Wood, O., Garrido-Martin, E. M., Chee, S. J., Mellows, T., Samaniego-Castruita, D., Singh, D., Seumois, G., Alzetani, A., Woo, E., Friedmann, P. S., King, E. v., Thomas, G. J., Sanchez-Elsner, T., Vijayanand, P., & Ottensmeier, C. H. (2017). Tissue-resident memory features are linked to the magnitude of cytotoxic T cell responses in human lung cancer. *Nature Immunology*, *18*(8), 940–950. https://doi.org/10.1038/ni.3775

Gebhardt, T., Wakim, L. M., Eidsmo, L., Reading, P. C., Heath, W. R., & Carbone, F. R. (2009). *Memory T cells in nonlymphoid tissue that provide enhanced local immunity during infection with herpes simplex virus*. https://doi.org/10.1038/ni.1718

Glennie, N. D., Yeramilli, V. A., Beiting, D. P., Volk, S. W., Weaver, C. T., & Scott, P. (2015). Skin-resident memory CD4+ T cells enhance protection against Leishmania major infection. *Journal of Experimental Medicine*, *212*(9), 1405–1414. https://doi.org/10.1084/jem.20142101

Goral, S. (2011). The three-signal hypothesis of lymphocyte activation/targets for immunosuppression. *Dialysis & Transplantation*, *40*(1), 14–16. https://doi.org/10.1002/DAT.20527

Haanen, J. B. A. G., Baars, A., Gomez, R., Weder, P., Smits, M., de Gruijl, T. D., von Blomberg, B. M. E., Bloemena, E., Scheper, R. J., van Ham, S. M., Pinedo, H. M., & van den Eertwegh, A. J. M. (2006). Melanoma-specific tumor-infiltrating lymphocytes but not circulating melanoma-

specific T cells may predict survival in resected advanced-stage melanoma patients. *Cancer Immunology, Immunotherapy*, *55*(4), 451–458. https://doi.org/10.1007/s00262-005-0018-5

Herndler-Brandstetter, D., Ishigame, H., Shinnakasu, R., Plajer, V., Stecher, C., Zhao, J., Lietzenmayer, M., Kroehling, L., Takumi, A., Kometani, K., Inoue, T., Kluger, Y., Kaech, S. M., Kurosaki, T., Okada, T., & Flavell, R. A. (2018). KLRG1+ Effector CD8+ T Cells Lose KLRG1, Differentiate into All Memory T Cell Lineages, and Convey Enhanced Protective Immunity. *Immunity*, *48*(4), 716-729.e8. https://doi.org/10.1016/j.immuni.2018.03.015

Hombrink, P., Helbig, C., Backer, R. A., Piet, B., Oja, A. E., Stark, R., Brasser, G., Jongejan, A., Jonkers, R. E., Nota, B., Basak, O., Clevers, H. C., Moerland, P. D., Amsen, D., & van Lier, R. A. W. (2016). Programs for the persistence, vigilance and control of human CD8 + lung-resident memory T cells. *Nature Immunology*, *17*(12), 1467–1478. https://doi.org/10.1038/ni.3589

Hu, G., Wu, P., Cheng, P., Zhang, Z., Wang, Z., Yu, X., Shao, X., Wu, D., Ye, J., Zhang, T., Wang, X., Qiu, F., Yan, J., & Huang, J. (2017). Tumor-infiltrating CD39+ γδTregs are novel immunosuppressive T cells in human colorectal cancer. *Oncoimmunology*, *6*(2). https://doi.org/10.1080/2162402X.2016.1277305

Hu, W., Sun, R., Chen, L., Zheng, X., & Jiang, J. (2019). Prognostic significance of resident CD103+CD8+T cells in human colorectal cancer tissues. *Acta Histochemica*, *121*(5), 657–663. https://doi.org/10.1016/j.acthis.2019.05.009

Huang, Y., Ma, C., Zhang, Q., Ye, J., Wang, F., Zhang, Y., Hunborg, P., Varvares, M. A., Hoft, D. F., Hsueh, E. C., & Peng, G. (2015). CD4+ and CD8+ T cells have opposing roles in breast cancer progression and outcome. *Oncotarget*, *6*(19), 17462. https://doi.org/10.18632/ONCOTARGET.3958

Iijima, N., & Iwasaki, A. (2014). A local macrophage chemokine network sustains protective tissue-resident memory CD4 T cells. *Science*, *346*(6205), 93–98. https://doi.org/10.1126/science.1257530

Kaech, S. M., Hemby, S., Kersh, E., & Ahmed, R. (2002). Molecular and functional profiling of memory CD8 T cell differentiation. In *Cell* (Vol. 111, Issue 6, pp. 837–851). Cell Press. https://doi.org/10.1016/S0092-8674(02)01139-X

Killelea, B. K., Yang, V. Q., Wang, S. Y., Hayse, B., Mougalian, S., Horowitz, N. R., Chagpar, A. B., Pusztai, L., & Lannin, D. R. (2015). Racial Differences in the Use and Outcome of Neoadjuvant Chemotherapy for Breast Cancer: Results From the National Cancer Data Base. *Journal of Clinical Oncology : Official Journal of the American Society of Clinical Oncology*, *33*(36), 4267–4275. https://doi.org/10.1200/JCO.2015.63.7801

Kumar, B. v., Ma, W., Miron, M., Granot, T., Guyer, R. S., Carpenter, D. J., Senda, T., Sun, X., Ho, S. H., Lerner, H., Friedman, A. L., Shen, Y., & Farber, D. L. (2017). Human Tissue-Resident Memory T Cells Are Defined by Core Transcriptional and Functional Signatures in Lymphoid and Mucosal Sites. *Cell Reports*, *20*(12), 2921–2934. https://doi.org/10.1016/j.celrep.2017.08.078

le Floc'h, A., Jalil, A., Franciszkiewicz, K., Validire, P., Vergnon, I., & Mami-Chouaib, F. (2011). Minimal engagement of CD103 on cytotoxic T lymphocytes with an E-cadherin-Fc molecule triggers lytic granule polarization via a phospholipase Cγ-dependent pathway. *Cancer Research*, *71*(2), 328–338. https://doi.org/10.1158/0008-5472.CAN-10-2457

Linehan, J. L., & Delamarre, L. (2019). Teamwork by different T-cell types boosts tumour destruction by immunotherapy. *Nature 2021 574:7780*, *574*(7780), 639–640. https://doi.org/10.1038/d41586-019-03106-1

Loi, S. (2013). Tumor-infiltrating lymphocytes, breast cancer subtypes and therapeutic efficacy. *Oncoimmunology*, *2*(7). https://doi.org/10.4161/ONCI.24720

Loi, S., Adams, S., Schmid, P., Cortés, J., Cescon, D. W., Winer, E. P., Toppmeyer, D. L., Rugo, H. S., de Laurentiis, M., Nanda, R., Iwata, H., Awada, A., Tan, A., Wang, A., Aktan, G., Karantza, V., & Salgado, R. (2017). *LBA13 Relationship between tumor infiltrating lymphocyte (TIL) levels and response to pembrolizumab (pembro) in metastatic triple-negative breast cancer (mTNBC): Results from KEYNOTE-086*. https://doi.org/10.1093/annonc/mdx440.005

Loi, S., Giobbie-Hurder, A., Gombos, A., Bachelot, T., Hui, R., Curigliano, G., Campone, M., Biganzoli, L., Bonnefoi, H., Jerusalem, G., Bartsch, R., Rabaglio-Poretti, M., Kammler, R., Maibach, R., Smyth, M. J., di Leo, A., Colleoni, M., Viale, G., Regan, M. M., … Schneier, P. (2019). Pembrolizumab plus trastuzumab in trastuzumab-resistant, advanced, HER2-positive breast cancer (PANACEA): a single-arm, multicentre, phase 1b–2 trial. *The Lancet Oncology*, *20*(3), 371–382. https://doi.org/10.1016/S1470-2045(18)30812-X

Loibl, S., Poortmans, P., Morrow, M., Denkert, C., & Curigliano, G. (2021). Breast cancer. *The Lancet*, *397*(10286), 1750–1769. https://doi.org/10.1016/S0140-6736(20)32381-3

Losurdo, A., Scirgolea, C., Alvisi, G., Brummelman, J., Errico, V., di Tommaso, L., Pilipow, K., Colombo, F. S., Fernandes, B., Peano, C., Testori, A., Tinterri, C., Roncalli, M., Santoro, A., Maria, E., Mazza, C., & Lugli, E. (n.d.). *Single-cell profiling defines the prognostic benefit of CD39 high tissue resident memory CD8+ T cells in luminal-like breast cancer*. https://doi.org/10.1038/s42003-021-02595-z

Mackay, L. K., Braun, A., Macleod, B. L., Collins, N., Tebartz, C., Bedoui, S., Carbone, F. R., & Gebhardt, T. (2015). Cutting Edge: CD69 Interference with Sphingosine-1-Phosphate Receptor Function Regulates Peripheral T Cell Retention. *The Journal of Immunology*, *194*(5), 2059–2063. https://doi.org/10.4049/jimmunol.1402256

Mackay, L. K., Minnich, M., Kragten, N. A. M., Liao, Y., Nota, B., Seillet, C., Zaid, A., Man, K., Preston, S., Freestone, D., Braun, A., Wynne-Jones, E., Behr, F. M., Stark, R., Pellicci, D. G., Godfrey, D. I., Belz, G. T., Pellegrini, M., Gebhardt, T., … van Gisbergen, K. P. J. M. (2016). Hobit and Blimp1 instruct a universal transcriptional program of tissue residency in lymphocytes. *Science*, *352*(6284), 459–463. https://doi.org/10.1126/science.aad2035

MacKay, L. K., Rahimpour, A., Ma, J. Z., Collins, N., Stock, A. T., Hafon, M. L., Vega-Ramos, J., Lauzurica, P., Mueller, S. N., Stefanovic, T., Tscharke, D. C., Heath, W. R., Inouye, M., Carbone, F. R., & Gebhardt, T. (2013). The developmental pathway for CD103+ CD8+ tissue-resident memory T cells of skin. *Nature Immunology*, *14*(12), 1294–1301. https://doi.org/10.1038/ni.2744

Mackay, L. K., Stock, A. T., Ma, J. Z., Jones, C. M., Kent, S. J., Mueller, S. N., Heath, W. R., Carbone, F. R., & Gebhardt, T. (2012). Long-lived epithelial immunity by tissue-resident memory T (TRM) cells in the absence of persisting local antigen presentation. *Proceedings of the National Academy of Sciences of the United States of America*, *109*(18), 7037–7042. https://doi.org/10.1073/pnas.1202288109

Maliszewski, C. R., Delespesse, G. J., Schoenborn, M. A., Armitage, R. J., Fanslow, W. C., Nakajima, T., Baker, E., Sutherland, G. R., Poindexter, K., & Birks, C. (1994). The CD39 lymphoid cell activation antigen. Molecular cloning and structural characterization. *The Journal of Immunology*, *153*(8).

Marquardt, N., Kekäläinen, E., Chen, P., Lourda, M., Wilson, J. N., Scharenberg, M., Bergman, P., Al-Ameri, M., Hård, J., Mold, J. E., Ljunggren, H.-G., & Michaëlsson, J. (2019). Unique transcriptional and protein-expression signature in human lung tissue-resident NK cells. *Nature Communications 2019 10:1*, *10*(1), 1–12. https://doi.org/10.1038/s41467-019-11632-9

Masopust, D., Choo, D., Vezys, V., Wherry, E. J., Duraiswamy, J., Akondy, R., Wang, J., Casey, K. A., Barber, D. L., Kawamura, K. S., Fraser, K. A., Webby, R. J., Brinkmann, V., Butcher, E. C., Newell, K. A., & Ahmed, R. (2010). Dynamic T cell migration program provides resident memory within intestinal epithelium. *Journal of Experimental Medicine*, *207*(3), 553–564. https://doi.org/10.1084/jem.20090858

McMaster, S. R., Wilson, J. J., Wang, H., & Kohlmeier, J. E. (2015). Airway-Resident Memory CD8 T Cells Provide Antigen-Specific Protection against Respiratory Virus Challenge through Rapid IFN-γ Production. *The Journal of Immunology*, *195*(1), 203–209. https://doi.org/10.4049/jimmunol.1402975

Milner, J. J., Toma, C., Yu, B., Zhang, K., Omilusik, K., Phan, A. T., Wang, D., Getzler, A. J., Nguyen, T., Crotty, S., Wang, W., Pipkin, M. E., & Goldrath, A. W. (2017). Runx3 programs CD8+ T cell residency in non-lymphoid tissues and tumours. *Nature*, *552*(7684), 253–257. https://doi.org/10.1038/nature24993

Motz, G. T., & Coukos, G. (2013). Deciphering and Reversing Tumor Immune Suppression. In *Immunity* (Vol. 39, Issue 1, pp. 61–73). Cell Press. https://doi.org/10.1016/j.immuni.2013.07.005

Mueller, S. N., & Mackay, L. K. (2016). Tissue-resident memory T cells: Local specialists in immune defence. In *Nature Reviews Immunology* (Vol. 16, Issue 2, pp. 79–89). Nature Publishing Group. https://doi.org/10.1038/nri.2015.3

Nagarajan, D., & Mcardle, S. E. B. (2018). biomedicines Immune Landscape of Breast Cancers. *Biomedicines*, *6*. https://doi.org/10.3390/biomedicines6010020

Naito, Y., Saito, K., Shiiba, K., Ohuchi, A., Saigenji, K., Nagura, H., & Ohtani, H. (1998). CD8+ T Cells Infiltrated within Cancer Cell Nests as a Prognostic Factor in Human Colorectal Cancer. *Cancer Research*, *58*(16).

Ohene-Yeboah, M., & Adjei, E. (2012). Breast Cancer in Kumasi, Ghana. *Ghana Medical Journal*, *46*(1), 8. /pmc/articles/PMC3353503/

Oja, A. E., Piet, B., van der Zwan, D., Blaauwgeers, H., Mensink, M., de Kivit, S., Borst, J., Nolte, M. A., van Lier, R. A. W., Stark, R., & Hombrink, P. (2018). Functional heterogeneity of CD4+ tumor-infiltrating lymphocytes with a resident memory phenotype in NSCLC. *Frontiers in Immunology*, *9*(NOV). https://doi.org/10.3389/fimmu.2018.02654

Park, M. H., Kwon, S. Y., Choi, J. E., Gong, G., & Bae, Y. K. (2020). Intratumoral CD103-positive tumour-infiltrating lymphocytes are associated with favourable prognosis in patients with triple-negative breast cancer. *Histopathology*, *77*(4), 560–569. https://doi.org/10.1111/his.14126

Park, S. L., Gebhardt, T., & Mackay, L. K. (2019). Tissue-Resident Memory T Cells in Cancer Immunosurveillance. In *Trends in Immunology* (Vol. 40, Issue 8, pp. 735–747). Elsevier Ltd. https://doi.org/10.1016/j.it.2019.06.002

Park, S. L., Zaid, A., Hor, J. L., Christo, S. N., Prier, J. E., Davies, B., Alexandre, Y. O., Gregory, J. L., Russell, T. A., Gebhardt, T., Carbone, F. R., Tscharke, D. C., Heath, W. R., Mueller, S. N., & MacKay, L. K. (2018). Local proliferation maintains a stable pool of tissue-resident memory T cells after antiviral recall responses article. *Nature Immunology*, *19*(2), 183–191. https://doi.org/10.1038/s41590-017-0027-5

Posavad, C. M., Zhao, L., Dong, L., Jin, L., Stevens, C. E., Magaret, A. S., Johnston, C., Wald, A., Zhu, J., Corey, L., & Koelle, D. M. (2017). Enrichment of herpes simplex virus type 2 (HSV-2) reactive mucosal T cells in the human female genital tract. *Mucosal Immunology*, *10*(5), 1259–1269. https://doi.org/10.1038/mi.2016.118

Pulsawatdi, A. V., Craig, S. G., Bingham, V., McCombe, K., Humphries, M. P., Senevirathne, S., Richman, S. D., Quirke, P., Campo, L., Domingo, E., Maughan, T. S., James, J. A., & Salto-Tellez, M. (2020). A robust multiplex immunofluorescence and digital pathology workflow for the characterisation of the tumour immune microenvironment. *Molecular Oncology*, *14*(10), 2384. https://doi.org/10.1002/1878-0261.12764

Purwar, R., Campbell, J., Murphy, G., Richards, W. G., Clark, R. A., & Kupper, T. S. (2011). Resident Memory T cells (TRM) are abundant in human lung: Diversity, function, and antigen specificity. *PLoS ONE*, *6*(1). https://doi.org/10.1371/journal.pone.0016245

Raczkowski, F., Rissiek, A., Ricklefs, I., Heiss, K., Schumacher, V., Wundenberg, K., Haag, F., Koch-Nolte, F., Tolosa, E., & Mittrücker, H.-W. (2018). CD39 is upregulated during activation of mouse and human T cells and attenuates the immune response to Listeria monocytogenes. *PLOS ONE*, *13*(5), e0197151. https://doi.org/10.1371/journal.pone.0197151

Reicher, B., & Barda-Saad, M. (2010). Multiple pathways leading from the T-cell antigen receptor to the actin cytoskeleton network. *FEBS Letters*, *584*(24), 4858–4864. https://doi.org/10.1016/J.FEBSLET.2010.09.002

Rosen, R. D., & Sapra, A. (2021). TNM Classification. *StatPearls NCBI*. https://www.ncbi.nlm.nih.gov/books/NBK553187/

Salgado, R., Denkert, C., Demaria, S., Sirtaine, N., Klauschen, F., Pruneri, G., Wienert, S., van den Eynden, G., Baehner, F. L., Penault-Llorca, F., Perez, E. A., Thompson, E. A., Symmans, W. F., Richardson, A. L., Brock, J., Criscitiello, C., Bailey, H., Ignatiadis, M., Floris, G., … Loi, S. (2015). The evaluation of tumor-infiltrating lymphocytes (TILS) in breast cancer: Recommendations by an International TILS Working Group 2014. In *Annals of Oncology* (Vol. 26, Issue 2, pp. 259–271). Oxford University Press. https://doi.org/10.1093/annonc/mdu450

Sallusto, F., Geginat, J., & Lanzavecchia, A. (2004). Central memory and effector memory T cell subsets: Function, generation, and maintenance. In *Annual Review of Immunology* (Vol. 22, pp. 745–763). Annual Reviews. https://doi.org/10.1146/annurev.immunol.22.012703.104702

Sallusto, F., Lenig, D., Förster, R., Lipp, M., & Lanzavecchia, A. (1999). Two subsets of memory T lymphocytes with distinct homing potentials and effector functions. *Nature*, *401*(6754), 708–712. https://doi.org/10.1038/44385

Sarrabayrouse, G., Corvaisier, M., Ouisse, L.-H., Bossard, C., Mével, B. le, Potiron, L., Meurette, G., Gervois, N., & Jotereau, F. (2011). Tumor-reactive CD4+CD8αβ+ CD103+ αβT cells: A prevalent tumor-reactive T-cell subset in metastatic colorectal cancers. *International Journal of Cancer*, *128*(12), 2923–2932. https://doi.org/10.1002/ijc.25640

Savas, P., Virassamy, B., Ye, C., Salim, A., Mintoff, C. P., Caramia, F., Salgado, R., Byrne, D. J., Teo, Z. L., Dushyanthen, S., Byrne, A., Wein, L., Luen, S. J., Poliness, C., Nightingale, S. S., Skandarajah, A. S., Gyorki, D. E., Thornton, C. M., Beavis, P. A., … Loi, S. (2018). Single-cell profiling of breast cancer T cells reveals a tissue-resident memory subset associated with improved prognosis. *Nature Medicine*, *24*(7), 986–993. https://doi.org/10.1038/s41591-018-0078-7

Schenkel, J. M., Fraser, K. A., Beura, L. K., Pauken, K. E., Vezys, V., & Masopust, D. (2014). Resident memory CD8 t cells trigger protective innate and adaptive immune responses. *Science*, *346*(6205), 98–101. https://doi.org/10.1126/science.1254536

Schnitt, S. J. (2010). Classification and prognosis of invasive breast cancer: From morphology to molecular taxonomy. *Modern Pathology*, *23*, 60–64. https://doi.org/10.1038/modpathol.2010.33

Scurr, M., Ladell, K., Besneux, M., Christian, A., Hockey, T., Smart, K., Bridgeman, H., Hargest, R., Phillips, S., Davies, M., Price, D., Gallimore, A., & Godkin, A. (2014). Highly prevalent colorectal cancer-infiltrating LAP + Foxp3 - T cells exhibit more potent immunosuppressive activity than Foxp3 + regulatory T cells. *Mucosal Immunology*, *7*(2), 428–439. https://doi.org/10.1038/mi.2013.62

Shin, H., & Iwasaki, A. (2012). A vaccine strategy that protects against genital herpes by establishing local memory T cells. *Nature*, *491*(7424), 463–467. https://doi.org/10.1038/nature11522

Skon, C. N., Lee, J.-Y., Anderson, K. G., Masopust, D., Hogquist, K. A., & Jameson, S. C. (2013). Transcriptional downregulation of S1pr1 is required for the establishment of resident memory CD8+ T cells. *Nature Immunology*, *14*(12), 1285–1293. https://doi.org/10.1038/ni.2745

Stack, E. C., Wang, C., Roman, K. A., & Hoyt, C. C. (2014). Multiplexed immunohistochemistry, imaging, and quantitation: a review, with an assessment of Tyramide signal amplification, multispectral imaging and multiplex analysis. *Methods (San Diego, Calif.)*, *70*(1), 46–58. https://doi.org/10.1016/J.YMETH.2014.08.016

Stanton, S. E., & Disis, M. L. (2016). Clinical significance of tumor-infiltrating lymphocytes in breast cancer. In *Journal for ImmunoTherapy of Cancer* (Vol. 4, Issue 1). BioMed Central Ltd. https://doi.org/10.1186/s40425-016-0165-6

Stark, A., Kleer, C. G., Martin, I., Awuah, B., Nsiah-Asare, A., Takyi, V., Braman, M., Quayson, S. E., Zarbo, R., Wicha, M., & Newman, L. (2010). African Ancestry and Higher Prevalence of Triple-Negative Breast Cancer: Findings From an International Study. *Cancer*, *116*(21), 4926. https://doi.org/10.1002/CNCR.25276

Steinbach, K., Vincenti, I., Kreutzfeldt, M., Page, N., Muschaweckh, A., Wagner, I., Drexler, I., Pinschewer, D., Korn, T., & Merkler, D. (2016). Brain-resident memory T cells represent an autonomous cytotoxic barrier to viral infection. *Journal of Experimental Medicine*, *213*(8), 1571–1587. https://doi.org/10.1084/jem.20151916

Steinert, E. M., Schenkel, J. M., Fraser, K. A., Beura, L. K., Manlove, L. S., Igyártó, B. Z., Southern, P. J., & Masopust, D. (2015). Quantifying memory CD8 T cells reveals regionalization of immunosurveillance. *Cell*, *161*(4), 737–749. https://doi.org/10.1016/j.cell.2015.03.031

Sun, Z., Nyberg, R., Wu, Y., Bernard, B., & Redmond, W. L. (2021). Developing an enhanced 7-color multiplex IHC protocol to dissect immune infiltration in human cancers. *PLOS ONE*, *16*(2), e0247238. https://doi.org/10.1371/JOURNAL.PONE.0247238

Svensson, H., Olofsson, V., Lundin, S., Yakkala, C., Björck, S., Börjesson, L., Gustavsson, B., & Quiding-Järbrink, M. (2012). Accumulation of CCR4+ CTLA-4hi FOXP3+CD25hi Regulatory T Cells in Colon Adenocarcinomas Correlate to Reduced Activation of Conventional T Cells. *PLoS ONE*, *7*(2), e30695. https://doi.org/10.1371/journal.pone.0030695

Szabo, P. A., Miron, M., & Farber, D. L. (2019). Location, location, location: Tissue resident memory T cells in mice and humans. In *Science Immunology* (Vol. 4, Issue 34, p. 9673). American Association for the Advancement of Science. https://doi.org/10.1126/sciimmunol.aas9673

Taube, J. M., Akturk, G., Angelo, M., Engle, E. L., Gnjatic, S., Greenbaum, S., Greenwald, N. F., Hedvat, C. v, Hollmann, T. J., Juco, J., Parra, E. R., Rebelatto, M. C., Rimm, D. L., Rodriguez-Canales, J., Schalper, K. A., Stack, E. C., Ferreira, C. S., Korski, K., Lako, A., … Bifulco, C. B. (2020). The Society for Immunotherapy of Cancer statement on best practices for multiplex immunohistochemistry (IHC) and immunofluorescence (IF) staining and validation. *Journal for ImmunoTherapy of Cancer*, *8*(1), e000155. https://doi.org/10.1136/JITC-2019-000155

Teijaro, J. R., Turner, D., Pham, Q., Wherry, E. J., Lefrançois, L., & Farber, D. L. (2011). Cutting Edge: Tissue-Retentive Lung Memory CD4 T Cells Mediate Optimal Protection to Respiratory Virus Infection. *The Journal of Immunology*, *187*(11), 5510–5514. https://doi.org/10.4049/jimmunol.1102243

Thomas, A. S., Kidwell, K. M., Oppong, J. K., Adjei, E. K., Osei-Bonsu, E., Boahene, A., Jiagge, E., Gyan, K., & Merajver, S. D. (2017). Breast Cancer in Ghana: Demonstrating the Need for Population-Based Cancer Registries in Low- and Middle-Income Countries. *Journal of Global Oncology*, *3*(6), 765. https://doi.org/10.1200/JGO.2016.006098

Tian, Y., Babor, M., Lane, J., Schulten, V., Patil, V. S., Seumois, G., Rosales, S. L., Fu, Z., Picarda, G., Burel, J., Zapardiel-Gonzalo, J., Tennekoon, R. N., de Silva, A. D., Premawansa, S., Premawansa, G., Wijewickrama, A., Greenbaum, J. A., Vijayanand, P., Weiskopf, D., … Peters, B. (2017). Unique phenotypes and clonal expansions of human CD4 effector memory T cells re-expressing CD45RA. *Nature Communications 2017 8:1*, *8*(1), 1–13. https://doi.org/10.1038/s41467-017-01728-5

Tøndell, A., Wahl, S. G. F., Sponaas, A.-M., Sørhaug, S., Børset, M., & Haug, M. (2020). Ectonucleotidase CD39 and Checkpoint Signalling Receptor Programmed Death 1 are Highly Elevated in Intratumoral Immune Cells in Non–small-cell Lung Cancer. *Translational Oncology*, *13*(1), 17. https://doi.org/10.1016/J.TRANON.2019.09.003

Tse, S. W., Radtke, A. J., Espinosa, D. A., Cockburn, I. A., & Zavala, F. (2014). The chemokine receptor CXCR6 is required for the maintenance of liver memory CD8+ T cells specific for infectious pathogens. *Journal of Infectious Diseases*, *210*(9), 1508–1516. https://doi.org/10.1093/infdis/jiu281

Wang, Z. Q., Milne, K., Derocher, H., Webb, J. R., Nelson, B. H., & Watson, P. H. (2016). CD103 and intratumoral immune response in breast cancer. *Clinical Cancer Research*, *22*(24), 6290–6297. https://doi.org/10.1158/1078-0432.CCR-16-0732

Wherry, E. J. (2011). T cell exhaustion. In *Nature Immunology* (Vol. 12, Issue 6, pp. 492–499). Nat Immunol. https://doi.org/10.1038/ni.2035

Yao, S., Cheng, T.-Y. D., Elkhanany, A., Yan, L., Omilian, A., Abrams, S. I., Evans, S., Hong, C.-C., Qi, Q., Davis, W., Liu, S., Bandera, E. v, Odunsi, K., Takabe, K., Khoury, T., & Ambrosone, C. B. (2021). Breast Tumor Microenvironment in Black Women: A Distinct Signature of CD8+ T-Cell Exhaustion. *JNCI: Journal of the National Cancer Institute*, *113*(8), 1036–1043. https://doi.org/10.1093/JNCI/DJAA215

Zaid, A., Hor, J. L., Christo, S. N., Groom, J. R., Heath, W. R., Mackay, L. K., & Mueller, S. N. (2017). Chemokine Receptor–Dependent Control of Skin Tissue–Resident Memory T Cell Formation. *The Journal of Immunology*, *199*(7), 2451–2459. https://doi.org/10.4049/jimmunol.1700571

Zarour, H. M. (2016). Reversing T-cell Dysfunction and Exhaustion in Cancer. *Clinical Cancer Research*, *22*(8), 1856–1864. https://doi.org/10.1158/1078-0432.CCR-15-1849

Zhang, N., & Bevan, M. J. (2013). Transforming growth factor-β signaling controls the formation and maintenance of gut-resident memory T cells by regulating migration and retention. *Immunity*, *39*(4), 687–696. https://doi.org/10.1016/j.immuni.2013.08.019